8-2016

New Insights Into An Old Interaction: Developing A Model For PAI-1:VN Interactions

Letitia Nichole Puster
University of Tennessee, Knoxville, lnpuster@gmail.com

To the Graduate Council:

I am submitting herewith a dissertation written by Letitia Nichole Puster entitled "New Insights Into An Old Interaction: Developing A Model For PAI-1:VN Interactions." I have examined the final electronic copy of this dissertation for form and content and recommend that it be accepted in partial fulfillment of the requirements for the degree of Doctor of Philosophy, with a major in Biochemistry and Cellular and Molecular Biology.

Cynthia B. Peterson, Major Professor

We have read this dissertation and recommend its acceptance:

Engin Serpersu, Liz Howell, Dan Roberts, Jeffrey M. Becker

Accepted for the Council:

Carolyn R. Hodges

Vice Provost and Dean of the Graduate School

(Original signatures are on file with official student records.)

New Insights Into An Old Interaction: Developing A Model For PAI-1:VN Interactions

A Dissertation Presented for the
Doctor of Philosophy
Degree
The University of Tennessee, Knoxville

Letitia Nichole Puster
August 2016

Dedication

This work is dedicated to the following individuals

My Husband

Dr. Brian Puster, Esq.

My Parents

Robin and Kent Olson

Acknowledgements

My parents have always supported and encouraged me, telling me that I could do anything, if only I would work hard. Their confidence and encouragement gave me the drive and courage that I needed to pursue higher education. Of all my siblings, I am the only one to achieve a post-baccalaureate degree, and there are many, including my parents, who contributed to my successful completion of this work.

First, I would like to acknowledge and thank my adviser, Cynthia B. Peterson. She has mentored and supported me throughout the past seven years. Despite career and university changes, she was never more than an email away. I would not be the scientist I am today without the opportunities and guidance she provided me. I would also like to thank my committee members, Drs. Jeff Becker, Liz Howell, Dan Roberts, and Engin Serpersu. They provided guidance and assistance throughout my graduate career, and were particularly helpful and supportive as I completed my degree following Cynthia's move to LSU. There were many other faculty members, staff, and collaborators who provided beneficial guidance and support throughout my time at UT. I particularly acknowledge and thank Dr. Ed Wright, Dr. Christopher Stanley, and Dr. Susan Kruger for all of the time and effort that they spent training and mentoring me. Also, thanks to the many members of the Peterson lab who filled the lab with science and smiles for many years. You made research in a windowless lab something to look forward to.

Next I would like to thank my family for the amazing support they have been to me throughout my educational journey. My parents and siblings have inspired and supported me

throughout this journey. They have listened to numerous practice presentations, helped me study, and threw a wonderful prelim passing party. They are always there to listen to my successes and failures in research, always encouraging me, helping me remain focused on my goals, yet also providing timely distractions when needed.

Finally, I want to thank my dearest friend in the world, my husband. He has endured the late nights and weekends, the stress of wedding planning during my prelim, cancelled dates, and the science jargon for seven years. He has cooked, cleaned, and cared for our "fur-babies" when I have been too busy to do so, all while pursuing his own education and career. Brian has been the best friend and husband I could have asked for and I could not have completed this project without his support.

Abstract

Active human Plasminogen Activator Inhibitor 1 (PAI-1) is most often found in complex with Vitronectin (VN), an ~62kDa glycoprotein. Research has shown PAI-1 and VN form higher order complexes in tissues, and our work indicates a 2:1 (PAI-1:VN) stoichiometry for these complexes. A logical model for PAI-1:VN interaction proposes that two PAI-1 molecules bind VN at separate sites. However, our small-angle neutron scattering (SANS) data suggest that there is a PAI-1: PAI-1:VN interaction, in which PAI-1 forms a dimer when in complex with VN. We tested this novel arrangement of PAI-1 within the complex by using a variety of biophysical methods. Through the use of VN binding deficient PAI-1 variants we were able to detect binding deficient PAI-1 in PAI-1:VN complexes, thus supporting the existence of a PAI-1:PAI-1:VN interaction. In addition to studying the PAI-1:VN complex assembly and macromolecular arrangement, we probed the disordered domain of VN in order to identify the effect of PAI-1 binding on the disordered nature of the domain. Additionally, we sought to examine the postulated binding site for PAI-1 in this domain. It is known that a class of proteins containing intrinsically disordered domains (IDDs) frequently undergoes a conformational change upon ligand binding. We present evidence that the disordered domain of VN can be classified as an IDD based on sequence composition and SANS data that demonstrate the IDD undergoes a disorder to order transition upon PAI-1 binding. Additionally, our SANS data support a model in which the IDD of VN interacts with the secondary binding site for VN on PAI-1. Overall, this work has greatly advanced the field, and has opened new paths of study for future research efforts in the Peterson lab.

Table of Contents

List of Tables

List of Figures

List of Abbreviations

14-1B	Stable PAI-1 Variant (contains four mutations)
AUC	Analytical Ultra Centrifucation
CD	Circular Dichroism
cvSANS	Contrast Variation Small Angle Neutron Scattering
ECM	Extra Cellular Matrix
ELISA	Enzyme-Linked Immunosorbent Assay
EOM	Ensemble Optimization Method
EG	Ethylene Glycol
FRET	Fluorescence Resonance Energy Transfer
HFIR	High Flux Isotope Reactor
HRP	Horseradish Peroxidase
IDD	Intrinsically Disordered Domain
IDP	Intrinsically Disordered Protein
JAK-STAT	Janus Kinase and Signal Transducer and Activator of Transcription proteins
LRP1	Low Density Lipoprotein Receptor Related Protein
MoRF	Molecular Recognition Feature
ORNL	Oak Ridge National Laboratory
PA	Plasminogen Activator
PAI-1	Plasminogen Activator Inhibitor – 1
PEG	Polyethylene Glycol

RCL	Reactive Center Loop
Rg	Radius of Gyration
ROCK1	Rho-associated, coil-coil –containing protein kinase 1
RU	Response Units
SANS	Small Angle Neutron Scattering
SAXS	Small Angle X-ray Scattering
Serpin	Serine Protease Inhibitor
SMB	Somatomedin B
SNS	Spallation Neutron Source
SPR	Surface Plasmon Resonance
tPA	Tissue type Plasminogen Activator
uPA	Urokinase type Plasminogen Activator
uPAR	Urokinase Receptor
VN	Vitronectin

Chapter 1 - A tale of two proteins: PAI-1 and Vitronectin

1.1 Introduction to Plasminogen Activator Inhibitor - 1

1.1.a An Overview of Plasminogen Activator Inhibitor - 1

Plasminogen Activator Inhibitor 1 (PAI-1) is found throughout the human body, both in circulation, and in the extracellular matrix (ECM). PAI-1 is expressed in the liver, adipose tissue, smooth muscle cells, and platelets. Tumor cells and other inflammation activated cells have also been shown to secrete PAI-1 [1, 2]. PAI-1 plays a role in a wide variety of physiological processes due to its involvement in fibrinolysis, ECM remodeling, and cell migration (figure 1.1) through inhibitory and non-inhibitory processes [3-5].

As the name implies, PAI-1 is involved in the delicate regulation of plasminogen activation. Plasminogen, the zymogen form of plasmin, is a ubiquitous protein expressed in all major tissues and organs. Plasminogen binding to cell surface receptors and fibrin renders it more readily activated through a cleavage mechanism [6]. Plasmin is a multifunctional, highly efficient protease that, if left unchecked, could lead to a hemorrhagic state within minutes due to its role in fibrin degradation. Plasminogen, and the active form plasmin, are both regulated at several levels in order to maintain a ready supply of the protein, and preserve the hemostatic integrity of the systems in which it is involved [7]. Plasminogen plays a key role in fibrinolysis, cell adhesion, cell migration, wound healing, clotting, inflammation, ECM degradation, and promotes hormone, and growth factor release [4, 7, 8]. Mice deficient in plasminogen have delayed wound healing, and deficiency in EMC remodeling. Additionally, plasmin also plays

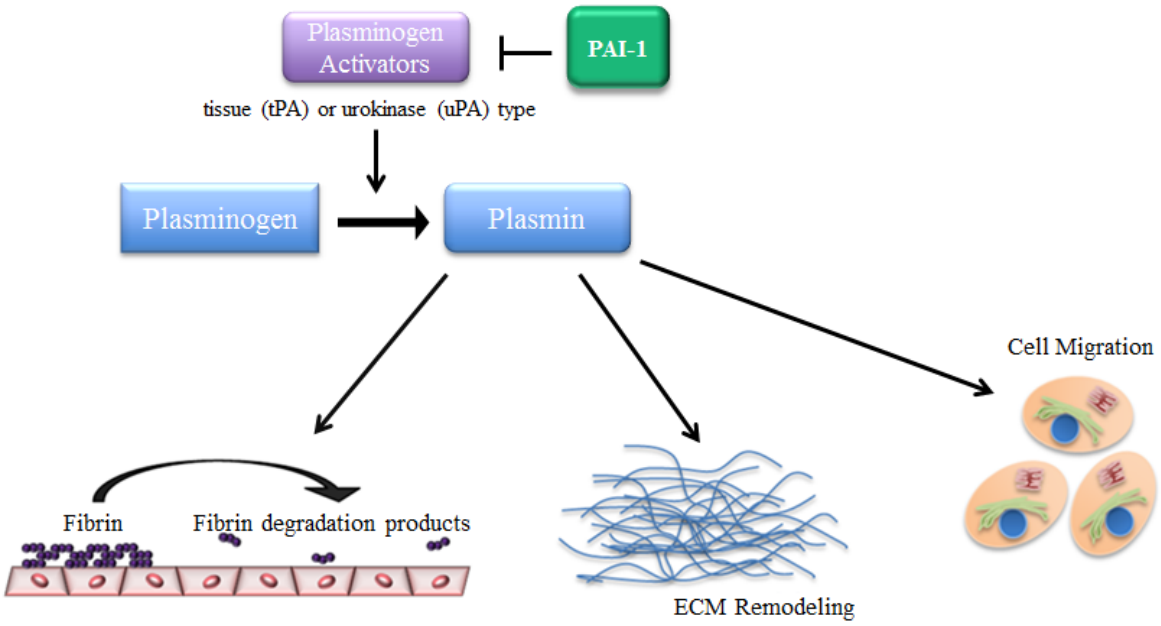

Figure 1.1 Physiological Role of PAI-1

PAI-1 inhibits plasminogen activators and through them the activation of plasminogen to plasmin. Through this inhibition, PAI-1 plays a role in fibrinolysis, ECM remodeling and cell-migration.

role in cancer progression, in which elevated levels typically result in a poor prognosis due to increased ECM remodeling [6, 9].

PAI-1 acts to limit the generation of plasmin by inhibiting tissue type and urokinase type plasminogen activators (known as tPA and uPA respectively) [10, 11]. This cleavage is consistent with the standard mechanism of serine proteases, a protein family to which tPA, uPA, and plasmin belong, and involves the recognition and binding of the protease to a specific peptide sequence, then cleavage through the formation of tetrahedral and acyl intermediates [12, 13]. Through this mechanism, tPA and uPA are able to generate the active protease, plasmin. PAI-1 inhibits this activation by permanently inactivating tPA and uPA through the classic serine protease inhibitor (serpin) mechanism (figures 1.2 and 1.3) wherein the PA cleaves the reactive center loop of PAI-1, triggering a mechanism that results in the translocation of the PA, and disruption of the PA active site [14, 15].

Through its role in regulating the activation of plasmin, PAI-1 plays a key role in the same processes that plasmin effects. PAI-1 also has non-inhibitory effects on cell migration and adhesion through its interaction with cell receptors and vitronectin (VN). PAI-1 binds to Low density lipoprotein receptor-related protein 1 (LRP1) and is endocytosed, along with the cell surface receptor. This mechanism not only clears PAI-1 from the system, but also leads to cellular migration through endocytosis of cellular receptors, as well as through the activation of the JAK/Stat pathway [16-19]. PAI-1 also has an anti-apoptotic effect through its activation of the PkP/Akt pathways [20].

Imbalances in PAI-1 levels, or alterations to the activity of PAI-1, are frequently associated with disease states. Low levels of PAI-1 are typically tied to mild or moderate

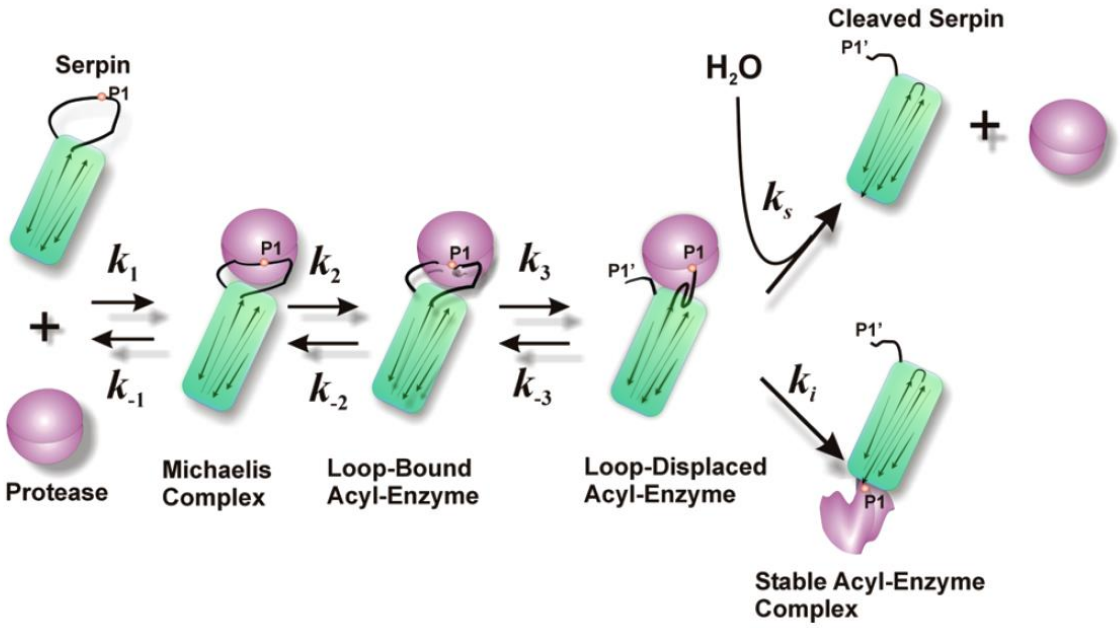

Figure 1.2 Serpin mechanism

Serpins structure includes a reactive center loop (RCL) which contains a region that mimics the consensus sequence of certain proteases. The protease binds to this region, forming a Michaelis complex. Once the protease has bound to the serpin, it forms the acyl intermediate and undergoes the first cleavage reaction, releasing one half of the RCL as the first product. At this point, there are two fates for the protease-serpin complex. In the first, cleavage of the RCL triggers a conformational change in the serpin, leading to the insertion of the RCL into the central β-sheet. This results in an ~70A translocation of the protease, leading to a conformational change in the protease active site that renders it unable to complete the final hydrolysis step that would release it from the serpin. The second fate occurs when the serpin is in a substrate form, and results in the protease completing the final hydrolysis step that allows it to release the RCL and escape in active form. Figure adapted from our work with Blouse *et al* 2009 [21].

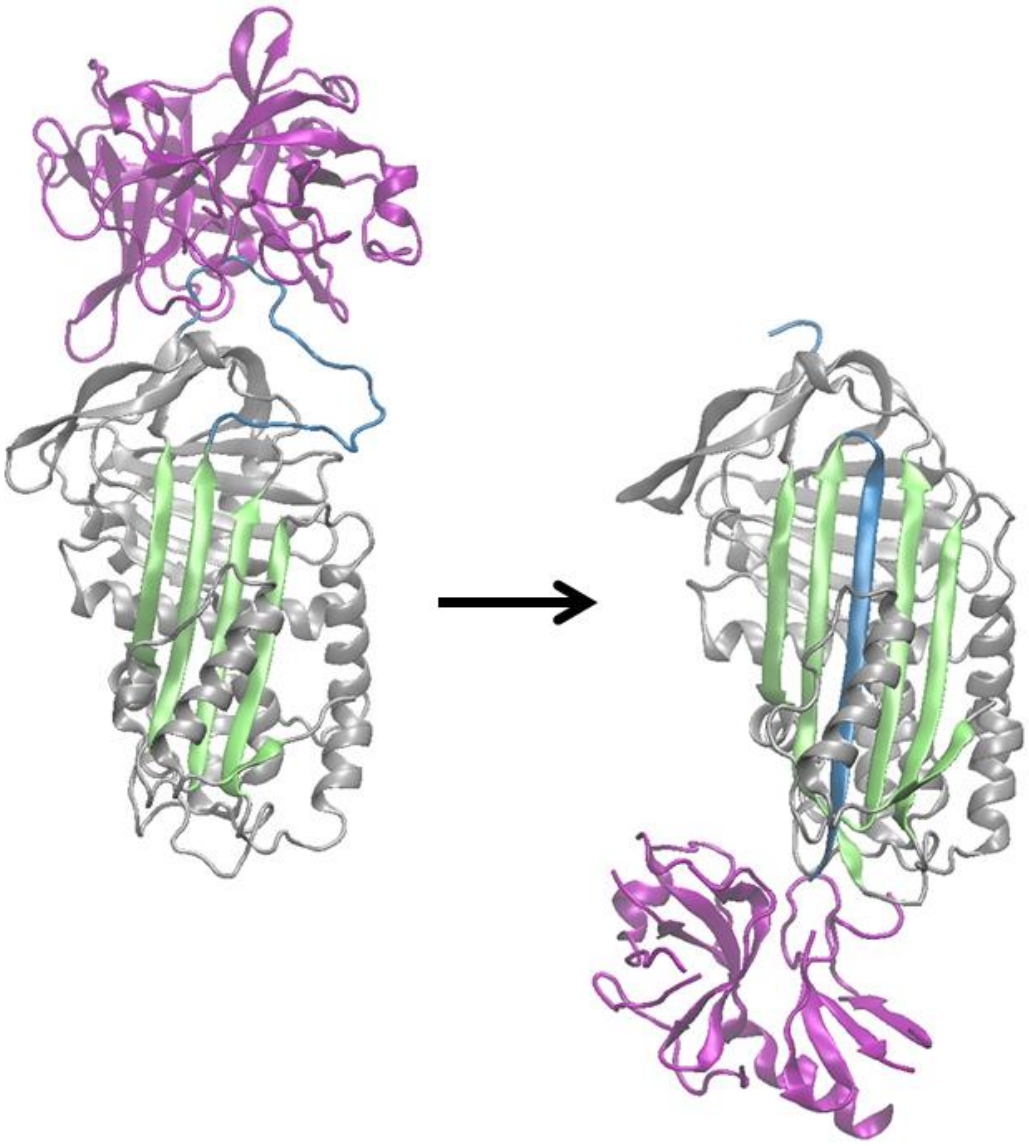

Figure 1.3 Serpin Inhibition of Serine Protease

Serpins utilize the RCL as "bait" to attract target serine proteases. Upon cleavage of the RCL by the serine protease, the RCL inserts into the central β-sheet, causing the serine protease to undergo a 70Å translocation which causes disruption of the proteases active site. This is a suicide inhibitory mechanism, as the proteins are now covalently attached. On the right is the PAI-1:uPA complex – pre cleavage [10]. On the left is the α-1-Antitrypsin:Trypsin complex – post cleavage. [14]

bleeding disorders and frequently go undiagnosed although severe deficiencies can be life threatening [22, 23]. These PAI-1 deficiencies manifest in abnormal bleeding following surgery, heavy menstruation, and are typically a heritable trait [24-26]. However, there is at least one case of acquired PAI-1 deficiency in a patient with cirrhosis of the liver [27].

On the other side of the balance, elevated PAI-1 levels are associated with a variety of pathological symptoms. Imbalances in PAI-1 levels are brought about by a variety of factors and PAI-1 not only serves as a marker for many disease states, but it also exacerbates several pathologies [28, 29]. High levels of PAI-1 are tied to disease states in cancer, skin fibrosis, insulin resistance syndrome, cardiovascular disease, multiple sclerosis, Alzheimer's, hypertension, and fibrosis [16, 30-36]. Additionally, elevated levels of PAI-1 are tied to genetic factors, as well as weight, diet, and other environmental factors [37-40]. Some studies have published conflicting data regarding the role of PAI-1 in disease states, however, when these studies are compared, it is found that the discrepancies are due to variances in experimental conditions, and the alternate roles of PAI-1 in different tissues [6, 18, 41, 42]. This is important to note as it demonstrates that PAI-1 adopts different roles based on its environment and interaction partners.

Because of the myriad of disease states PAI-1 is involved in, particularly cancer, it has become a promising subject for study as science seeks to understand the physiological role that PAI-1 plays, so that it can be utilized as a therapeutic agent [23, 29, 42-49]. Many approaches have been taken to modulate PAI-1 function with synthetic inhibitors [45, 50]. One method is to target the flexible joint region of PAI-1 in order to render it unable to inhibit plasminogen activation, either through speeding the latency transition, or converting PAI-1 to the substrate form [51-53]. Other groups have sought to alleviate elevated PAI-1 prior to the translation phase

[43, 54]. Still other groups have turned to naturally existing substances to find a way to lower elevated PAI-1 [55, 56]. Unfortunately, while many of these inhibitors were effective in vitro, very few function in vivo at levels that would allow them to be adopted for widespread therapeutic use. Successful inhibitors need further refinement to improve on current options with features such as a higher affinity for PAI-1, ability to bind PAI-1 when it is in complex with VN, the ability to bind glycosylated PAI-1, greater solubility, and a longer half-life in vivo [5, 53, 57]. This struggle to identify effective PAI-1 inhibitors highlights the need for further research into PAI-1 and its interaction partner VN as a piece in the puzzle that is therapeutic targeting of PAI-1.

1.1.b PAI-1 and its Role as a Serine Protease Inhibitor.

PAI-1 belongs to the protein superfamily known as serpins (serine protease inhibitors). There are over 3,000 serpins throughout eukarya, bacteria, archaea and certain viruses [58, 59]. The serpin superfamily of proteins acts to regulate thrombolysis and apoptosis, control cell development and survival, maintain homeostasis, and function as part of the host defense system vs pathogens and predators. Due to the many processes that serpins regulate, imbalances in normal levels, high or low, of serpins are frequently linked to disease states. Their primary mode of action is inhibition of serine and cysteine proteases. However, it has also been found that some serpins can act as chaperones, and hormone transporters. [58-63]. Inhibitory serpins serve as protease inhibitors via a highly conserved mechanism (shown in figure 1.2) wherein the reactive center loop (RCL) on the serpin functions as “bait” for the protease, and upon cleavage, inserts into the central β-sheet, disrupting the protease active site in the process [12]. Serpins share a common three-dimensional structure consisting of three beta-sheets, nine alpha-helices, and a

reactive center loop that contains the scissile bond recognized by the target serine proteases [12] (figure 1.4). This RCL is a crucial component of the serpin inhibitory mechanism and as such the length is highly conserved despite variations in amino acid composition [64].

While PAI-1 shares the key structural and mechanistic features of other serpins, there are differences between PAI-1 and the rest of the serpin family. Unlike many other serpins, PAI-1 is highly metastable. Where nearly all serpins remain in the stressed, or active, state until cleaved by a serine protease, PAI-1 will spontaneously convert to the latent, or relaxed, state under physiological conditions and does so more rapidly than other members of the serpin family. [59, 65, 66] (figure 1.4). The latency conversion occurs when the reactive center loop spontaneously inserts into the central beta sheet of PAI-1, without a protease cleavage event, rendering the protein inactive for future inhibitory activity [59, 67]. This difference, likely part of a delicate control mechanism to regulate activity [59, 68], is thought to be due to variations in the protein sequence [69, 70]. Several factors influence the rate of latency transition in PAI-1 including pH, and ligand binding [71, 72].

While the metastable nature of PAI-1 helps regulate the delicate balance of plasminogen activation, the metastable nature of PAI-1 makes study of this serpin difficult. PAI-1 has a half-life of only 60 minutes [66, 73] at 37° C. Because of this, mutations in the PAI-1 sequence have been generated that lengthen the half-life of PAI-1 considerably. The first stable PAI-1 variant, commonly referred to as “14-1B” PAI-1, contains four separate mutations (N150H, K154T, Q319L, and M354I) and was the first active PAI-1 construct to be crystalized [74, 75].

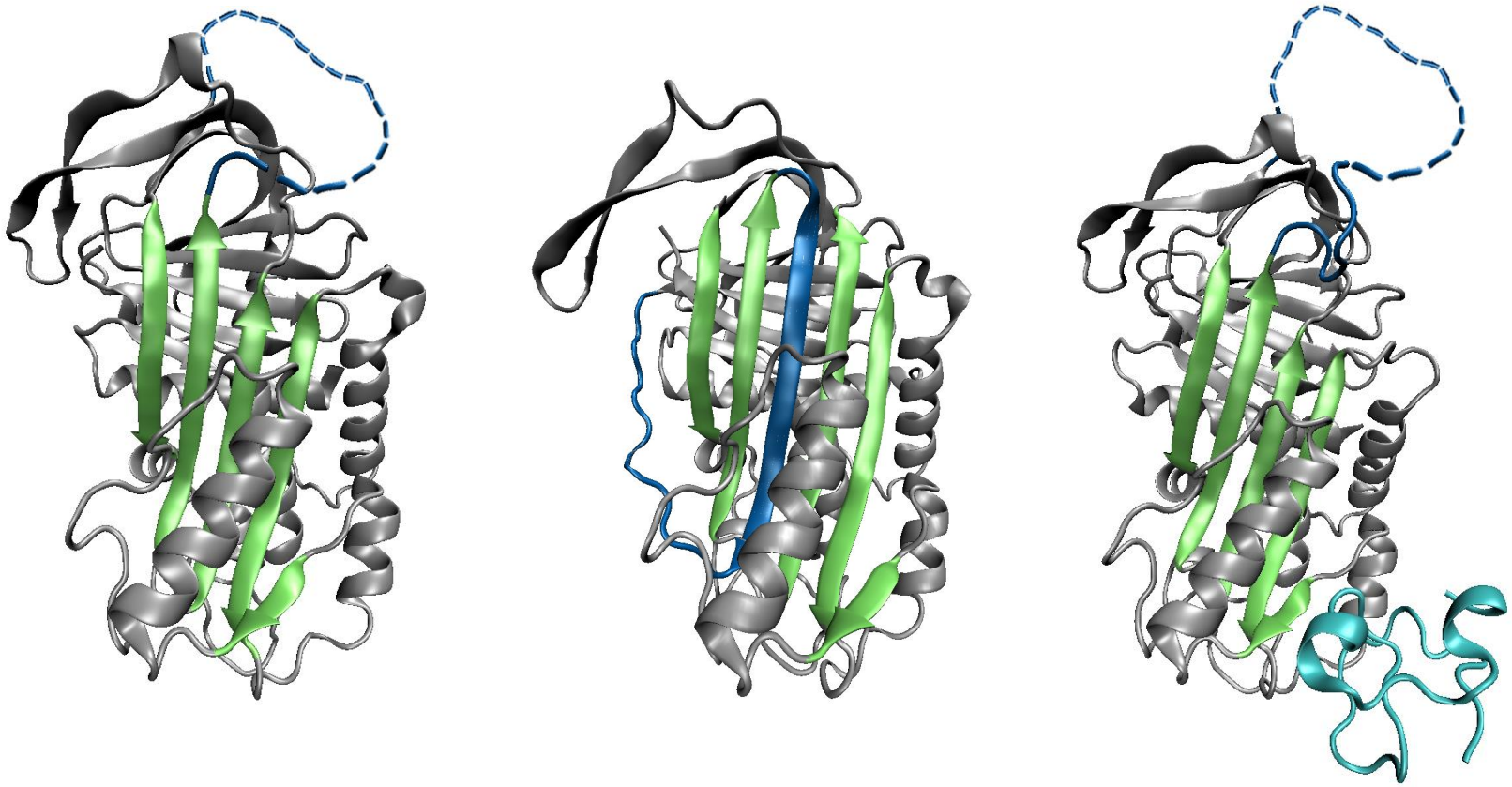

Figure 1.4 Structures of PAI-1

Three PAI-1 structures are displayed above. The central β-sheet is highlighted in green, and the RCL is shown in blue. Because of the inherent flexibility of the RCL in active PAI-1 it is missing from the crystal structures. A dashed blue line is included in active structures to represent the RCL. The leftmost structure is the active form of W175F PAI-1. This active structure is shown, rather than 141B, as the W175F PAI-1 construct is used throughout this work. The center structure is latent Wt PAI-1. In this structure the RCL has inserted into the central β-sheet as strand 4. The rightmost structure is the co-crystal structure of 141B PAI-1 and the SMB domain of VN. The SMB domain is shown in cyan. [76-78]

A second stable PAI-1 variant has also been crystalized more recently, known by its point mutation W175F. This PAI-1 variant slows the latency transition by restricting pre-insertion of the RCL [76, 79]. W175F PAI-1 has been shown to have a similar thermodynamic stability in comparison with wild type PAI-1 (Wt PAI-1) [76, 79], unlike 14-1B PAI-1 which is much more thermodynamically stable than Wt PAI-1. A study using epitope specific PAI-1 antibodies, as well as several PAI-1 variants, has demonstrated that 14-1B PAI-1 contains structural differences compared with Wt PAI-1 that affect interaction with VN, antibodies, and small peptides [80]. These discrepancies have demonstrated that 14-1B PAI-1 is a less than ideal model for studying PAI-1 in a physiologically relevant way. W175F PAI-1, contains a much more conservative mutation, and is considered to be a more appropriate stable PAI-1 variant for physiological relevance. Consequently, this study used W175F PAI-1for all experiments in which a stable PAI-1 variant was needed.

In addition to the metastable nature of PAI-1, there is another distinction between PAI-1 and other serpins. Many serpins form multimers in solution, which lead to the development of a class of pathological states referred to as serpinopathies. Often these multimers are formed through domain swapping when the RCL on one serpin inserts into the central β-sheet of another. This interaction causes disease through formation of polymers and depletion of functional serpins [61, 62]. This "self-interaction" is a feature that PAI-1 does not share when alone in solution, under physiological conditions. PAI-1 does have the ability to polymerize when under low pH and high salt conditions. However, even these PAI-1 polymers differ from other polymerized serpins in that they can dissociate back into functional PAI-1 monomers [81].

1.2 Introduction to Vitronectin

1.2.a An Overview of Vitronectin

Vitronectin (VN) is an abundant glycoprotein found in plants, algae, insects, and vertebrates and fungi. In higher vertebrates it is primarily synthesized in the liver. However, it is a diffusible protein and is consequently found in many bodily fluids and nearly all tissues. Despite this broad distribution of VN, it is primarily found in circulation and the ECM, though it is also stored in platelets [82, 83]. VN has a significant role in cell migration, tissue repair, fibrinolysis, platelet aggregation, and membrane attack complex formation. It also enhances the inflammatory response [82, 84, 85]. Many of the biological functions of VN are dependent on its conformational state, which is in turn dependent on ligand interactions. These binding partners include PAI-1, fibrinogen/fibrin, thrombin, urokinase, plasminogen/plasmin, heparin, intergrins, and other cell surface receptors [82, 86-88]. This multifunctional aspect of VN is in part, due to the multiple VN domains [83].

VN is composed of four domains, the somatomedin B domain (SMB), the intrinsically disordered domain (IDD), the central domain, and the C-terminal domain (figure 1.5). The central and C-terminal domains have been computationally predicted to fold into a β-propeller type structure and β-blade (half a propeller) type structure respectively [83, 89]. The only VN domain with experimentally derived structural data is the SMB domain. The SMB has been crystalized in complex with PAI-1 and the solution structure has also been determined via NMR. The SMB only contains two structural features, a single turn α-helix and a partial 3-10 helix. The rest of the SMB domain is comprised of unstructured loops, linked into a knot via disulfide bonds [90-93]. No full length crystal structure is available for VN. However, a three

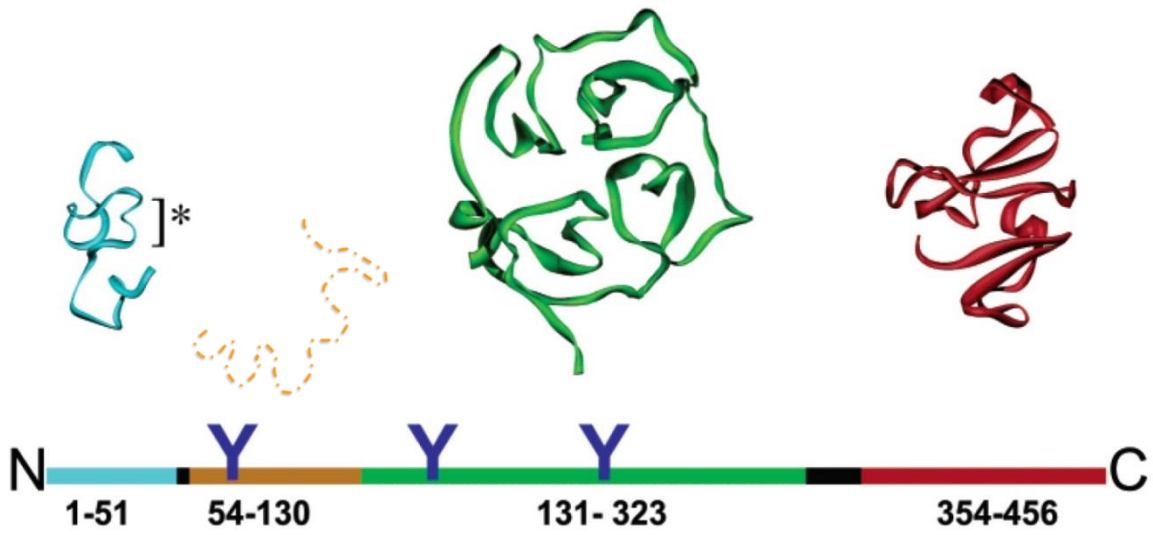

Figure 1.5 Structure of VN domains

Model of the four domains of VN. The somatomedin B domain is shown in blue. This is the only domain of VN to have an experimentally determined structure available [90, 93, 94]. The IDD is shown in orange. The Central and C-terminal domains are shown in red and green respectively. These two domain structures were generated via computational predictions. Figure adapted from our work with Lynn *et al. [95]*

dimensional model has been proposed based on computational modeling of small-angle x-ray scattering (SAXS) data (figure 1.6).

Through interaction with its multitude of partners, VN accumulates at sites of injury and stabilizes platelet-fibrinogen/fibrin bridges, also concentrating PAI-1 at the site of fibrin clots to prevent early lysis. The expression of VN is upregulated under stress conditions as part of the pro-inflammatory response and also serves to facilitate wound healing [87, 96]. VN also interacts with components in the ECM and with cell surface receptors and intergrins to regulate cell migration [97, 98]. It accumulates in the extravascular space and in the interstitial space through interaction with cell surface receptors, playing a role in cell motility and adhesion. This function of VN is important for hemostasis and wound healing, but also is appropriated by cancers and several pathogens [85, 97, 99]. Due to a role in some disease states, VN has also been the target of therapeutic research though not as heavily targeted as PAI-1 [96, 100, 101].

1.2.b The Field of Intrinsically Disordered Domains and How it Applies to VN

Intrinsically disordered proteins (IDPs) and intrinsically disordered domains (IDDs) represent an enigmatic face of protein structure research that, until the last decade, had been largely understudied. For decades, the overarching doctrine was that function required structure [102, 103]. The difficulty of studying IDPs and IDDs certainly contributed to their time in the shadows of biochemistry. However, in the eighties, disordered proteins got a second look. Highly dynamic regions of proteins were assigned function and disorder was characterized as an aspect of protein structure [104]. Now, many significant biological functions are known to directly depend on disorder. IDPs are common across all domains of life, particularly among

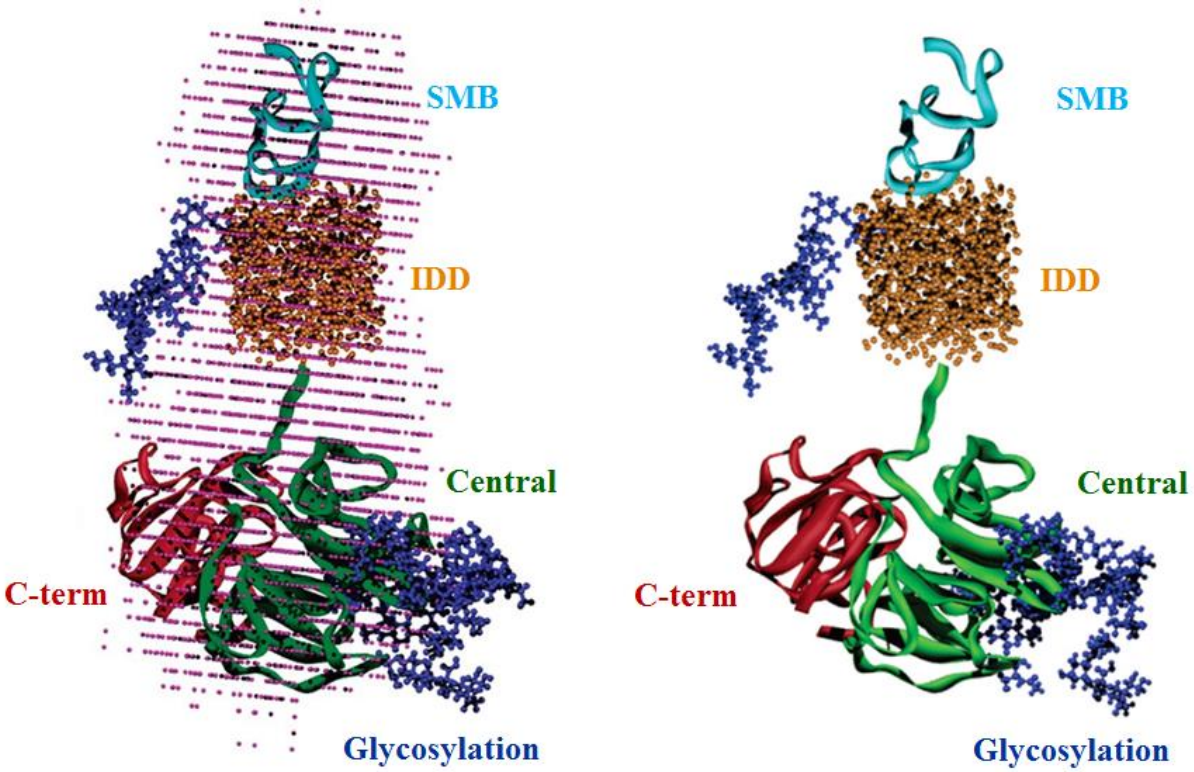

Figure 1.6 Three Dimensional Model of VN Using SAXS

Using small-angle x-ray scattering our group, in collaboration with others, was able to create a spatial envelope for VN in solution. This envelope was then used to orient the four VN in three-dimensional space to generate a model for full-length VN. At the top portion of the SAXS envelope, the SMB domain is fitted. In the neck of the SAXS envelope an orange cylinder is used to represent the disordered VN domain. The central and C-terminal domains are aligned in the bottom of the SAXS envelope. This figure is adapted from Lynn *et al [95]*.

eukaryotes. Disorder is a common feature in proteins involved in neural development, synaptic transmission, and cell cycle regulation [105, 106]. Signaling sequences are commonly located in disordered regions and scaffolding proteins utilize intrinsic disorder to facilitated mechanisms which enhance function [107-111]. Intrinsic Disorder is now acknowledged as a powerful tool to facilitate the complexity of living systems [112].

Disorder defines the ability of some proteins to serve as promiscuous binders. This feature of IDPs is demonstrated by the many proteins in sub-nuclear organelles, many of which are enriched in disorder [113]. RNA binding proteins and domains are also rich in disorder. The long disordered regions that exist in these proteins establish extended, conserved interfaces that specifically interact with RNA partners via an induced fit mechanism, yet possess multifunctional binding due to their disordered state [114]. IDPs have also been shown to adopt secondary structure when interacting with different binding partners. A notable example of this is found in p53 which can adopt different secondary structural features upon binding to its myriad of partners [115]. This disorder to order transition allows for versatility in binding partners, while still forming specific interactions [110, 116]. Not all disorder to order transitions are beneficial for IDPs however. Nearly 20% of disease causing mutations in IDPs cause disorder to order transitions, drastically affecting the function and role of the IDP [117]. Many more mutations that affect the disorder properties of IDPs have also been shown to cause disease [118].

The newly recognized importance of intrinsic disorder has led to the development of databases and prediction tools to identify disorder and has also resulted in a concerted effort to define what makes an IDP [119-121]. Not all unstructured sections of a protein are considered to be IDDs. In fact, a recent study analyzed a database of proteins/protein domains and found

several traits that are present in IDDs and IDPs when compared to other proteins with minimal (<5%) secondary structure. Notably, IDPs are enriched in glutamate (E), aspartate (D), and glutamine (Q), and simultaneously depleted of glycine (G) and cysteine (C). These findings demonstrate that there is more to IDPs than a simple lack of secondary structure [122]. In comparing the second domain of VN to these qualifications, we note that nearly 30% of the second domain of VN is composed of aspartate, glutamate, and glutamine. Additionally, the disordered domain of VN has a number of negative charge repulsive interactions within four residues, as opposed to positive charge repulsions, which is another characteristic of IDPs. These findings support the classification of the disordered region in VN as an IDD.

1.3 Interactions between PAI-1 and VN

1.3.a An Overview of PAI-1:VN interactions

VN and PAI-1 are well characterized binding partners. VN is known to localize PAI-1, bringing PAI-1 to sites of function through interactions with proteins such as fibrin [123]. VN binding stabilizes PAI-1, increasing the length of time that PAI-1 is able to function as a protease inhibitor [124]. This stabilization, and other protective effects, is accomplished through restriction of movement in β-sheet A, particularly the movement of strand 5 (s5A) [69, 125, 126]. VN and PAI-1 also serve to expand their respective physiological roles through binding induced conformational changes [21, 127, 128]. For instance, PAI-1, when bound to VN, has expanded protease functions and is able to inhibit thrombin, and also to protect against cardiac fibrosis [129, 130]. Indeed, VN binding has been demonstrated to affect the conformation of the RCL, causing the scissile bond to be more solvent exposed [131]. PAI-1 also serves to expand the function of VN, which remains in a monomeric, non-adhesive state until PAI-1 binding at

both the primary and secondary sites, inducing a permanent conformational change in the glycoprotein [132].

PAI-1 and VN are primarily found in plasma, the ECM, and platelets. Indeed, the largest pool of PAI-1 is stored in platelets, ready for deposition at sites of injury [83, 97]. However, only 5% of the PAI-1 present in platelets is active [133]. VN is also stored in platelets, in the multimeric form, due to PAI-1 interactions. Upon secretion of PAI-1 and VN, the multimeric VN promotes aggregation of the platelets while active PAI-1 prevents fibrin breakdown and latent PAI-1 promotes wound healing through LRP1 mediated cell migration [16, 83, 124]. PAI-1 and VN also serve to modulate the migratory properties of each other. Notably, the PAI-1:VN complex is non-motogenic, whereas each protein has pro-migratory roles when not in complex with the other. Imbalances in PAI-1:VN levels, and disruption of the complex through PAI-1 activity or latency transition, free both partners to promote cell migration [16, 17, 134, 135].

1.3.b Interactions between PAI-1 and VN. The PAI-1 Perspective

PAI-1 and VN interact at two distinct and separate sites. The first site of interaction to be characterized between these two proteins was between the somatomedin B (SMB) domain of VN and the shutter region of PAI-1 (specifically helices E and F and strand 1 of β-sheet A) [136]. This site has been well characterized, and a co-crystal structure of PAI-1 and the SMB domain was published in 2003 (figure 1.3) [77] . PAI-1 and the SMB domain of VN have a very tight binding affinity (K_d ~1 nM), so much so that all active PAI-1 in circulation is in complex with VN [21, 77]. This tight binding is only applicable to the active form of PAI-1 however. Even though VN, and the SMB domain, are able to stabilize PAI-1, over time a latency transition still

occurs and the affinity for PAI-1 is reduced (K_d ~100nM) , resulting in a dissociation of PAI-1 from the protein complex [77, 137].

The secondary, lower affinity (K_d = 29nM), binding site for VN, on PAI-1, was characterized in 2008 [137, 138]. A series of point mutations in PAI-1 were used to pinpoint the location of the secondary site at which PAI-1 interacts with VN (outside the SMB domain). In order to test this, a VN construct, lacking the SMB domain was used. Schar *et al.* found that an extended region of PAI-1 serves as the binding interface for ΔSMB VN, and that PAI-1 and ΔSMB VN interact with a 1:1 stoichiometry while in circulation [137].

PAI-1 and the VN fragments, that only contain a single PAI-1 binding site, interact in a 1:1 ratio. Additionally, PAI-1 and full-length VN interact in a 1:1 ratio in circulation. However, PAI-1 and VN have been shown to interact with a 2:1 stoichiometry when in the ECM and *in vitro* [132]. This difference in stoichiometry is due in part to PAI-1 concentrations in circulation versus the concentration in the platelets and the ECM where higher PAI-1 concentrations (~200ng/mL) make binding at the secondary, lower affinity, site more likely [21, 128, 139].

The 2:1 stoichiometry for PAI-1:VN interaction was first by Podor *et al* in 2000 using sedimentation equilibrium Analytical Ultracentrifugation (AUC) [140]. The existence of a 2:1 complex was a novel discovery that greatly advanced the field, and clarified controversy that had arisen due to the observation of multiple PAI-1 binding sites on VN. Podor *et al* demonstrated that both PAI-1 binding sites can be occupied simultaneously and that the newly discovered 2:1 complex can go on to form higher order oligomers. In 2005, Minor *et al* expanded upon the observations made by Podor in 2000 by demonstrating that the 2:1 complex serves as an intermediary in the assembly of higher order PAI-1:VN complexes [128]. They noted that the

formation of the 2:1 complex only occurs under higher concentrations of PAI-1 and that sequential binding of PAI-1 results in the formation of the 2:1 complex. This 2:1 complex then acts as a modular unit in assembly of higher order PAI-1:VN oligomers. In 2008, Schar *et* al measured the distance between the two PAI-1 molecules in a 2:1 PAI-1 VN complex using FRET and found that the two PAI-1 molecules are separated by 57Å [138]. The discovery of the 2:1 complex and development of techniques to study the higher order PAI-1:VN interactions greatly advanced the field and laid the ground work for this study.

In 2009, Blouse *et al* measured the distance between PAI-1 molecules using fluorescence measurements and stopped –flow. They discovered that PAI-1 binding to full-length VN is a rapid, biphasic, process. The first phase of binding occurred rapidly, and the second phase occurred more slowly, or at a lower affinity site than the first. Notably, PAI-1 binding to the SMB is a monophasic interaction identical to the first phase of binding for PAI-1 and VN. These data reveal that a single PAI-1 binds to both sites on VN in relatively quick succession. Blouse *et al* also discovered that PAI-1 binding induces a structural change in VN that occurs more rapidly that VN oligomerization, indicating that the conformational change precedes VN oligomerization [21]. Their data, and that of Schar [137], support a model in which the first PAI-1 binds to VN at two separate interfaces and the second PAI-1 is recruited following a conformational change induced when the first PAI-1 binds [21].

1.3.c Interactions between PAI-1 and VN: The VN perspective

The primary site of interaction between PAI-1 and VN occurs in and around the single turn α-helix of the SMB domain. This interaction doubles the half-life of PAI-1 from

approximately 60 minutes to around 120 minutes. Interestingly, while SMB type domains exist throughout biology, only the VN SMB domain is able to bind PAI-1, demonstrating that binding specificity between these proteins is linked to a specific sequence, in addition to tertiary structure [141]. A secondary binding site for PAI-1 exists within VN, outside of the SMB domain. This site is still uncharacterized; however, two regions have been proposed to house the second PAI-1 binding domain. One site is at the C-terminal end of the IDD, discovered using bacterial protease V8 to digest VN. The other proposed site is in the heparin binding region of the central domain, isolated through CNBr cleavage [142-144].

While VN has many interaction partners, including cell surface receptors, PAI-1 is a key partner of VN in both the ECM and in circulation and has a significant effect on the biological functions of VN, and competes with other binding partners of VN [97, 145, 146]. The concentration of VN in plasma is significantly higher than that of PAI-1 (3-6μM VN compared to <1.5nM PAI-1) [1, 5, 124]. When in circulation, all active PAI-1 is bound to VN in a 1:1 stoichiometry. This is not surprising as the K_d for PAI-1 interacting with the SMB domain is ~1nM, and the K_d for PAI-1 interactions with the second PAI-1 binding domain is ~30nM. In the ECM and platelets, PAI-1 is found at higher concentrations and PAI-1 and VN are usually found in higher order oligomeric complexes with a 2:1 stoichiometry of PAI-1 to VN. This oligomerization is brought about by a permanent conformational change in VN that occurs upon interaction with PAI-1. Indeed, once PAI-1 becomes latent and dissociates with VN, the VN molecules remain in an oligomeric adhesive state. In this way, PAI-1 and VN serve as a molecular switch, wherein their interaction and subsequent dissociation sends each protein on to a new biological role [127, 132].

1.4 Preliminary Data from Peterson Lab

1.4.a Small Angle Neutron Scattering Data

A few years ago, in order to gain better insight in the interaction between PAI-1 and VN, our lab performed contrast variation, small angle neutron scattering experiments (cvSANS). The power of SANS comes from the scattering properties of neutrons as they refract off of different elements. In particular, neutrons experience a negative scatter when hitting hydrogen, and a positive scatter when hitting deuterium. This difference in scattering means that the signal from a deuterated protein will be distinct from that of a hydrogenated protein (figure 1.7) allowing for the identification of scattering signal from individual proteins within a complex.

Taking advantage of this scattering property of neutrons, we mixed deuterated W175F PAI-1, and protonated VN and measured neutron scattering. W175F PAI-1 was used for these experiments for two key reasons. First, W175F PAI-1 has a significantly longer half-life (>7hours) [137], which allowed the PAI-1:VN complex to remain stable over the time course of the SANS experiments. Second, W175F PAI-1 has been observed to have reduced higher order complex formation beyond 4:2 complexes, and the concentration of PAI-1 and VN in 4:2 complexes would simplify data analysis. Next, the D_2O composition of the buffer was varied in order to feature different components of the complex by exploiting the change in scattering that occurs when deuterium is present (figures 1.8 and 1.9). By collecting data at multiple buffer D_2O percentages, we were able to fade components of the complex from the scattering data, and use the data gathered to build a low resolution model of the complex in solution.

Analysis of the cvSANS data for the PAI-1:VN complex revealed that PAI-1 and VN interact in with a 2:1 stoichiometry and formed a 4:2 complex. This intermediate oligomerization state is in agreement with previously published [140]. However, the 4:2 complex we observed does not

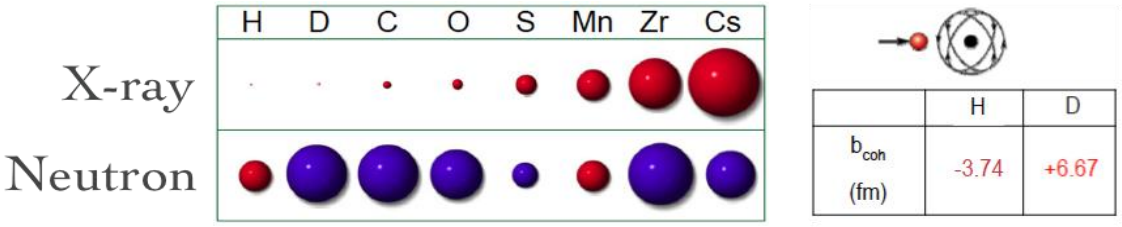

Figure 1.7 Small Angle Neutron Scattering Differentiates between atoms

Neutrons exhibit different scattering properties upon interaction with hydrogen and deuterium. This property makes neutron scattering a valuable tool for studying protein complexes using deuterium labeled protein.

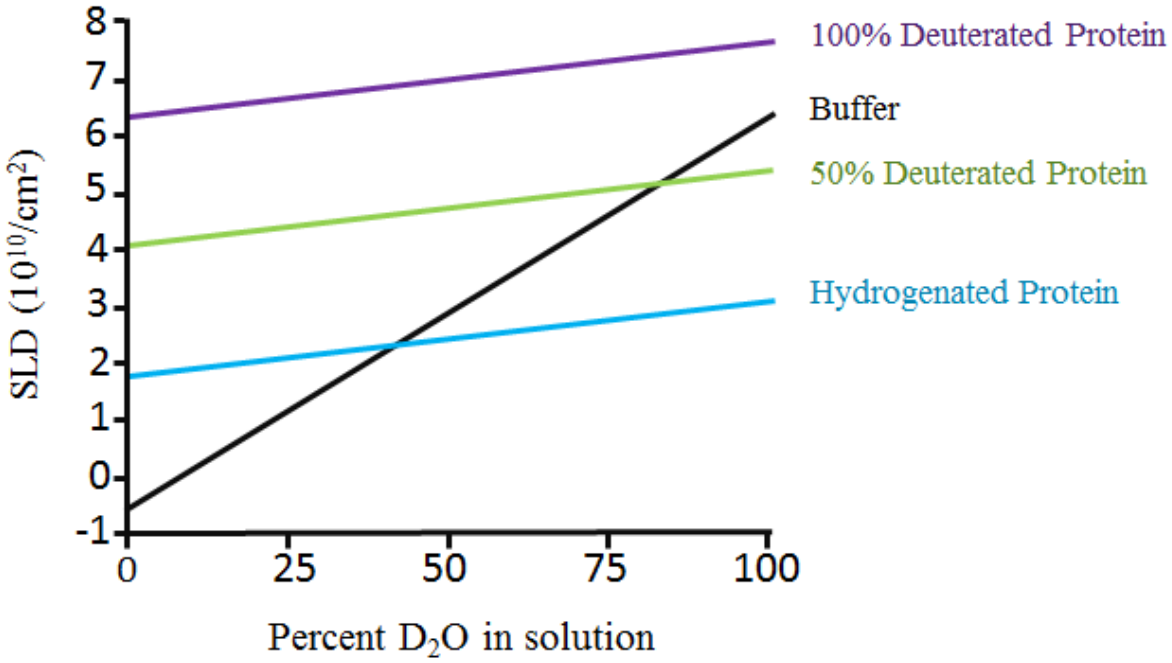

Figure 1.8 Graph of Neutron Scattering Properties

The scattering length density (SLD) of neutrons changes in relation to the molecule of interest as well as the D_2O percentage found in the buffer. This allows for differentiation between elements of a multicomponent complex.

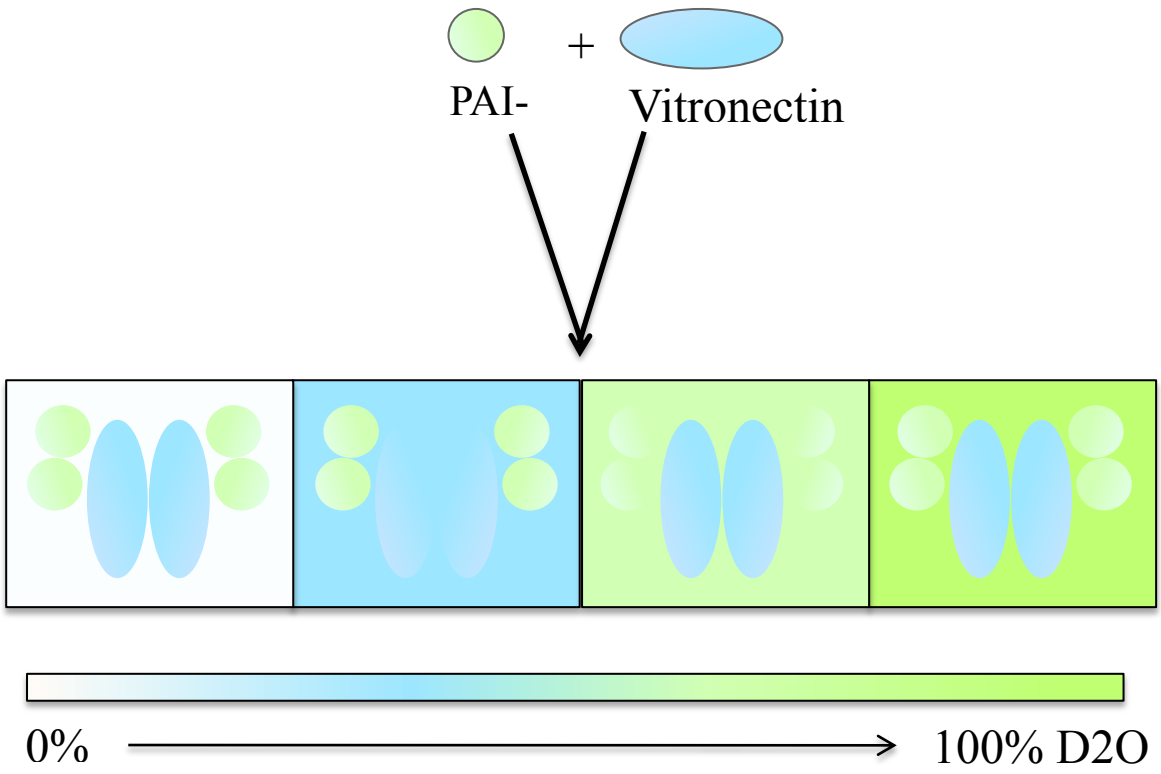

Figure 1.9 Contrast Variation Small Angle Neutron Scattering Scheme for PAI-1:VN

Contrast variation SANS involves collecting data on the sample of interest in buffer with varied D_2O compositions. Deuterated PAI-1 was mixed with protonated VN and the buffer composition was varied in order to change the signal contribution from each of the complex components. Neither of the complex components are completely matched out in any buffer condition with this method, but the buffer variation allows on component of the complex to dominate the signal.

agree with the current accepted model wherein PAI-1 interacts at two separate sites on the VN molecule [128]. In all of our models, we show PAI-1, interacting with another PAI-1, which interacts with VN. This 2:1 stoichiometric unit interacts with another identical unit via VN in a 'V' shaped pattern (figure 1.10) [147]. These data break through several barriers currently found in the literature. Not only is it the first experimentally determined structure of the PAI-1:VN complex, it also provides insight into the mechanism by which PAI-1 may polymerize following conformational changes induced upon interaction with VN at the both the primary and secondary sites.

1.5 Research Goals

1.5.a New Model for PAI-1:VN interactions

While our preliminary data are novel, they are not without support in the current literature. The two PAI-1 molecules in the 2:1 PAI-1 VN stoichiometric ratio, have been shown to be close in proximity when bound to VN [21]. Also, in the literature, it has been demonstrated that only binding at the primary site of interaction between PAI-1 and VN has a stabilizing effect on the PAI-1 molecule. Binding at the secondary site alone does not stabilize PAI-1 [137]. This difference in the two binding sites for PAI-1 has raised questions about the role that the secondary PAI-1 binding site plays. If the two binding sites actually form an extended interaction with a single PAI-1 molecule, the lack of stabilization from the second binding site is not concerning. Finally, the ability of PAI-1 to form functional polymers has been demonstrated, however a conformational change must occur in order for this polymerization to take place [81]. The model suggested by our SANS data provides potential answers to each of these concerns, building and expanding upon present knowledge.

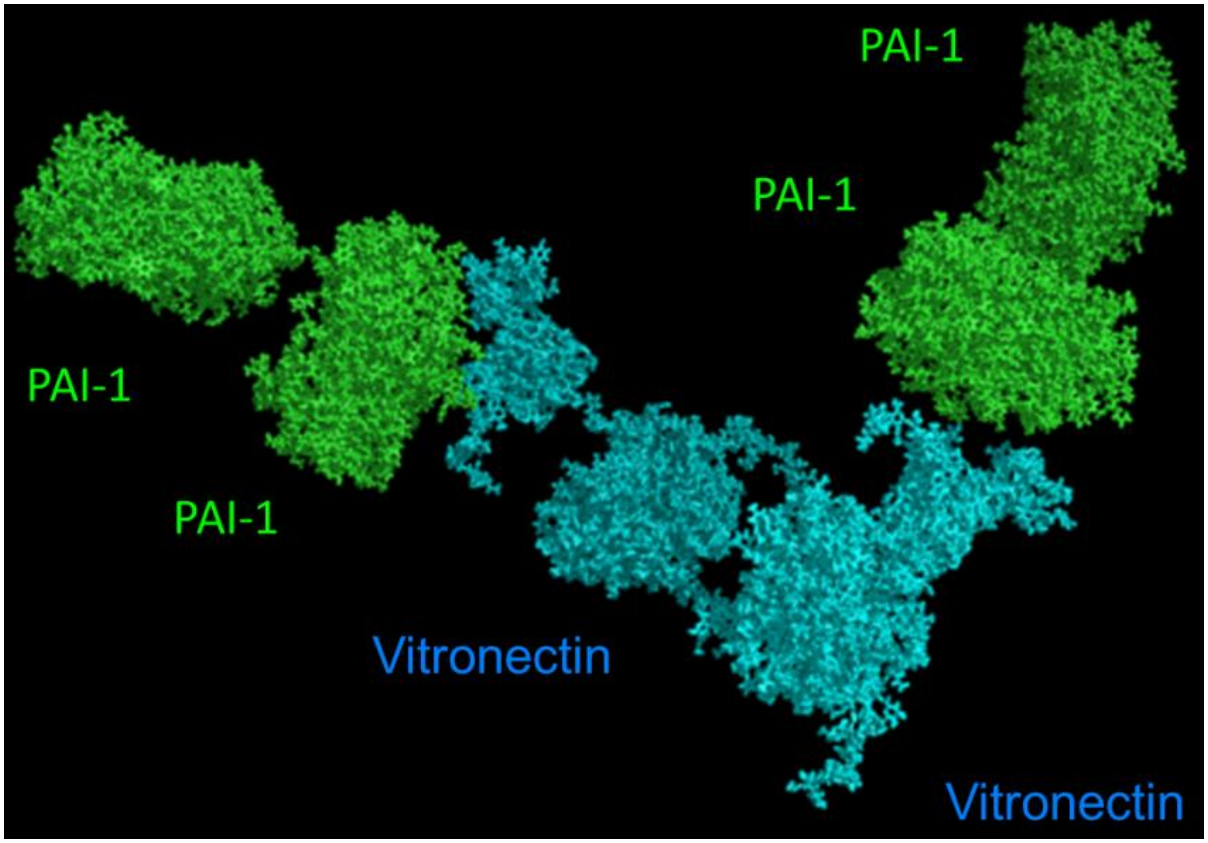

Figure 1.10 SANS Model of the PAI-1:VN complex

Representative model from analysis of the SANS data on PAI-1:VN [147]. Several models were generated and each had small variations. However, all models shared important core features. These data show that the 4:2 PAI-1 and VN complex exists in a "V" shaped pattern. This model also demonstrates that PAI-1 forms a dimer when in complex with VN. Due to the low resolution of this model, no conclusions can be drawn regarding the sites of interaction between the proteins. However, it is reasonable to suggest that the region of VN interacting with the PAI-1 molecule contains the SMB domain. Additionally, the region of VN that is interacting with the second VN molecule likely contains the central and C-terminal domains. This latter conclusion comes from the organization of domains shown in figure 1.6 and the understanding that the C-terminal domain of VN plays a role in multimerization [148].

This current work aimed to further test the model that has been revealed by the SANS data for the PAI-1:VN complex. The hypothesis that drove this work is that PAI-1 interacts with another PAI-1 when in complex with VN (figure 1.11). In order to probe this hypothesis, we generated a VN binding deficient PAI-1 which was then labeled in order to provide a means of studying its incorporation into a PAI-1:VN complex. We then performed experiments to determine if the addition of VN binding PAI-1 was able to rescue the incorporation of binding deficient PAI-1 into the PAI-1:VN complex.

1.5.b Elucidating the role of the IDD in PAI-1:VN interactions

This work also sought to better understand the role of the IDD of VN in PAI-1:VN interactions. While the secondary binding site of PAI-1 has not been identified, one potential site of interaction is found in the IDD. This, along with a desire to further understand the role that IDD of VN plays in the PAI-1 VN interaction prompted this branch of the project. We used SANS, and other techniques, to study the effect of PAI-1 binding on the IDD. The hypotheses that drove this work were that PAI-1 binding affects the structure of the IDD, causing the IDD to become more compacted, possibly through the adoption of secondary structural elements and that the IDD contains the secondary binding site for PAI-1 on VN.

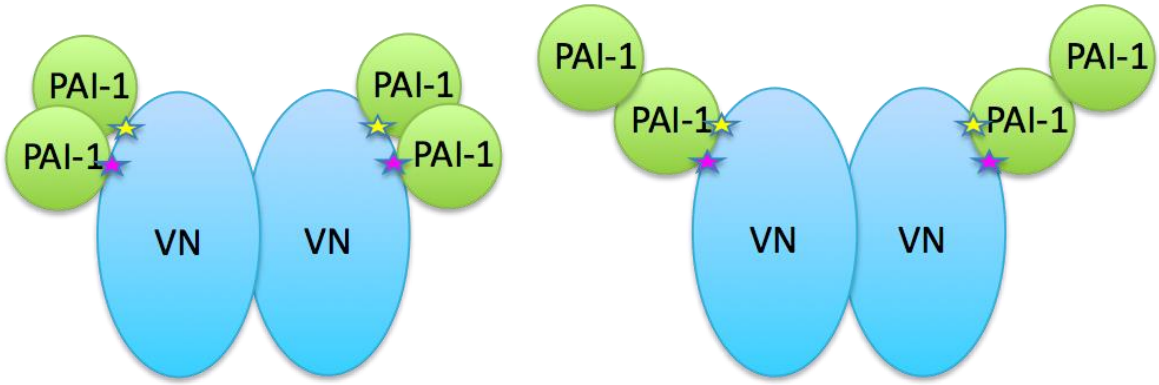

Figure 1.11 Proposed Model of PAI-1:VN Interactions

On the left is shown the current model for PAI-1:VN interactions. On the right is the model that our SANS data supports. This work seeks to test the existence of the model on the right though PAI-1:VN binding studies.

Chapter 2 - Materials and Methods

2.1 Materials

PAI-1 cloned into the pET 24d expression vector was obtained from Dr. Grant Blouse (Henry Ford Health Sciences Center, Detroit, MI) as a gift. Rabbit anti-PAI-1 polyclonal antibody, and mouse anti-VN "1E9" monoclonal antibody were purchased from Molecular innovations Inc, Southfield, MI. Secondary, peroxidase labeled anti-mouse and anti-rabbit, antibodies were purchased from Vector Labs, Burlingame, CA. Rosetta 2(DE3)pLysS cells were purchased from EMD Millipore Corp, Billerica, MA. The QuikChange II XL and QuikChange Lightning Multi-Site kits used for mutagenesis were purchased from Agilent Technologies, Santa Clara, CA. Primers for the PCR mutagenesis reactions were purchased from Invitrogen™ Custom DNA Oligos. DH5α cells were purchased from Thermo Scientific, Rockford, IL, and Rosetta 2(DE3)pLysS and Rosetta gami 2(DE3)pLysS cells were purchased from EMD Millipore Corp, Billerica, MA. Wizard® Plus SV Minipreps DNA purification system was purchased from Promega, Madison, WI. Protease inhibitor cocktail P8465 was purchased from Sigma Aldrich Corp., St. Louis, MO. Freshly frozen human plasma was purchased from Red Cross and Tennessee Blood Services. PD-10 columns were purchased from GE Healthcare, Piscataway, NJ. NHS activated Sepharose Fast Flow, DEAE Sephacel, blue Sepharose Fast Flow, heparin Sepharose, SP Sepharose Fast Flow, chelating Sepharose Fast Flow, high-resolution Sephacryl S100, and S200 resins were purchased from GE Healthcare, Piscataway, NJ. Invitrogen™ IANBD amide was purchased from Fisher Scientific, Pittsburg, PA. Biotin EX link Iodoacetyl-LC-Biotin was purchased from Thermo Scientific, Rockford, IL. Spectrozyme® tPA was purchased from American Diagnostica Inc, Stamford, CT. HPLC column, BioSep-

SEC-S2000 was purchased from Phenomenex, Torrance, CA. CM5 SPR chip, HBS EP Buffer, and Acetate 5.0 buffer were all purchased from GE Healthcare, Piscataway, NJ. Spectra/Por® Dialysis membranes were purchased from Spectrum Laboratories, Inc., Rancho Dominguez, CA. Slide-A-Lyzer® Dialysis Cassettes were purchased from Thermo Scientific, Rockford, IL. Nitrocellulose Membranes, 0.45µm were purchased from BioRad Laboratories, Hercules, CA. 96-well, polystyrene, maxisorp C8 lockwell plates, and TMB substrate kit were purchased from Thermo Scientific, Rockford, IL. Deuterated osmolytes were purchased from Cambridge Isotope Lab, Tewksbury, MA, and hydrogenated osmolytes were purchased from Sigma-Aldrich Corp., St. Louis, MO. All chemicals used, but not explicitly mentioned above were purchased from Fisher Scientific, Pittsburg, PA.

2.2 Methods

2.2.a Mutagenesis

In order to mutate the PAI-1 sequence to generate the amino acid substitutions shown in table 2.1, PCR mutagenesis was carried out on the PAI-1 cDNA cloned into the pet24d vector. The primers used for these reactions are shown in table 2.2. The protocol for the QuikChange kits was followed to generate 50uL reactions. The PCR conditions are shown in figure 2.1.

2.2.b DPN1

PCR product DNA was digested using DPN1 provided with the QuikChange kit. 25µL of PCR product was transferred to a new .2mL thin walled tube and .5µL DPN1 was added to the

Table 2.1 PAI-1 Variant Constructs

Table of PAI-1 variants constructed for use in this study.

PAI-1 Constructs
Wt
S338C
W175F
Q123K
Q123K, S338C
Q123K, W175F
Q123K, W175F, S338C
Q123K, R115E, R118E
Q123K, R115E, R118E, S338C
Q123K, R115E, R118E, W175F
Q123K, R115E, R118E, W175F, S338C
R101A, M110A, Q123A
R101A, M110A, Q123A, S338C
R101A, M110A, Q123A, W175F
R101A, M110A, Q123A, W175F, S338C

Table 2.2 PAI-1 Mutagenic Primer Sequences

Sequence of primers used in site directed mutagenesis.

Primer Name	Primer Sequence
R101A forward (5’ → 3’)	CGTCCAGGCGGATTTGAAGCTG
R101A reverse (3’ → 5’)	CAAACCCGCCTGGACGAAGATCG
M110A forward (5’ → 3’)	GGCTTCGCCCCACTTC
M110A reverse (3’ → 5’)	GTGGGGCGCGAAGCCCTGGACC
Q123K forward (5’ → 3’)	CGGAGCACGGTCAAGAAAGTGGACTTTTCAGAG
Q123K reverse (3’ → 5’)	CTCTGAAAAGTCCACTTTCTTGACCGTGCTCCG
Q123A forward (5’ → 3’)	GGTCAAGGCAGTGGACTTTCAG
Q123A reverse (3’ → 5’)	GTCCACTGCCTTGACCGTGCTCCGG
W175F forward (5’ → 3’)	CTACTTCAACGGCCAGTTTAAGACTCCCTTCCCCG
W175F reverse (3’ → 5’)	GATGAAGTTGCCGGTCAAATTCTGAGGGAAGGGGC
S338C forward (5’ → 3’)	GTGGCCTCCTCATGCACAGCTGTCATAGTC
S338C Q123A reverse (3’ → 5’)	CACCGGAGGAGTACGTGTCGACAGTATCAG
PAI-1 middle sequencing primer forward (5’ → 3’)	CTTGGGAAAGGAGCCGTGGA
PAI-1 middle sequencing primer reverse (3’ → 5’)	AAGTAGAGGGCATTCACCA

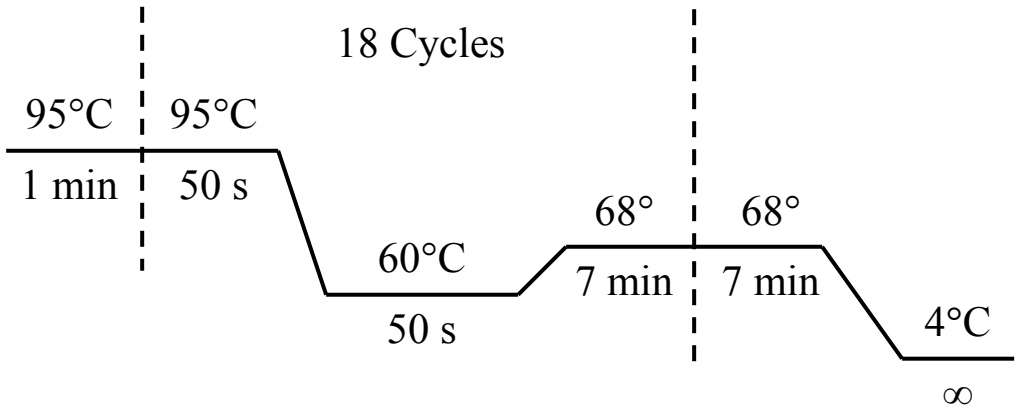

Figure 2.1 PCR Cycle Parameters

Cycle parameters used for site directed mutagenesis.

PCR product. This mixture was incubated at 37°C for 1hr and then stored at 4°C until further use.

2.2.c Transformation

DPN1 digested PCR product was transformed into DH5α following standard transformation protocols. 5µL of DNA was added to 20-50uL of DH5α cells. The cells were then incubated on ice for 15-30 minutes. Cells were then incubated in a 42°C water bath for 30s, followed by an immediate incubation on ice for 2min. 300µL of SOC media was then added to the cells, and the cells were agitated at ~200rpm at 37°C for at least one hour. Cells were then streaked on an LB agar + Kanamycin (50µg/mL) plate and incubated at 37°C over-night.

2.2.d DNA Purification

Single colonies were selected from a plate and used to inoculate a 5-10mL culture of LB + Kanamycin (50µg/mL). Cultures were incubated overnight (15-18 hours) at 37°C shaking at ~200rpm. Cells were then spun down at 14,000xg for eight minutes and the supernatant was discarded. Pellets were then either frozen at -20°C or immediately moved to the next step.

DNA was harvested from cell pellets according to the Wizard SV mini prep kit protocol with minor modifications. Cell pellets were resuspended with 250µL resuspension buffer, then 10µL alkaline protease and 250µL lysis buffer were added. Mixture was inverted then allowed to incubate at room temperature for five minutes. Neutralization solution was added, and the sample was spun in 2mL microfuge tubes at 14,000xg for 10 minutes. The supernatant was then added to the spin columns and spun for 2 min. Following the binding of DNA to the spin column, the columns were washed with 750µL of the wash solution twice, followed by 250µL, and then a two minute dry spin to ensure that all ethanol was removed. 60µL of H_2O was then

added and allowed to incubate for 10 minutes prior to a final spin in order to elute the DNA. Purified plasmid concentrations were determined using a fluorimeter.

2.2.e Sequencing

DNA samples were submitted to the UTK core sequencing facility for sequence confirmation. T7 forward primer and a PAI-1 reverse primer were used to ensure full sequence coverage.

2.2.f Transformation into expression cell lines

Sequence confirmed DNA containing mutations in the PAI-1 sequence was transformed into the Rosetta 2(DE3)pLysS cell line following standard transformation protocol as described above. Cells were plated on LB agar + Kanamycin (50µg/mL) + Chloramphenicol (34µg/mL) and incubated overnight at 37°C.

2.2.g Small Scale Induction Screens

Single colonies (3-4) were selected from the plate and cultured in TB + Kanamycin (50µg/mL) + Chloramphenicol (34µg/mL). These cultures were grown to an OD_{600} of ~1 at 37°C shaking at ~200rpm. Cultures were then transferred to 15°C, shaking at 220, and induced with 1µM IPTG overnight (15-18 hours). Prior to induction a sample of un-induced cells was taken, part was spun down, and the cell pellet frozen at -20°C. The other sample portion was mixed with glycerol and frozen at -80°C.

The next day a sample of the induced cells was taken, spun down and the supernatant discarded. Un-induced and induced cells were resuspended in H_2O and concentrations were normalized according to OD_{600}. Samples were taken and boiled with reducing dye for three minutes. Samples were then loaded on a 10% polyacrylamide gel with a protein ladder for standard comparison. The gel was then run at a constant 120-150V, with SDS PAGE running buffer, for ~60 minutes.

The gel was then partially transferred onto nitrocellulose, using a semidry blot transfer system, at 15V for 10 minutes. The gel was then stained with Coomassie Blue buffer while gently shaking. Once gel had been allowed to adequately stain, the dye was poured off and a destain solution was added and allowed to soak the gel while gently shaking until gel was destained.

The western blot was blocked with 10% Non-Fat Milk (NFM) in PBS + .01% Tween 80 for one hour at room temperature while gently shaking. The blot was then washed three times with PBS buffer before being incubated with primary PAI-1 antibody, at a 1:2000 dilution, for one hour at room temperature. The blot was washed again, as before, before being incubated with the anti-Rabbit-HRP conjugated secondary antibody, at a 1:4000 dilution, for one hour at room temperature. Finally, the blot was washed as before, and a mixture of 15mL PBS + 3mL 3mg/mL 4-Chloro-1-Napthol in Methanol + 10µL H_2O_2 was added to the blot and allowed to react with the secondary antibody. Once bands were visible, the blot was washed and imaged using the gel doc system. The western blot and gel were then analyzed to determine which cell stock had optimal PAI-1 expression.

2.2.h Large Scale Expression

Glycerol stocks were used to inoculate 10-15mL TB + Kanamycin (50µg/mL) + Chloramphenicol (34µg/mL) cultures. These cultures were grown overnight at 37°C shaking at ~200rpm. The following morning, these starter cultures were used to inoculate 4L of TB + Kanamycin (50µg/mL) + Chloramphenicol (34µg/mL). The 1L cultures were incubated at 37°C while shaking at 220rpm until the OD_{600} of the cultures was ~1. Cultures were then cooled to 15°C for one hour prior to induction with 1µM IPTG overnight (15-18hours). Un-induced samples were taken for a gel prior to induction and treated as mentioned above. The following morning, cells were pelleted at 15000rpm for 10 minutes. Cell pellets were harvested and stored at -80°C until further use.

2.2.i Purification of PAI-1

PAI-1 constructs were purified following a common protocol, with minor alterations for PAI-1 variants. All buffers used to purify a PAI-1 construct containing the S338C mutation contained 1mM DTT. PAI-1 constructs containing mutations that reduced protein pI were purified in a lysis/SP buffer at pH 5.5 to ensure binding to the SP column. PAI-1 constructs with a pI near that of wild type PAI-1 were purified in the same buffer, at pH 6.5.

Cell pellets were resuspended in lysis buffer (50mM NaH_2PO_4, 1mM EDTA, pH 6.5) with 20mg lysozyme and 1mg protease inhibitor per 100mg cell pellet. The pellet, buffer mixture was stirred at room temperature for approximately one hour, until the pellet was fully dissolved. Resuspended cells were then lysed by sonication (30s pulse, 60s pause, cycled until 15min

runtime achieved). The sonicator was set to pulse level 7, and the resuspended cells were stirring on ice to keep the mixture cool during sonication.

Cell debris was removed by centrifugation at 15000rpm for 30 minutes at 4°C. All further purification steps were carried out at 4°C to maintain PAI-1 activity. The supernatant was loaded on a SP sepharose column (2.5 x 25cm), pre-equilibrated with lysis buffer containing 80mM $(NH_4)_2SO_4$ (designated hereafter as "SP buffer"). Following loading of the lysate, the column was washed with SP buffer. Protein was eluted off the column with a linear gradient of 80mM – 500mM $(NH_4)_2SO_4$ in SP buffer. Total gradient volume was 800mL, with 10mL fraction size for the elutions. Fractions were collected using a Pharmacia-LKB-SuperFrac Fraction collector, and BioRad Econo pumps, and flow adaptors were used to maintain constant flow.

The A_{280} of every other fraction was taken, and SDS PAGE and western blotting were performed to identify the elutions containing PAI-1. These elutions were then pooled and dialyzed, using 14,000 MWCO tubing, into imidazole buffer (50mM NaH_2PO_4, 500mM NaCl, 20mM imidazole, pH 7.0). The following day, the PAI-1 was loaded onto a chelating Sepharose column (2.5 x 10cm), pre-charged with nickel and equilibrated with imidazole buffer. The column was then washed with imidazole buffer. Protein was eluted off the column with a linear gradient of 20mM – 220mM imidazole. Total gradient volume was 400mL, with 10mL fraction size. Fractions were collected in tubes containing 2mL of collection buffer (500 mM K_2HPO_4, 300 mM NaCl, 30 mM EDTA, pH 6.25) The A_{280} of every other fraction was taken, and SDS PAGE and western blotting were performed to identify the elutions containing PAI-1. These elutions were then pooled and concentrated, with a 30kD MWCO, to 2-5mL, and loaded onto a high resolution Sephacryl S-100 column (2.5 x 115cm), pre-equilibrated with S-100

buffer(50mM NaH_2PO_4, 300mM NaCl, 1mM EDTA, pH 6.25). Elution was carried out at .5mL/min with S-100 buffer, fraction size was 3mL. The A_{280} of every other fraction was taken, and SDS PAGE and western blotting were performed to confirm the elutions containing PAI-1. Western transfer was performed on a BioRad Trans-Blot SD Cell Semi-Dry system. Fractions were pooled and concentrated, then frozen at -80°C. PAI-1 concentration was determined by measuring A_{280} and using ε_{280} = .93 $mL*mg^{-1}*cm^{-1}$ and a molecular weight of 43760g/mol (as calculated from the amino acid sequence).

2.2.j NBD and Biotin Labeling

PAI-1 constructs containing the S338C mutation were labeled with Biotin and NBD for detection purposes. Biotin labeling was performed by preparing 1mL of PAI-1 at ~4mg/mL in "reaction buffer" (0.05M Tris-HCl, 5mM EDTA pH 8.0). A PD-10 column was equilibrated with reaction buffer, then the PAI-1 was loaded on the column to de-salt it prior to biotin labeling. Following PAI-1 addition to the column, it was then eluted with 2mL of reaction buffer. All steps were carried out at 4°C under gravity flow. After PAI-1 was de-salted, 100µL of 2mg/mL Biotin (in DMSO) was added to the PAI-1 and the mixture was incubated on ice, in the dark, overnight. The following day, Biotin labeled PAI-1 was dialyzed into PBS pH 7.4 to remove free biotin, then frozen at -80°C until use.

NBD labeling was performed by preparing 1-3mg of protein in 2.5mL of "reaction buffer" (50mM NaH_2PO_4, 300mM NaCl, 1mM EDTA, pH 6.6). A PD-10 column was equilibrated with reaction buffer, after which the PAI-1 was loaded on the column to de-salt it prior to NBD labeling. Following PAI-1 addition to the column, it was then eluted with 3.5mL

of reaction buffer. All steps were carried out at 4°C under gravity flow. The eluted PAI-1 was then concentrated to ~200µL and 20x molar excess of NBD (in DMSO) was added and the mixture was incubated on ice, in the dark, overnight. The following day, free NBD was separated from the labeled protein by passage over a second PD-10 following the same protocol as before. NBD labeled protein was frozen at -80°C until use.

2.2.k Activity Assays (Gel and Plate)

PAI-1 was assayed for activity using two methods. The first method, referred to as a "plate assay," utilized a spectroscopic tPA substrate to measure PAI-1 activity. In this plate assay, Spectrozyme tPA, PAI-1, and tPA were individually diluted in (100 mM Tris, 1% BSA, 1 mM EDTA, pH 7.4 @ 37°C). Once stock concentrations were generated, PAI-1 and tPA were mixed at various ratios. The PAI-1:tPA mix was then incubated at room temperature for 30 minutes in microfuge tubes. Following incubation, the PAI-1:tPA mixture was added to a 96 well plate and mixed with the Spec tPA substrate. The plate was immediately placed in a plate reader and data were collected over the course of 20 minutes. The data were then analyzed to determine the ratio of PAI-1:tPA at which PAI-1 is able to effectively inhibit the ability of tPA to cleave the substrate. A ratio of 1:1, or 1:1.25 is considered to be an appropriate activity level.

The second method by which the activity of PAI-1 was measured was a "gel assay." In which PAI-1 and single chain tPA were mixed at varying ratios, as before, and incubated at room temperature for one hour at room temperature. Samples were then analyzed by SDS-PAGE under non-reducing conditions at 150V for 2 hr on a 10% acrylamide gel. Complex formation was assessed and again, a ratio of 1:1 or 1.25:1 PAI-1:tPA was considered to be active PAI-1.

2.2.l VN purification from Human Plasma

Monomeric, full length, VN was purified from human plasma using a modified version of the protocol published by Dahlback & Podack [149]. This method was standardized by previous members of the Peterson lab, Dr. Sumit Goswami, and Dr. Larry Thompson [147]. 2L of freshly frozen plasma, with sodium citrate as the anticoagulant agent, was thawed gently in a cool water bath. The plasma was then subjected to $BaCl_2$ precipitation, followed by $(NH_4)_2SO_4$ added to the plasma at 50% saturation. All future steps were carried out at 4°C.

After an overnight incubation the precipitant was harvested by ultracentrifugation, and resuspended in 1L of "DEAE buffer" (20mM NaH_2PO_4, 0.1 mM EDTA, pH 7.0) containing 1mM dinitrothiobenzoate (DTNB) and centrifuged again. The supernatant was dialyzed twice against 22L of the DEAE buffer, overnight at 4°C. Protein was then loaded on a pre-equilibrated DEAE Sephacel column (5 x 21.5cm), then washed with DEAE buffer, then eluted with a 0 - 0.5M NaCl linear gradient. Total gradient volume was 4.4L, with 40mL fraction size for the elutions. Fractions containing VN were pooled and precipitated with $(NH_4)_2SO_4$ added to the pool at a 72.7% saturation.

In two batches, the precipitated DEAE elution pool was centrifuged and the pellet containing VN was resuspended in "blue Sepharose buffer" (50mM Tris, 0.1mM EDTA and 150 mM NaCl pH 7.4) and dialyzed twice against 22L of the blue Speharose buffer, overnight at 4°C. Protein was then loaded on a pre-equilibrated blue Sepharose column (5 x 21.5cm), followed by a wash with the same buffer. VN was then eluted with a 0.15 - 3M NaCl linear gradient. Total gradient volume was 4.4L, with 40mL fraction size for the elutions. Fractions containing VN were pooled and concentrated, then precipitated with $(NH_4)_2SO_4$ added to the pool at a 72.7% saturation.

In two batches, the precipitated blue Sepharose elution pool was centrifuged and the pellet containing VN was resuspended in "heparin buffer" (20mM Tris, 20mM NaCl, and 0.1mM EDTA pH 7.4) and dialyzed once against 22L of heparin buffer over-night at 4°C. Protein was then loaded on a pre-equilibrated heparin Sepharose column (2.5 x 15cm) followed by a wash with the heparin buffer. VN was then eluted with a 0.02 – 1.0M NaCl linear gradient. Total gradient volume was 800mL, with 10mL fraction size for the elutions. Fractions containing VN from both column runs were pooled, then run over the column again.

The final heparin column pool was concentrated to ~10mL, and loaded onto a high resolution Sephacryl S-200 column (2.5 x 115cm), pre-equilibrated with "S-200 buffer" (50mM Tris, 150mM NaCl, and 0.1mM EDTA pH 7.4). Elution was carried out at .5mL/min with S-200 buffer, fraction size was 3mL. Fractions containing VN were pooled, and stored at 4°C under $(NH_4)_2SO_4$ precipitation at 70 % saturation. VN concentration, prior to precipitation, was determined at A_{280} and using ε_{280} = 1.0 mL*mg^{-1}*cm^{-1} and a molecular weight of 62,000g/mol.

2.2.m Generation of the PAI-1 Affinity Column

W175F PAI-1 was expressed and purified, then bound to an NHS linked Sepharose column by cycling the W175F PAI-1 mixture over the column overnight. The next day, the column was blocked with Ethanolamine.

2.2.n VN fragment purification from *E. Coli* expression

A plasmid containing the cDNA for the SMB-IDD fragment of VN was cloned into Rosetta gami (DE3) cells. This fragment was attached to a thioredoxin tag to prevent proteolysis of the

disordered VN domain. Following standard transformation protocol as described above. Cells were plated on LB agar + Kanamycin (50µg/mL) + Chloramphenicol (34µg/mL) + Tetracycline (12µg/mL) and incubated overnight at 37°C. Colonies were then selected and grown in TB + Kanamycin (50µg/mL) + Chloramphenicol (34µg/mL) + Tetracycline (12µg/mL). These cultures were then used to perform a small scale induction screen as described above, and a cell stock expressing SMB-IDD was then utilized for large scale expression.

Large scale expression of the SMB-IDD VN fragment was altered somewhat from the PAI-1 large scale expression. Cultures were grown at 37°C and induced at 20°C overnight with 0.5µM IPTG once cultures reached an OD_{600} of ~ 1.

Cells were lysed, while stirring on ice, by sonication at amplitude 7 (30s on 160s off, for 20 cycles). All further steps, unless otherwise noted, were performed at 4°C. Following lysis, the lysate was spun at 10000xg for 30 min, and the supernatant was loaded onto a chelating Sepharose column (2.5 x 10cm), pre-charged with nickel and equilibrated with imidazole buffer. The column was then washed with imidazole buffer. Protein was eluted off the column with a linear gradient of 20mM – 1.0M imidazole. Total gradient volume was 800mL, with 10mL fraction size. The A_{280} of every other fraction was taken, and fractions containing SMB-IDD were pooled and placed into dialysis against 4L of "thrombin buffer" (20mM Tris, 150mM NaCl, 2.5mM $CaCl_2$ pH 8.3) overnight.

Protein was separated into ~45mL fractions, and 5U of biotinylated thrombin was added to each in order to remove the thioredoxin tag. This mixture was then agitated over night at room temperature. The following day, .4mL resuspended streptavidin agarose beads were added to each ~45mL aliquot of digested protein. This mixture was then agitated for ~15min at room

temperature, then the beads were removed by passing the cleaved protein mixture through .22µm filter. This solution was then dialyzed over-night into sodium phosphate buffer (50mM NaH_2PO_4, 300mM NaCl, 1mM EDTA pH7.4).

SMB-IDD was loaded onto the pre-equilibrated W175F PAI-1 affinity column ~5mL at a time. A PAI-1 affinity column was used to ensure that our final SMB-IDD pool would only contain VN fragments that had proper disulfide bond formation in the SMB domain. The column was then washed with sodium phosphate buffer (pH 7.4) for 10m minutes, then with pH 4.0 buffer for 5 minutes, followed by pH 3 buffer for 15 minutes. The column was then re-equilibrated, and the process repeated until all SMB-IDD had been affinity purified.

2.2.o AUC

Sedimentation velocity experiments were performed on a Beckman Coulter Optima XL-1 Analytical Ultracentrifuge. PAI-1 and full length VN were combined at at concentrations of 2-10µM. Prior to loading the AUC cells, proteins were dialyzed in Slide-A-Lyzer dialysis cassettes (10kD MWCO), over-night into PBS pH 7.4 at 4°C. Protein was then spun at 14000xg for 15 minutes to pellet any precipitant that formed during dialysis. Proteins were then mixed to desired concentrations then loaded into the sample sector of preassembled cells. AUC cells were assembled with a double sector, charcoal-filled epon (12mm path length) centerpiece and sapphire lenses. The cells were tightened to 130psi, then loaded with 400µL of protein samples in the sample sector and filtered dialysis buffer in the reference sector. Cells were then aligned in an 8-hole 50 Ti rotor that had been temperature equilibrated inside the centrifuge under

vacuum for at least two hours. Once the rotor and optics were assembled in the instrument, the chamber was allowed to equilibrate to 25°C under vacuum for one hour.

The instrument was brought up to speed in stages in order to perform radial calibration and check laser offset settings for each cell. Once the speed reached 50,000rpm, scans were taken every 50s, for ~16 hours. Data analysis was carried out using the continuous c(s) distribution model, described by the lamb equation, with Sedfit [150].

2.2.p HPLC

HPLC experiments were performed on and Hewlett-Packard series 1100 instrument. A Phenomenex SEC-2000 size exclusion column was used to separate PAI-1:VN complexes. The column was run using PBS as the washing and eluting buffer. Between column uses the column was cleaned with water and .1%TFA. Prior to injecting the proteins of interest on the column, known protein standards were injected onto the column to identify the retention time of our proteins and protein complexes. 20µL of protein were injected onto the column at a time. PBS buffer was then flowed over the column at .5mL/min for 30 min. After this period of time the column had returned to baseline and was ready for the next protein injection.

2.2.q ELISA

Various ELISA methods were tested. Described here is the method most commonly utilized, any deviation from this method will be noted in the experimental sections of this work. The following description of the ELSA methods used, are also depicted in figure 2.2.

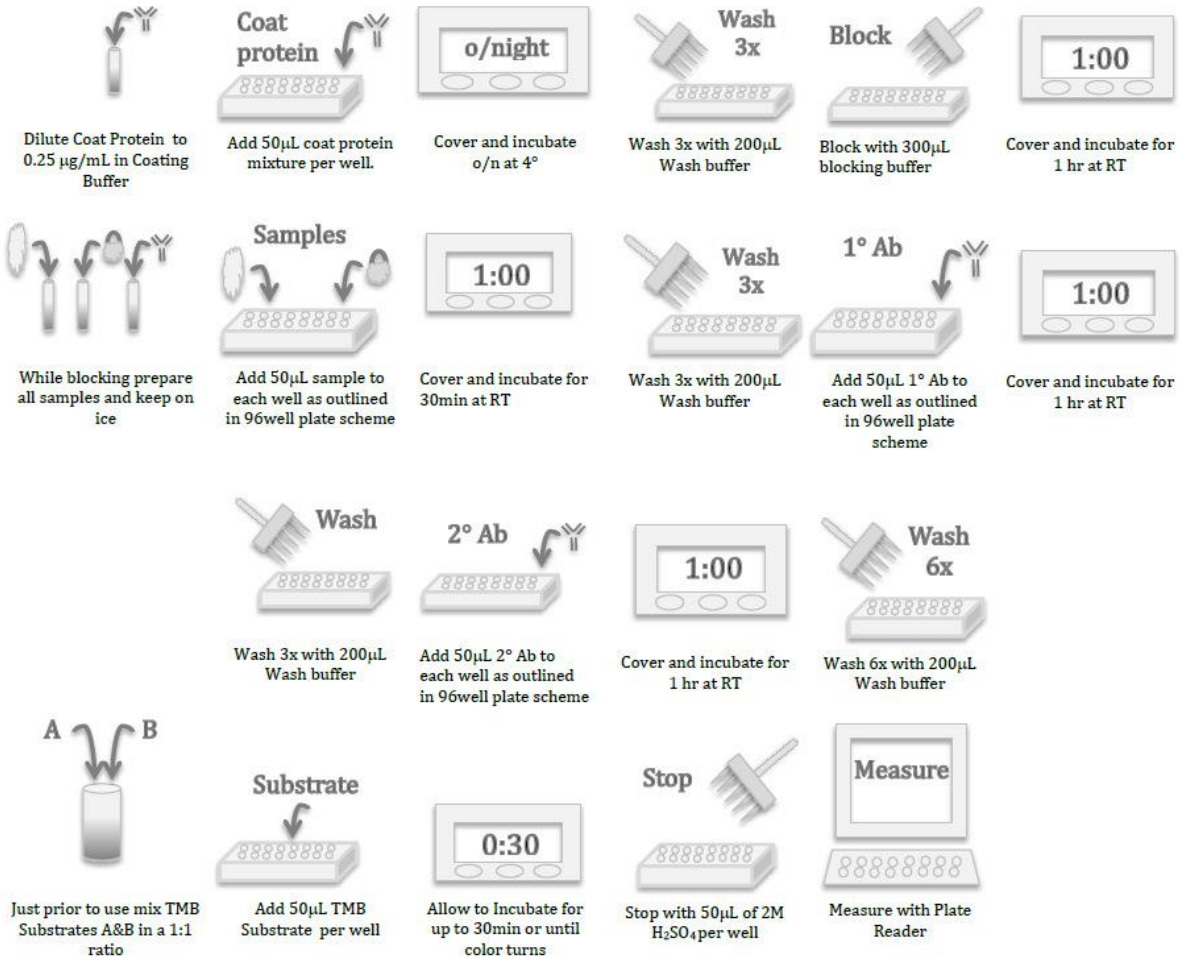

Figure 2.2 Illustrated ELISA Method

Detailed scheme of ELISA method.

PAI-1 or VN were diluted into “coat buffer” (.2M Sodium Citrate pH 9.0) and 50µL was added to wells on a high binding 96 well plate and allowed to incubate overnight at 4°C. The plates were then washed three times with 200µL of a Tris wash buffer (.02M Tris and .15M NaCl pH 7.4) and blocked with 300µL Pierce® protein free blocking buffer for one hour at room temperature. Samples of PAI-1 and VN were mixed in serial dilutions, in the blocking buffer immediately prior to addition of 50µL of each sample, in duplicate, to the plate. The samples were then incubated for 30 minutes at room temperature. Following sample incubation the plate was washed with 200µL of Tris buffer, followed by the addition of 50µL of antibody diluted in blocking buffer. The primary antibody was then incubated for one hour at room temperature, followed by another wash step and addition of the secondary antibody. Following a one hour incubation of the secondary antibody, the plate was washed six times. TMB substrate (3,3′,5,5′-Tetramethylbenzidine) was mixed and 50µL added to the wells. Once sufficient color change had occurred, the reaction was stopped with 2M H_2SO_4. Absorbance at 450nm was then measured using a plate reader, and data were plotted in Excel.

2.2.r SPR

Surface Plasmon Resonance (SPR) experiments were performed on a Biacore-3000 instrument. A CM5 chip was used to study the interaction between PAI-1 and VN. A preprogramed immobilization protocol was used to facilitate VN immobilization. Between 2100 and 2500 Response Units (RU) of VN was covalently immobilized on the CM5 chips with a 10mM sodium acetate buffer pH5.0 using 1-ethyl-3-(dimethylaminipropyl)carbodimide hydrochloride (EDC) and N-hydroxysulfosuccinimide (NHS). Following immobilization, the chip was blocked with ethanolamine.

SPR experiments were all performed using the HBS-EP buffer commercially available from Biacore (.01M HEPES, .15M NaCl, 3mM EDTA, pH 7.4). PAI-1 variants were injected over the chip for multiple conditions and concentrations. Between injections the chip was regenerated by injecting 10mM glycine pH 2.0 at 30µL/min for 60s followed by injecting .05% SDS at 30µL/min for another 60s. Data were analyzed using the built in tools in the BiaEvaluation software package.

2.2.s Deuteration of PAI-1

PAI-1 was deuterated by two different methods for this project. Initially, PAI-1 was deuterated using commercially available deuterated rich media. Glycerol stocks of *E. coli* expressing the W175F PAI-1 variant were used to inoculate this deuterated rich media and grown under the same conditions as un-deuterated PAI-1 (described in 2.2.h).

Later, we utilized minimal media and fermentation to more efficiently and cost effectively deuterate PAI-1. In order to deuterate the PAI-1 in this manner we worked with the Bio-deuteration lab at ORNL. The cells were grown to an OD_{600} of ~35 in a deuterated minimal media. The cells were then cooled to 15°C and induced overnight according to standard PAI-1 expression protocol.

In both cases, cells were then harvested and stored at -80°C until purification (see 2.2.i). In nearly all cases, protein was immediately dialyzed into D_2O PBS buffer (pH of 7.4) and then used in SANS experiments. The final expression using fermentation resulted in more protein than necessary for a single experiment. Excess protein was frozen at -80°C. Prior to use of frozen protein it was run over an S-100 size exclusion column to ensure all PAI-1 was monomeric.

Percent deuteration was determined computationally or experimentally via MALDI-TOF Mass Spec.

2.2.t SANS

Multiple SANS experiments were performed at the two SANS facilities at ORNL. Scattering data were collected on the BioSANS line at the High Flux Isotope Reactor (HFIR) and the EQ SANS line at the Spallation Neutron Source (SNS).

Original PAI-1 VN Experiments were performed at HFIR. Deuterated PAI-1 and protonated VN were mixed in quartz cells and placed in the neutron beam at various D_2O buffer percentages. Scattering data were gathered with the detector at a distance of .3m and again at 6m in order to fully capture the scatter.

SMB-IDD:Osmolyte Experiments were performed at HFIR. Protonated SMB-IDD was mixed with varying concentrations of deuterated osmolytes in a fixed D_2O buffer. Samples were placed in quartz cells and exposed to the neutron beam. Scattering data were gathered with the detector at a distance of .3m and again at 6m in order to fully capture the scatter.

SMB-IDD:PAI-1 Experiments were performed at HFIR and SNS. Protonated SMB-IDD was mixed with deuterated W175F PAI-1 at various D2O buffer percentages. A 1:1 mixture of SMB-IDD:PAI-1 was studied at SNS in 0%, 10%, 20%, 85%, and 100% D_2O. Samples were placed in quartz cells and exposed to the neutron beam. Due to the nature of the neutrons on the EQ SANS line, the detector could be left at a fixed distance for data collection. A 2:1 mixture of SMB-IDD was studied on the Bio SANS line at HFIR in 0%, 10%, 85%, and 100% D_2O.

Scattering data were gathered with the detector at a distance of .3m and again at 6m in order to fully capture the scatter.

2.2.u Analysis of SANS Data using MONSA and SUPCOMB

MONSA and SUPCOMB are part of the ATSAS program suite [151]. MONSA is designed to generate low resolution models of biological macromolecules in solution [151, 152]. In this study, a 70Å sphere of closely packed dummy atoms was used as the dummy atom molecule (DAM) to ensure a large enough radius for the entire PAI-1: SMB-IDD complex to be modeled within. The scattering curves were then fit within this DAM and a .pdb file was generated containing low resolution information for the PAI-1 and SMB-IDD components of the complex.

SUPCOMB, was used to super impose the 3D crystal structure for PAI-1 and the SMB domain of VN onto the low resolution structure generated by MONSA [153]. SUPCOMB works by finding the minimum distance between points in each model and generates a normalized .pdb file of the two structures.

2.2.v Analysis of SANS Data using EOM

Ensemble Optimization Method (EOM), part of the ATSAS program suite, was used to generate 10,000 independent structures based on sequence and known structural information [151, 154-156]. The small angle scattering data were then compared with the 10,000 structures. 1,000 structures were selected that best fit the experimental conditions for SMB-IDD in the presence of ethylene glycol (EG).

This process was repeated with the 100% D_2O data for deuterated PAI-1 and SMB-IDD complex. The data for the SMB-IDD were then isolated from the complex and the Radius of gyration (Rg) of the ensemble was then plotted and compared to the Rg of a random coil pool to study the change in the IDD of VN

2.2.w Analysis of SANS Data using SASSIE

SASSIE [157] is a suite of software tools that can be used to create high resolution models of protein complexes from experimental scattering data. In order to generate these models a series of steps were performed. Several energy minimized "starting structures" were created as starting points for further analysis.

The PAI-1:SMB co crystal structure (PDB 1OC0)[77] was used as the core for all starting structures. First, the PAI-1 and SMB portion of the co-crystal structure were separated. Next the B chain from the W175F PAI-1 structure (PDB 3Q02) [76] was isolated, and the E and F helices of the W175F PAI-1 structure were aligned to PAI-1 from the co-crystal structure and it was determined that the alignment was good enough to continue using the PAI-1 component from the co-crystal structure. The W175F point mutation was added to this structure as were the five missing N-terminal residues and the missing portion of the RCL. The RCL was energy minimized for 1000 steps using NAMD [158]. Then the entire PAI-1 was energy minimized for a further 1000 steps. Torsion angle MD (10ps) was run on the RCL of the minimized PAI-1 and the last frame was used for the PAI-1 component of all structures.

Starting Structure 1: The VN portion of the complex (SMB and IDD domains) was constructed using the SMB component from the co-crystal structure in order to preserve the PAI-

1:VN interface. An additional 10 disordered residues were added to the "SMB" based on their presence in the NMR solution structure [94]. For starting structure 1, the IDD residues were added and set to be completely flexible, with no added constraints, such as secondary structure. This structure was then minimized for 1000 steps using NAMD and became the SMB-IDD portion of starting structure 1. The PAI-1 and VN components were built back into a single structure and minimized for 1000 steps to generate starting structure 1.

Starting structure 2: The second starting structure was constructed similarly to structure 1. The first and second structures differ in that some structural constraints were introduced into the IDD portion of VN for structure 2. Specifically, the IDD portion of starting structure 2 was compacted, so that the starting structure better agreed with the experimentally determined Rg. To predict possible helical structures PSIPRED, PHYRE2, and Chou-Fasman, GOR and neural network were used [159-165]. While short regions of helicity were predicted in some cases, there was no region that was consistently predicted to adopt helical structure between any of these methods. Consequently, no helical structure was deliberately introduced into the IDD. However, PSIPRED produced a more compact structure for this region, so this more compact structure was used in place of the fully extended flexible tail in structure 1. This structure was then minimized for 5000 steps to generate starting structure 2.

Starting structure 3: Starting structure 3 was constructed such that part of the IDD wrapped around PAI-1, across the "front" of the central β-sheet in order to create a starting structure that had a center of mass value that better agreed with the center of mass value calculated from the experimental data. The interactive MD option within VMD [166] was used to apply force to the IDD (defined as residues 44 – 130) from starting structure 2 in order to

position the IDD on the opposite side of PAI-1 from the SMB. This structure was then minimized for 5000 steps to generate starting structure 3.

From each of these starting 50,000 structures were generated. These structures were then analyzed for goodness of fit to the experimental data.

Chapter 3 - Probing the global PAI-1:VN complex

3.1 Introduction to PAI-1:VN Interactions

The interaction between PAI-1 and VN has been under investigation since the two proteins were discovered to interact in the late 80's [167]. A plethora of binding studies have been performed in an effort to identify the binding affinity and the site of interaction between PAI-1 and VN, both in circulation, as well as in the ECM. Studies have also been performed to identify the effect that binding has on the conformational state of each protein, and how the PAI-1:VN interaction affects the function of each protein's physiological role [127, 132].

3.1.a Identification of VN Binding Domains in PAI-1

The discovery of the primary PAI-1:VN interaction site, as with many protein complexes, was made in bits and pieces. Early studies that demonstrated the presence of PAI-1 in the ECM noted that the interaction between PAI-1 and VN was not electrostatic due to the inability of 2M NaCl to release PAI-1 from the ECM [168]. PAI-1 was later shown to interact solely with VN in the ECM, confirming that the inability of high salt to remove PAI-1 from the ECM was due to the fact that the interaction between PAI-1 and VN is non-ionic [169]. The eventual co-crystal structure of PAI-1 and the SMB domain of VN confirmed the finding that the primary binding site for VN is composed of predominantly hydrophobic interactions [77].

In 1994, two studies were published that served to localize the primary site of VN binding on PAI-1. In one study, antibodies were used to localize a site of interaction to helix E (hE), strand 1in β-sheet A (s1A), and helix F (hF) [170] shown in figure 3.1. The second study

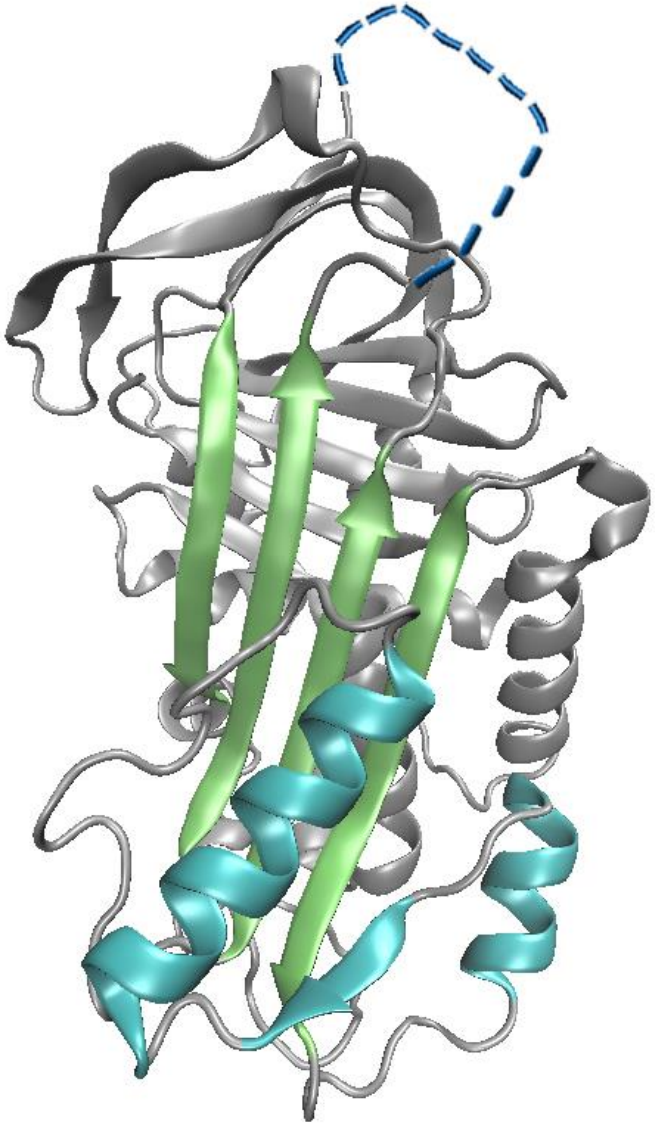

Figure 3.1 Primary Binding Site for VN on W175F PAI-1 Structure

The active PAI-1 crystal structure (3Q02), derived from W175F PAI-1, is shown with the central β-sheet in green for orientation purposes. The missing RCL residues have been added in as a dashed line. The regions important for interacting with VN, more specifically the SMB domain of VN, are highlighted in cyan. This primary interaction between PAI-1 and VN is hydrophobic.

randomly mutagenized the PAI-1 sequence coding for amino acids 13-147. Five point mutations were identified that selectively disrupted PAI-1:VN interactions while still retaining inhibitory activity. All five residues are surface exposed, and several form a cluster in the three-dimensional structure despite being separated in the primary sequence, indicating the importance of three-dimensional structure for PAI-1:VN interactions [171].

The identification of this primary binding site for VN on PAI-1 was a significant advancement in the field. However studies showed that it wasn't the only site of interaction between the two proteins. A mutational study of hE demonstrated that the primary binding site was not solely responsible for all interactions between PAI-1 and VN [172]. A ΔSMB VN construct was used to confirm the presence of a secondary binding site for VN on PAI-1. This ΔSMB VN was studied in conjunction with a variety of PAI-1 variants that contained one or more amino acid substitutions. This process was used to identify an extended interaction surface comprised of individually weak interactions between PAI-1 and VN near the heparin binding domain in PAI-1 [137, 173] shown in figure 3.2.

3.1.b Identification of PAI-1 Binding Domains in VN

The primary binding site for PAI-1 on VN was originally identified through a series of cleavage experiments. VN was subjected to acid and cyanogen bromide (CNBr) cleavage and the resulting fragments were tested for the ability to interact with PAI-1. The fragment spanning residues 1-51, known as the SMB domain, retained the ability to bind PAI-1 [174]. Later experiments demonstrated that PAI-1 is able to bind to bind to a fragment comprised of residues 1-40, but not to a fragment only containing residues 1-30 [136]. When the co-crystal structure of PAI-1 and the SMB domain was published, key residues for interaction with PAI-1 were

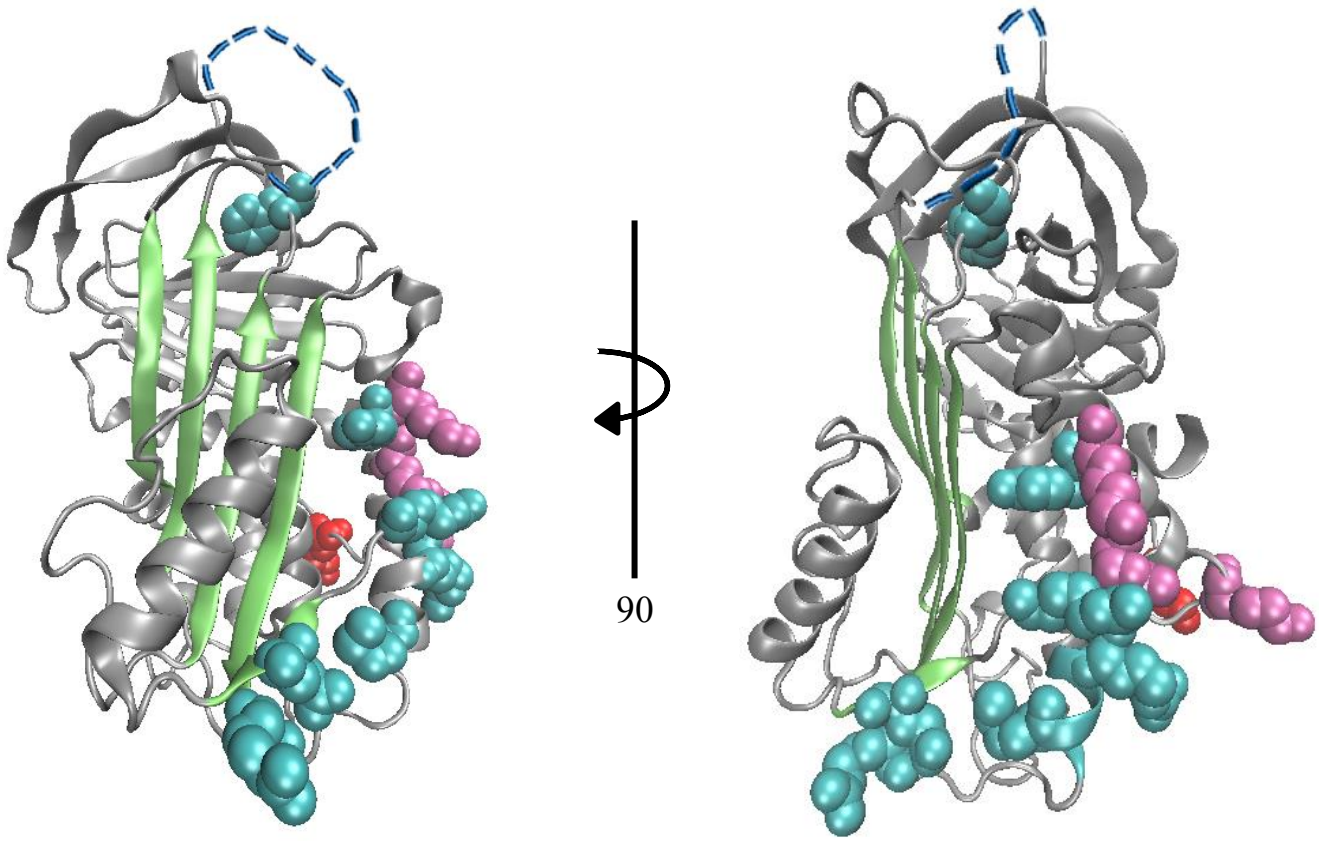

Figure 3.2 Secondary Binding Site for VN and the Heparin Binding Site on W175F PAI-1 Structure

The active PAI-1 crystal structure (3Q02), derived from W175F PAI-1, is shown with the residues identified as important for binding to VN outside of the SMB [137] in cyan. The residues identified as important for heparin binding [173] are shown in red. Residues that explicitly overlap both binding sites are shown in light purple. This overlay demonstrates that the secondary VN binding site and the heparin binding site overlap. The central β-sheet is shown in green for orientation purposes. The missing RCL residues have been added in as a dashed line. This secondary interaction between PAI-1 and VN is electrostatic.

identified [77]. Together these studies demonstrate the importance of primary and tertiary structure in the PAI-1:SMB interaction.

Notably, when a fragment of VN, spanning residues 1-45, was studied in competition assays with full length VN, it was found that the N-terminal fragment of VN only partially competed with full-length VN for PAI-1 binding. This strengthened speculation that more than one binding site for PAI-1 existed on VN. It was proposed that the secondary binding site exists near the primary site in three dimensional space [175]. Other studies concur with the three dimensional proximity of the two binding sites. However, two separate regions have been proposed to house this secondary domain. Some studies have localized a PAI-1 binding site in the heparin binding region of the C-terminal domain of VN [144] while others have identified a PAI-1 binding site within the IDD [143]. No consensus has been reached in the literature regarding the location of the second binding site at this time. However, studies with monoclonal antibodies demonstrated that the two binding sites in each protein are occupied simultaneously [140].

3.1.c Conformational Effects of Complex Formation

An important consequence of the PAI-1:VN interaction is the stabilizing effect that VN has on PAI-1 [176]. This stabilization results from the primary interaction between PAI-1 and the SMB domain, and is due to a restriction of flexibility in β-sheet A, slowing the rate of RCL insertion [77, 171]. Beyond this stabilization effect, the PAI-1:VN interaction induces a conformational change in both PAI-1 and VN, particularly following interaction at both the primary and secondary sites. It is important to note that the conformational change that occurs in

VN is permanent, and persists even after PAI-1 dissociates from the complex following latency transition or cleavage by PAs [21, 177]. The conformational change induced in VN by active PAI-1 enables VN to form multimers, of as many as 16 subunits, and act as an adhesive glycoprotein, which it is unable to do in the native monomeric state [148, 178, 179].

While VN exists as a multimeric adhesive protein in the ECM, the monomeric form is predominant while in circulation. This is likely due to the low concentration of PAI-1 (0-60ng/mL, approximately 0 – 1.4nM) in relation to the comparatively high concentration of VN (~200 – 700µg/mL, approximately 3.2 – 11.3µM) [5, 180, 181]. The association between PAI-1 and VN is strong enough at the primary site ($K_d \approx 1$nM) that this low concentration still allows binding. However, PAI-1 and VN exhibit weaker binding ($K_d \approx 30$nM) at the secondary binding site, with an ~10 fold difference in K_d making interaction at the secondary site unlikely while in circulation [138].

This circulating pool of PAI-1 and VN is functionally distinct from that which exists inside of platelets. Although 90% of the 200-300ng/mL of PAI-1 in platelets is inactive [5] it is likely that much of the platelet PAI-1 was in complex with the platelet pool of VN at some point as platelet derived VN is multimeric and codistributes with PAI-1 following platelet lysis [182]. In tissues, higher local concentration of PAI-1, and a greater affinity for multimeric VN facilitate PAI-1:VN interactions and the "activation" of more VN molecules through conformational change, expanding the reactivity of VN greatly [124, 183].

3.1.d Research Goals

In this portion of the project we sought to gain insight into the PAI-1:VN complex. Preliminary data from our lab (figure 1.10) demonstrate that the PAI-1 VN complex interacts in a way that is unique from the model that currently exists in the literature. These data provide experimental evidence of a PAI-1 dimer when in the presence of VN. While many serpins are able to polymerize [184], free PAI-1 does not polymerize under native conditions. However, it is able to polymerize under conditions that induce conformational changes. Furthermore, PAI-1 polymerization under these conditions results in dimers that retain inhibitory function [81]. These data, combined with the knowledge that PAI-1:VN interactions induce a conformational change in PAI-1, provide support for the PAI-1 dimer observed in our preliminary data. Additionally, previous publications from our group have suggested that the primary and secondary binding sites, between PAI-1 and VN, comprise an extended binding interface rather than two separate binding sites for two separate PAI-1 molecules [21, 137]. This too supports the revised model that we observed with SANS.

Our goal was to experimentally determine, if PAI-1 is indeed able to interact with another PAI-1 molecule in the presence of VN. The hypothesis that guided this project is PAI-1 and VN interact in a PAI-1:PAI-1:VN manner when in higher order complexes. In order to test our hypothesis, we generated a series of VN binding deficient PAI-1 mutants. These mutants were then labeled so that we could monitor their incorporation into PAI-1:VN complexes (figure 3.3).

If our hypothesis is correct then we will have significantly advanced the field by developing a more accurate model for the PAI-1:VN interaction (figure 3.4). We will have offered a rationale for some of the questions that have long remained unanswered about the PAI-

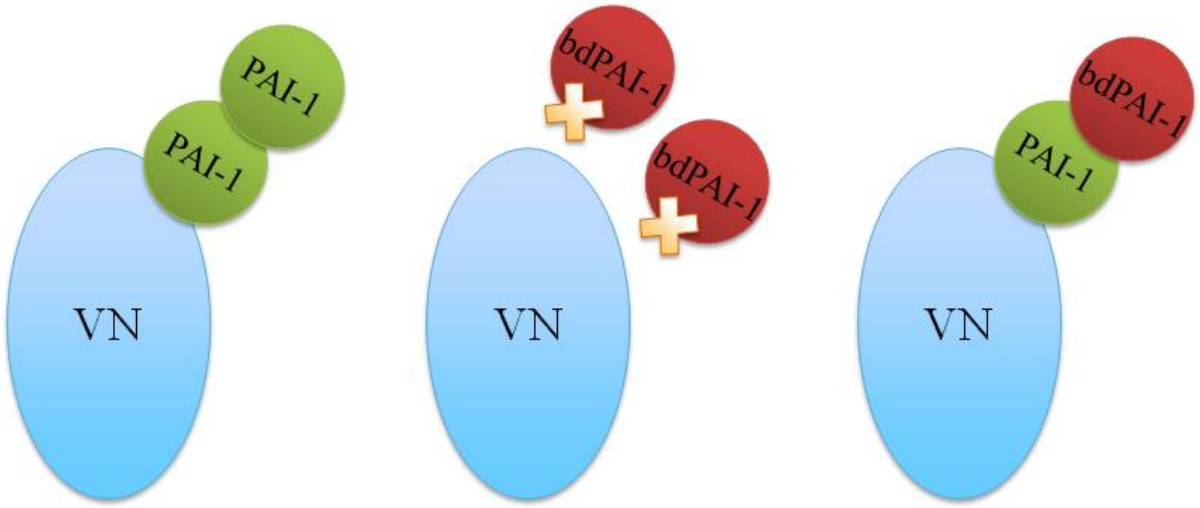

Figure 3.3 Experimental Design for PAI-1:VN binding studies

We hypothesize that PAI-1 forms a dimer when in a 2:1 complex with VN. In order to test this hypothesis, we generated VN binding deficient PAI-1 (bdPAI-1) variants and experimentally confirmed their inability to interact with VN. We will then mix this bdPAI-1 variant with PAI-1 constructs that retain VN binding and monitor incorporation of the bdPAI-1 into PAI-1:VN complexes. Incorporation of bdPAI-1 into PAI-1:VN complexes would confirm our hypothesis that PAI-1 forms a dimer when in a 2:1 complex with VN.

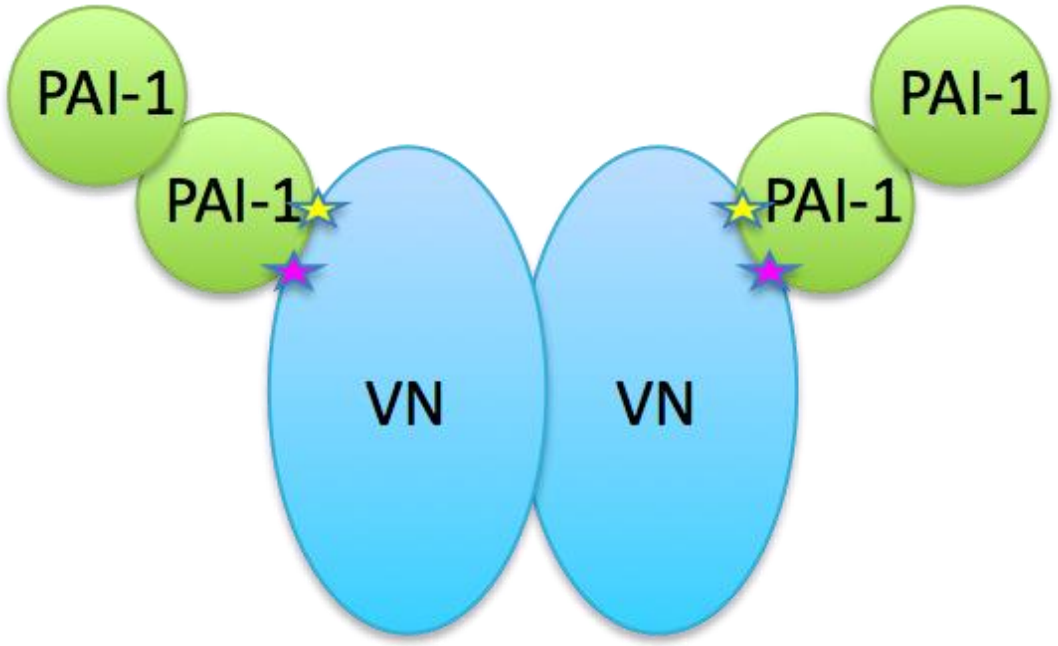

Figure 3.4 A New Model for PAI-1 VN Interaction

We propose a new model for PAI-1:VN interactions in a 4:2 complex. Our data support a model in which PAI-1 is able to form a PAI-1:PAI-1 dimer upon interaction with VN. We propose that this previously unseen dimerization of PAI-1 under physiological conditions is able to occur due to the conformational change induced by VN binding. We also propose that this dimerization is unlike that of other serpins, and does not result in a serpinopathy.

1:VN complex, and we will have demonstrated that PAI-1 can dimerize under physiological conditions, and does so as part of its normal interaction with VN.

3.2 Methods

3.2.a Generation of PAI-1 Constructs

In order to probe the hypothesis of a PAI-1:PAI-1:VN complex several PAI-1 variants were created via site directed mutagenesis (table 3.1). The point mutations that were created within the PAI-1 sequence have previously been shown to reduce PAI-1:VN binding. The Q123K mutation was demonstrated to drastically reduce the ability of PAI-1 and VN to interact and is considered to be deficient for binding at the primary site based on its location in the PAI-1 molecule [171]. The R115E and R118E double mutation was shown to diminish binding at the secondary interaction site [137]. W175F is a stabilizing mutation [76] and also diminishes the ability of PAI-1 and VN to form higher order oligomers beyond the 4:2 complex [147], but still allows for 4:2 and lower order complex formation. The S338C mutation was used to introduce a cysteine in the Reactive Center Loop (RCL) to allow for labeling of the variants. This mutation has been repeatedly used in the literature as a means of labeling PAI-1 and studying RCL movements. Neither the mutation, nor labeling at this position significantly alter PAI-1 activity or VN binding [185-187].

Following purification of the PAI-1 variants, each was analyzed for activity to ensure that PAI-1 was still functional as described in 2.2.k. All variants were reasonably active when compared to normal wild type PAI-1 activity. PAI-1 variants containing the S338C mutation

Table 3.1 Key Characteristics of PAI-1 Constructs

List of the PAI-1 variants used in this study. A "Y" in one or both of the VN binding columns indicates that no mutations have been made that alter the VN binding capacity of the PAI-1 construct to the primary or secondary site of interaction. A "-" in one or both of the VN binding columns indicates that the PAI-1 construct has reduced binding at the primary or secondary site. Labeling accessibility indicates that the S338C mutation has been added to allow for labeling with Biotin or NBD.

PAI-1 Constructs	Shorthand For PAI-1 Variants	Key Characteristics of PAI-1 Mutants		
		Primary Binding	Secondary Binding	Accessible for Labeling
Wt	Wt	Y	Y	-
S338C	P9	Y	Y	Y
W175F	W175F	Y	-	-
Q123K	Q	-	Y	-
Q123K, S338C	QP	-	Y	Y
Q123K, W175F	QW	-	-	-
Q123K, W175F, S338C	QWP	-	-	Y
Q123K, R115E, R118E	QRE	-	-	-
Q123K, R115E, R118E, S338C	QREP	-	-	Y
Q123K, R115E, R118E, W175F	QREW	-	-	-
Q123K, R115E, R118E, W175F, S338C	QREWP	-	-	Y
R101A, M110A, Q123A	RMQ	-	-	-
R101A, M110A, Q123A, S338C	RMQP	-	-	Y
R101A, M110A, Q123A, W175F	RMQW	-	-	-
R101A, M110A, Q123A, W175F, S338C	RMQWP	-	-	Y

were labeled with Biotin or NBD for use in differentiation between PAI-1 molecules in complexes with VN. Further details on the labeling procedure can be found in 2.2.j.

3.2.b AUC

Proteins samples were mixed with a small volume of 10x PBS, to prevent precipitation, and dialyzed overnight at 4°C in 4L of 1x PBS pH 7.4. The following day, protein samples were spun at 14,000xg for 15 -20 min in order to remove any particulates or precipitated protein. Additionally, ~10mL of the dialysis buffer was harvested and filtered with a .22µM filter for use in mixing samples and as the buffer blank in the AUC cells. All AUC experiments were performed using sapphire lenses so that absorbance and interference data could be collected.

Samples were mixed in .6mL microfuge tubes, and immediately loaded into preassembled AUC cells. The cells were placed in a 50Ti rotor, and then allowed to incubate in the AUC chamber at 25°C for 45-60min. Sedimentation velocity experiments were performed at 50,000rpm, 25°C for ~20hours with scans taken every 50 seconds. Analysis of AUC data were performed in Sedfit using the continuous c(s) model described by the Lamm equation [150, 188, 189]. Additional method details can be found in 2.2.o.

3.2.c HPLC

A size exclusion column was used to separate PAI-1, VN, and PAI-1:VN complexes. Prior to injection onto the column protein samples were mixed and allowed to incubate at room temperature for 30 minutes. Following incubation, 20µL of sample was injected onto the

column, followed by a .5mL/min flow of PBS buffer at pH 7.4. A more complete description of this method can be found in 2.2.p

3.2.d ELISA

VN was diluted into .2M Sodium Citrate at pH 9.0. 50µL of this mixture was then added to each well on a high-binding 96 well plate. In some cases PAI-1 was used as the coat protein, and was added to the plate according to the same method as VN. A side by side comparison of protein directly bound to the plate versus an antibody coat followed by protein binding showed no significant difference between the methods, so the direct addition of protein to the plate was used for further experiments. Incubation was carried out overnight at 4°C or for 2hr at room temperature. Side by side comparisons demonstrated no significant difference between these two methods so the overnight incubation was used for further experiments. Tris-HCl buffered wash and blocking buffer were used for all further steps. PAI-1 samples were mixed and 50uL/well was promptly added to the plate. Samples were incubated on the plate for 30min at room temperature. Antibody and TMB substrate detection steps were carried out as described in 2.2.q. The TMB substrate reaction was quenched with 2M H_2SO_4 and absorbance at 450nM was detected using a plate reader. These data were then plotted and analyzed in Excel.

3.2.e SPR

A Biacore CM5 chip, with a matrix of carboxymethylated dextran covalently attached to a gold surface was used for immobilization of PAI-1and VN in order to measure PAI-1:VN interactions. Use of the PAI-1 chip was soon eliminated due to the tendency toward latency,

even with a stable PAI-1 construct, as well as the high background from VN accumulating on the chip over time, and not being fully removed by a variety of regeneration protocols. Further experiments all used a VN chip with PAI-1 and streptavidin as the analytes. Following each injection, the chip was regenerated using a combination of 10mM glycine at pH 2.0 and .05% SDS. Data were analyzed using BiaEvaluation Software. Further detail can be found in 2.2.r.

3.3 Results

3.3.a Generation of PAI-1 Constructs

Over the course of our study, several PAI-1 constructs were generated in order to study the PAI-1:VN interaction. These variants and their hypothesized binding deficiencies are shown in table 3.1. The first set of binding deficient PAI-1 constructs was designed to eliminate binding at the primary (Q123K) and secondary (R115E/R118E) sites of interaction between PAI-1 and VN [137, 171]. We also generated a stable variant of these constructs containing the W175F mutation [76] as well as introduced a cysteine that could be used to label PAI-1 (S338C) (figure 3.5). Later in this study, we also generated a PAI-1 variant with three mutations (R101A/M110A/Q123A) that had been shown to be unable to bind VN [190]. Each PAI-1 variant was tested for activity via a gel and/or spectroscopic plate assay, to confirm that the mutation did not affect function in addition to VN binding. A representative selection of data is displayed in figure 3.6.

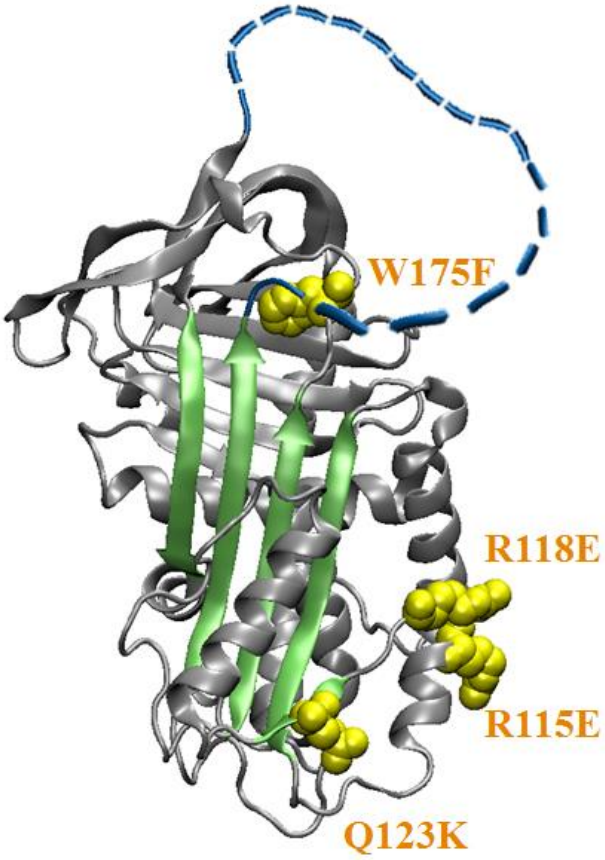

Figure 3.5 First Binding Deficient PAI-1 Constructs

The first set of mutations that we introduced to PAI-1 were designed to target the primary and secondary VN binding sites. Q123K has been shown to diminish VN binding at the primary site of interaction. R115/R118E has been shown to diminish VN binding at the secondary site of interaction. W175F was introduced as a stabilizing mutation. S338C (P9 in the RCL) was introduced to allow labeling of the PAI-1 construct.

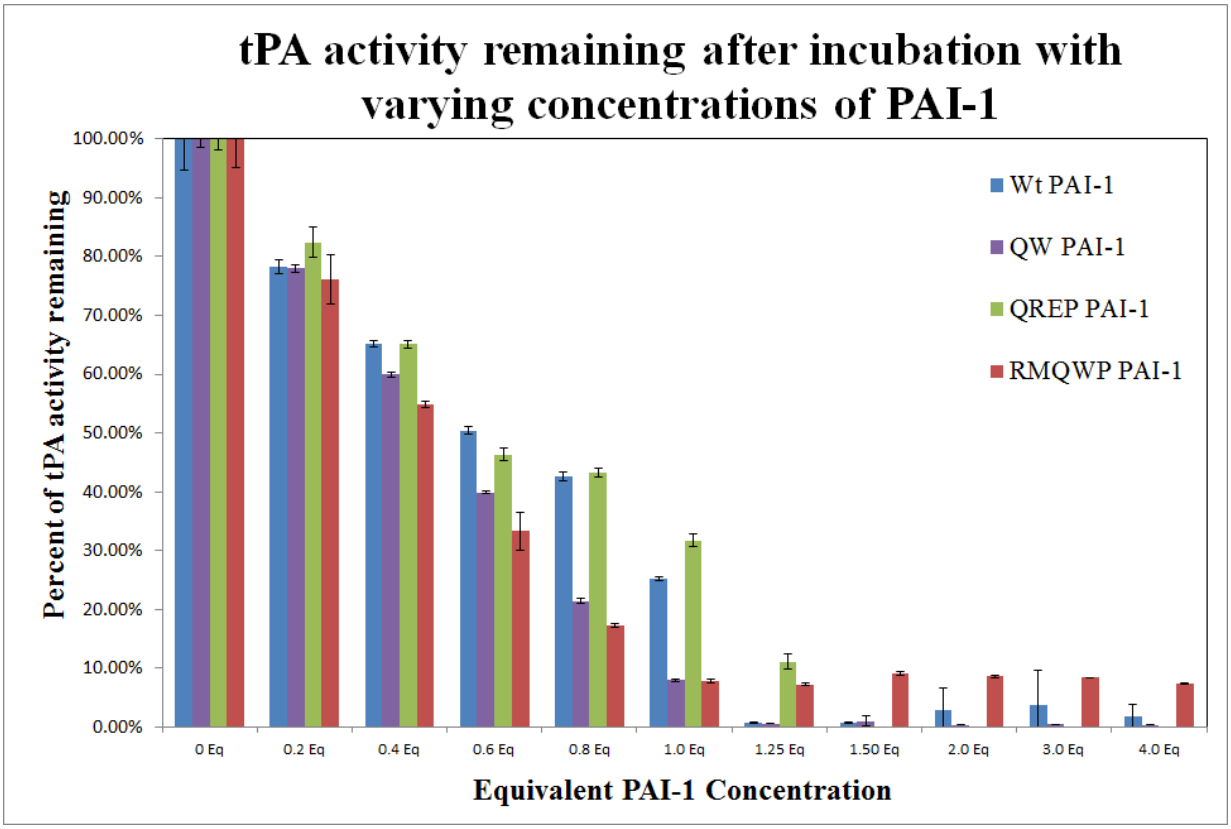

Figure 3.6 Representative Data From PAI-1 Activity Assay (Plate)

Activity of PAI-1 constructs was assessed using a spectroscopic tPA substrate. Following incubation of tPA with PAI-1, the substrate was added and color change detected. Data were normalized so that tPA alone, "0Eq" on the x-axis, is set at 100% activity. As increasing amounts of PAI-1 are added, the activity of tPA decreases through the inhibitory action of PAI-1. At 1.25 equivalents of PAI-1 to tPA there should be virtually no tPA activity remaining. As can be seen from this representative data set, tPA mixed with QREP PAI-1 and RMQWP still retains some activity. However, even these PAI-1 have >90% inhibitory activity.

3.3.b Probing the PAI-1:VN complex with AUC – The Early Studies

In order to test the for the existence of PAI-1 dimers in the presence of VN we designed a series of AUC experiments. Previous to this work, our lab published a study with the

sedimentation coefficients for PAI-1, VN and PAI-1:VN oligomers [128]. The sedimentation coefficient for key PAI-1:VN species is shown in figure 3.7.

Our studies initially utilized the VN binding deficient variant Q123K PAI-1. This single alteration had been shown to disrupt binding to VN at the primary site of interaction between the two proteins [171]. As can be seen in figure 3.8, this mutation was not sufficient to completely disrupt PAI-1:VN interactions when studied at the micromolar concentrations necessary for AUC experiments. Our next course was to add mutations that had been demonstrated to diminish VN binding at the secondary site of interaction between PAI-1 and VN (R115E R118E and W175F). Once again, these mutations were not sufficient to eliminate PAI-1:VN interactions at micromolar concentrations (Figure 3.8). Interestingly, while W175F causes a reduction in higher order complex formation beyond 4:2 complexes, the addition of the W175F mutation to PAI-1 increased the overall complex formation between PAI-1 and VN (Figure 3.9). This increase is likely due to the enhanced stability of PAI-1 containing the W175F mutation, which allows it to remain in complex with VN for longer periods of time.

These results demonstrated that we would need a more severe mutation to study the interaction of PAI-1 and VN at such a high concentration. Alternatively, we would need to change the method used to one that would allow us to study the complex at lower protein concentrations. Both of these alternative approaches were utilized in our studies.

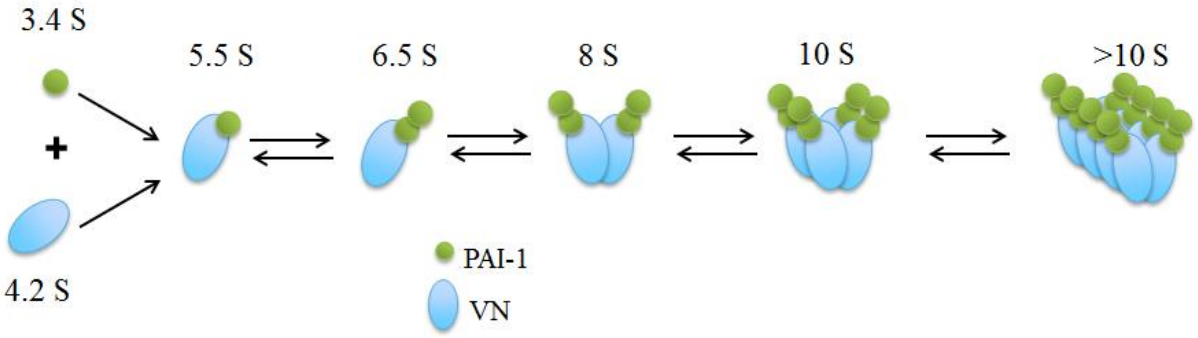

Figure 3.7 Order of Assembly for PAI-1:VN Complexes and Associated Sedimentation Coefficients

PAI-1 and VN are believed to assemble into higher order complexes via a stepwise mechanism illustrated above. These complexes are distinguishable by their sedimentation coefficients in AUC studies (shown in figure), as well as their molecular weights (PAI-1 monomer molecular weight: ~43kD, VN monomer molecular weight: ~70kD).

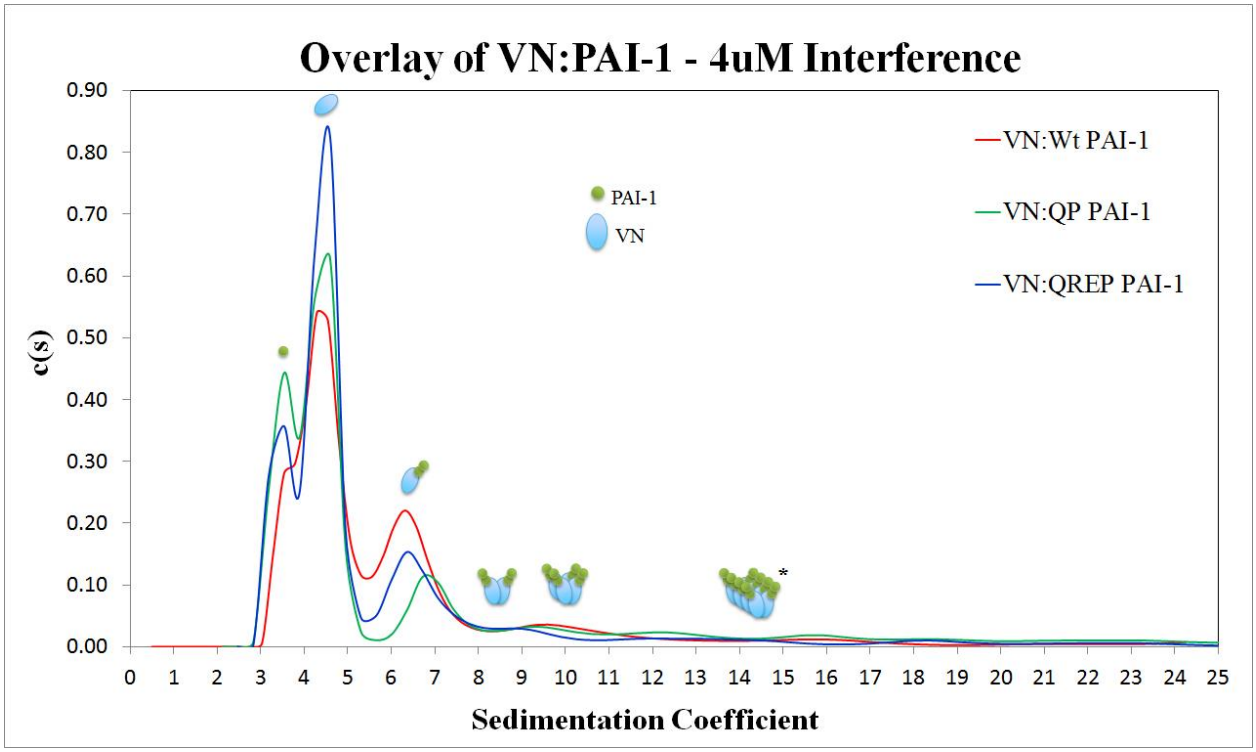

Figure 3.8 AUC Results for Early PAI-1:VN Binding Studies

A mixture of PAI-1 variants and VN was studied using AUC. PAI-1 and VN were mixed at equimolar concentrations (4µM of each protein). The AUC data are overlaid with cartoons representing the species that each peak is composed of. The sedimentation coefficients of each of these species were identified previously [128]. Green circles represent PAI-1, and blue ovals represent VN. In each sample there is some un-complexed PAI-1 and VN seen in the peaks spanning sedimentation coefficient values from 3 to ~5. Peaks higher than 5.5S are from higher order complexes. This is represented by the cartoons of PAI-1 VN complexes at their respective sedimentation coefficients. Above 10S are higher order oligomers, represented by the complex with an asterisk. The VN:Wt PAI-1 data set, shown in red, has the highest amount of higher order complex formation. QP PAI-1 and QREP PAI-1, shown in green and blue respectively, have diminished complex formation, but still exhibit VN binding at 4µM concentrations.

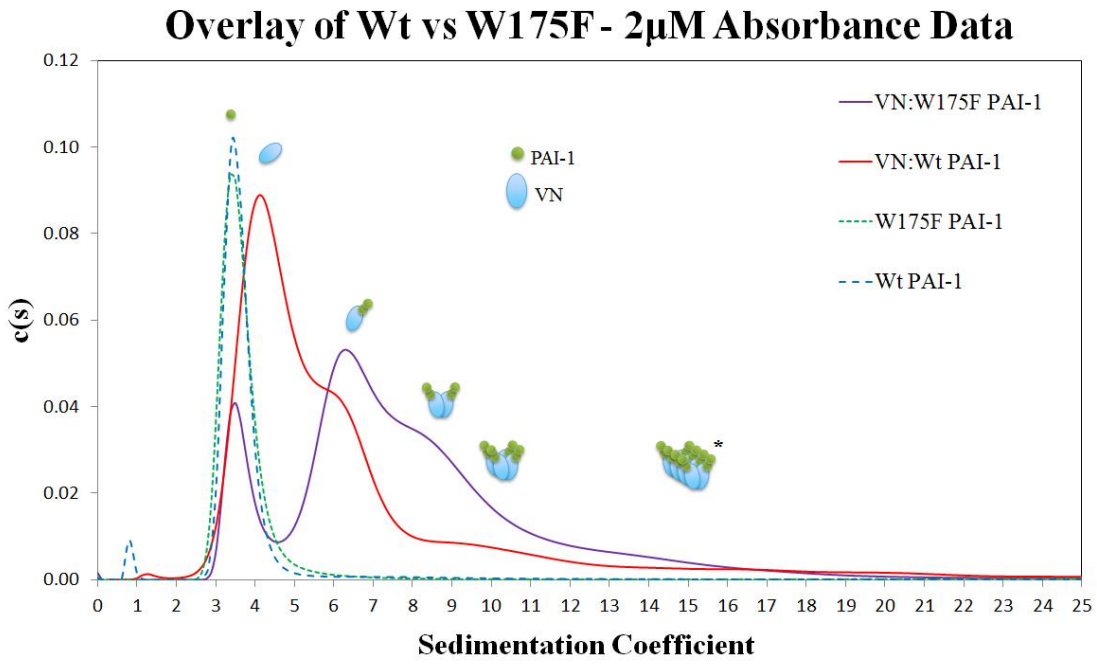

Figure 3.9 AUC Results – Wt PAI-1 vs W175F PAI-1 complex formation with VN

A mixture of PAI-1 variants and VN was studied using AUC. PAI-1 and VN were mixed at equimolar concentrations (2µM of each protein). The AUC data are overlaid with cartoons representing the species that each peak is composed of. The sedimentation coefficients of each of these species were identified previously [128]. Green circles represent PAI-1, and blue ovals represent VN. In each sample there is some un-complexed PAI-1 and VN seen in the peaks spanning sedimentation coefficient values from 3 to ~5. Peaks higher than 5.5S are from higher order complexes. This is represented by the cartoons of PAI-1 VN complexes at their respective sedimentation coefficients. Above 10S are higher order oligomers, represented by the complex with an asterisk. Free PAI-1 samples are shown in green (W175F) and blue (Wt) dashed lines. The VN:Wt PAI-1 mixture, shown as a solid red line, has un-complexed VN and PAI-1 present in addition to higher order complexes. The VN:W175F PAI-1 mixture, shown as a solid purple line, has un-complexed PAI-1 and a greater amount of complex formation than seen in the VN:Wt PAI-1 sample. This difference is likely due to the increased stability afforded by the W1175F mutation. During the course of an AUC experiment, Wt PAI-1 will convert to the latent form much more rapidly than W175F PAI-1, eliminating its ability to participate in a VN:PAI-1 complex.

3.3.c Studying PAI-1:VN interactions with HPLC

In our efforts to probe our hypothesis, we sampled several alternative experimental methods. We first attempted to use size exclusion High Pressure Liquid Chromatography (HPLC) to study the interaction between PAI-1 and VN. Using an S2000 column we were able to successfully identify the retention time for the different protein species. However, it soon became apparent that this method presented the same challenges as AUC. We were unable to fully test the interaction, or lack thereof, between the binding deficient PAI-1 variant and VN, as the micromolar concentration needed for the experiments was high enough to overcome the binding deficiency introduced by our mutations.

3.3.d Studying PAI-1:VN interactions with ELISA

Our next experimental approach took advantage of the sensitivity of Enzyme-Linked Immunosorbent Assays (ELISA) to study the PAI-1:VN interaction (figure 3.10). Following optimization of ELISA conditions for our system, preliminary data indicate that we could detect binding differences between VN and the different PAI-1 constructs. However, once again, the original binding deficient PAI-1 variants still demonstrated a residual ability to bind to VN in the assay (figure 3.11).

After the generation of the RMQ set of PAI-1 variants (figure 3.12) we were able to observe a marked decrease in the binding between the VN and the RMQW PAI-1 (figure 3.13) With this promising result, we progressed to analysis of the RMQW PAI-1 construct in PAI-1:PAI-1:VN complexes (figure 3.14). We observed that both Wt PAI-1 and W175F PAI-1 were able to

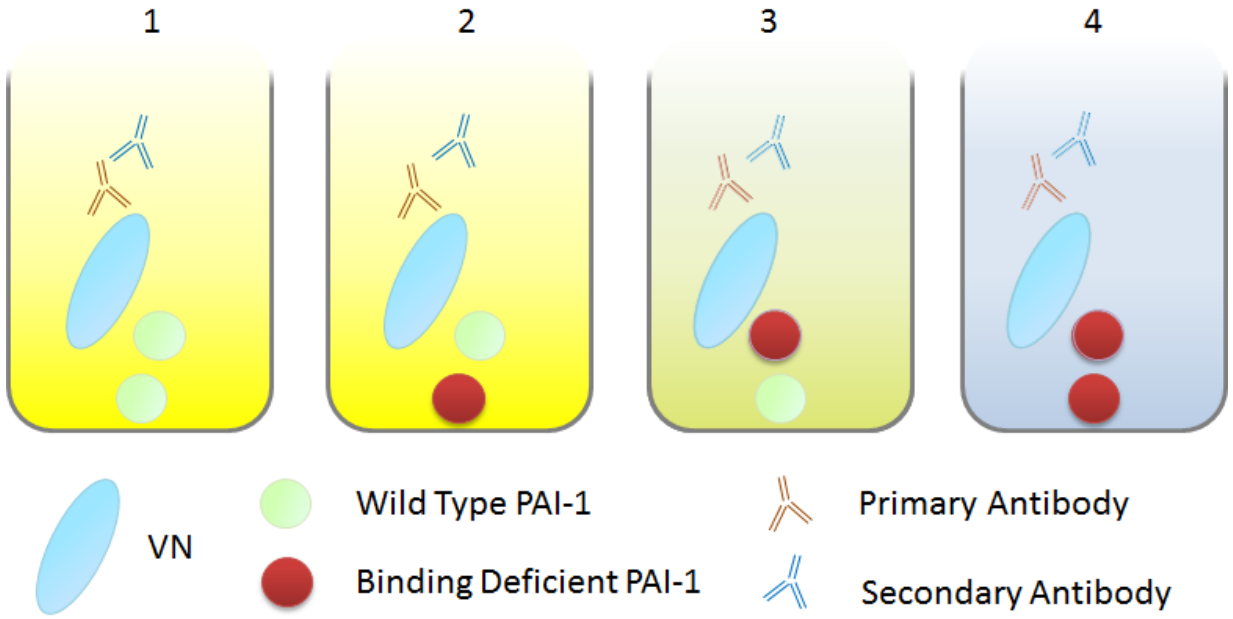

Figure 3.10 Experimental Concept for ELISA Studies

In order to study PAI-1:VN binding with ELISAs we conducted a series of experiments based on the concept illustrated above. PAI-1 was used as the coat protein. Subsequent to the blocking step a mixture of PAI-1 and VN was added to the wells. Next the primary, rabbit anti-VN, antibody was added, followed by a secondary, goat anti-rabbit, HRP-antibody. The above figure illustrates the results we expected if our hypothesis was correct. In the first two wells, we expected to see that the addition of Wt PAI-1 and VN would result in a color change. Well 1 would serve as the positive control, while well 2 would serve as a test of our hypothesis that Wt PAI-1 could mediate an interaction between bd PAI-1 and VN (figure 3.3). We expected that well 3 could have some color change (indicative of VN binding to the coat protein), but did not expect that it would have as distinct of a response. Well 4 served as a negative control, with two bdPAI-1 molecules there should be no color change occurring.

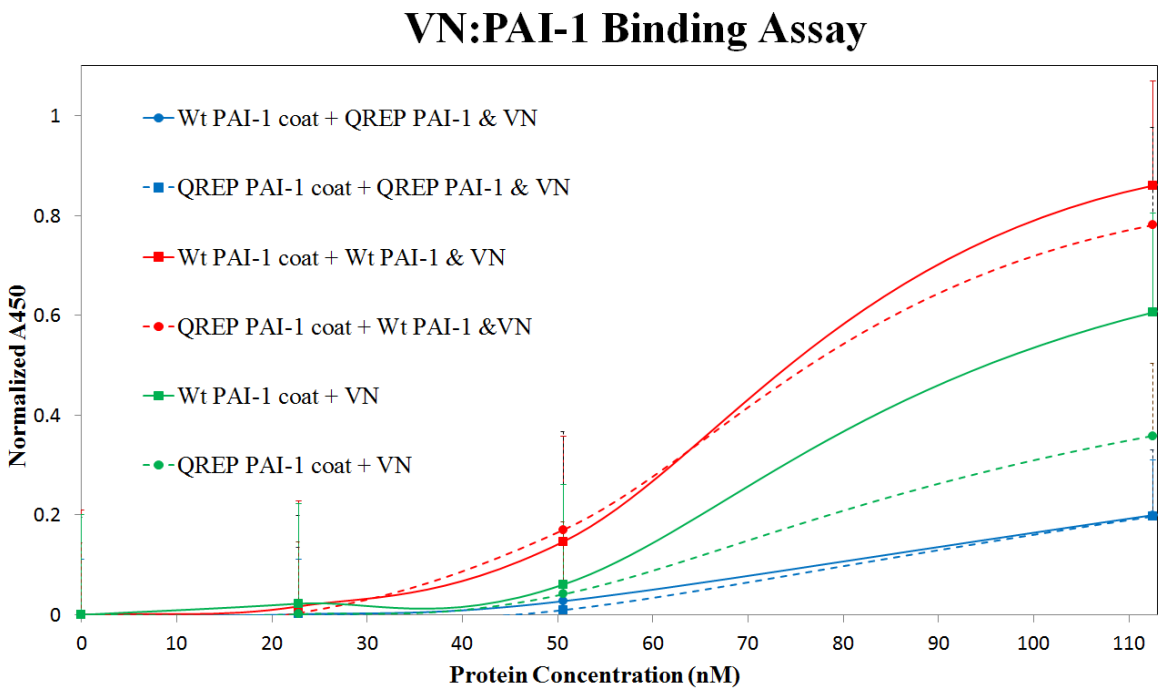

Figure 3.11 ELISA Results for Early PAI-1 Variants

PAI-1 was immobilized on the ELISA plate, and VN, or equimolar mixtures of PAI-1 and VN were added prior to detection via a polyclonal rabbit αVN antibody that was generated by our lab. Binding curves were generated by creating serial dilutions of VN alone or equimolar mixtures of PAI-1 and VN. Data were normalized to the highest A_{450} value for this experiment to render the data more easily comparable. Solid lines represent data collected when Wt PAI-1 was the coat protein. Dashed lines represent data collected when QREP PAI-1 was the coat protein. The data shown in green are VN binding to each PAI-1 construct alone. The data shown in red are from equimolar mixtures of Wt PAI-1 and VN added to the plate (0.5, 2, 4, 10, 20, 50, and 100nM of each protein). As can be seen from the red dashed line, addition of Wt PAI-1 alleviated some of the binding deficiency of QREP PAI-1. However, the data shown in blue, from equimolar mixtures of QREP PAI-1 and VN, (0.5, 2, 4, 10, 20, 50, and 100nM of each protein) indicate that the residual binding between QREP PAI-1 and VN is enough to limit interaction with the coat protein, and also suggest that the QREP mutation may interfere with possible PAI-1:PAI-1 interactions when QREP PAI-1 is acting as the primary PAI-1 molecule in the complex.

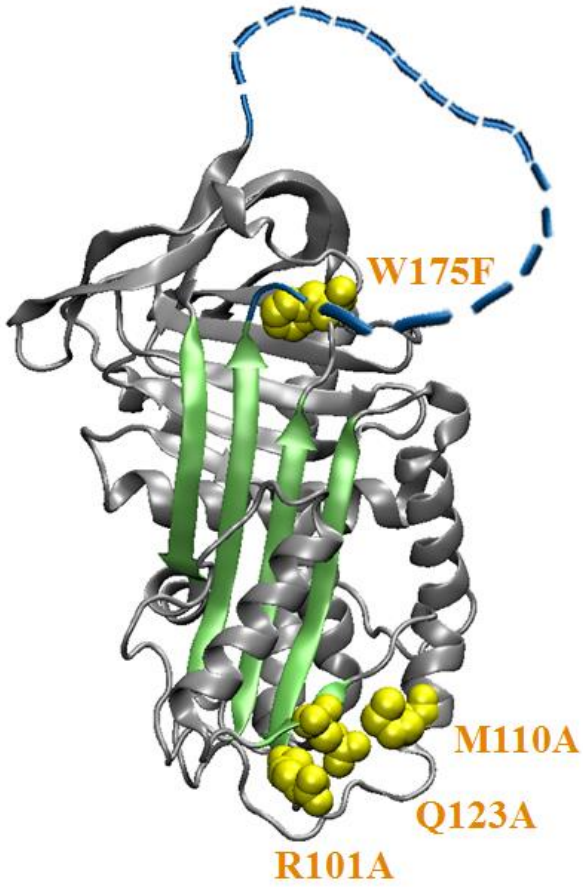

Figure 3.12 Second Set of Binding Deficient PAI-1 Constructs

The second set of mutations that we introduced to PAI-1 were based off of a set of mutants published by Jensen *et al* [190]. R101A, M110A, and Q123A have been shown to diminish VN binding. W175F was introduced as a stabilizing mutation. S338C (P9 in the RCL) was introduced to allow labeling of the PAI-1 construct.

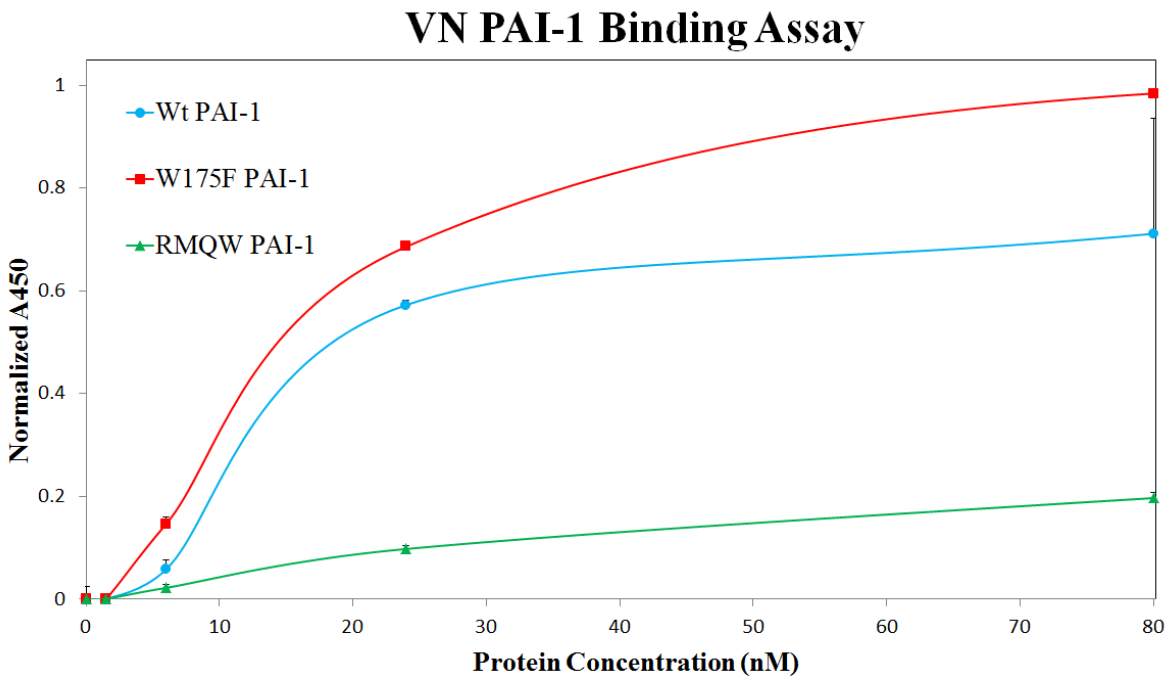

Figure 3.13 ELISA Results for PAI-1 Variants Binding to VN

VN was immobilized on the ELISA plate, and PAI-1 variants were added prior to detection via a polyclonal rabbit αPAI-1 antibody purchased from Molecular Innovations. Binding curves were generated by creating serial dilutions of PAI-1. Data were normalized to the highest A_{450} value for this experiment to render the data more easily comparable. Data from Wt PAI-1 are shown in blue, data from W175F PAI-1 are shown in Red, and data shown in green is from RMQW PAI-1. RMQW PAI-1 display a marked reduction in binding to VN in comparison with Wt and W175F PAI-1. The increased binding of W175F PAI-1 in comparison with Wt PAI-1 is likely due to the increased stability of the W175F PAI-1 construct.

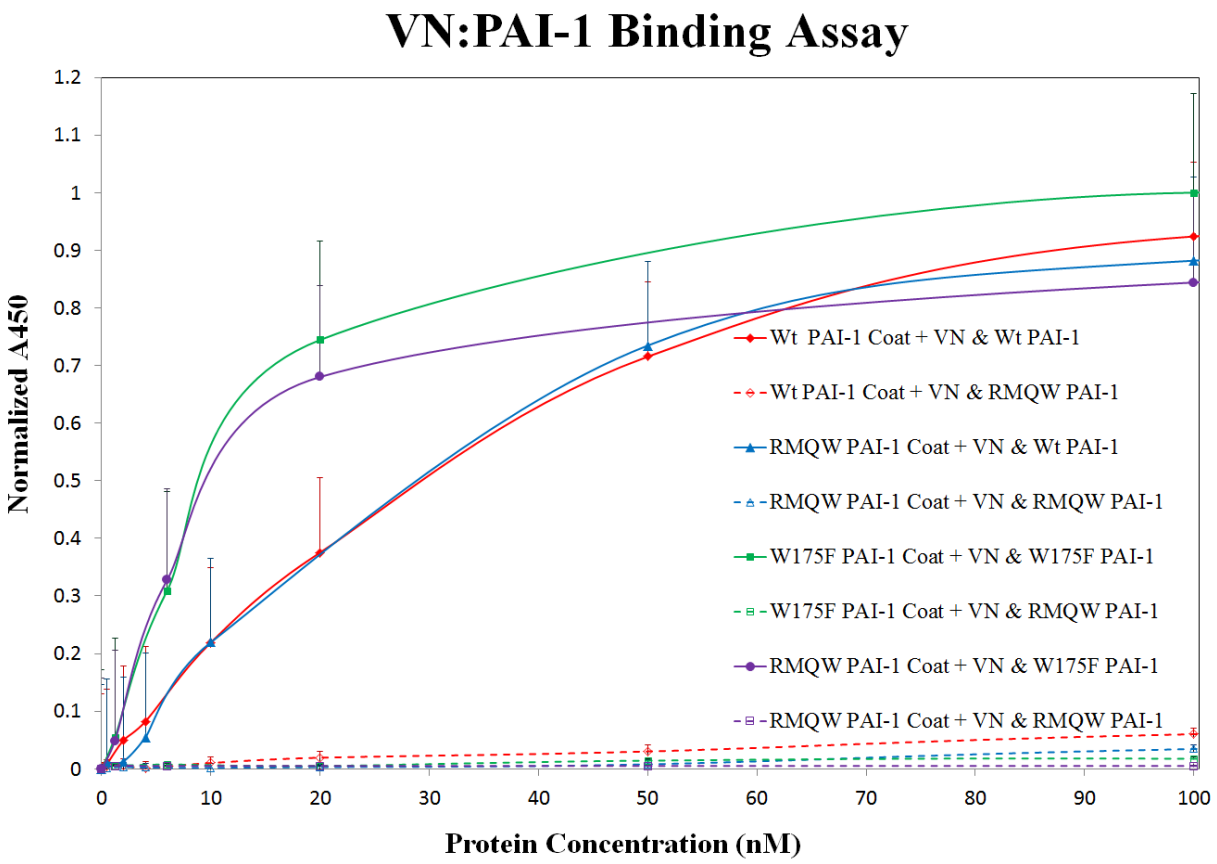

Figure 3.14 ELISA Results for Later PAI-1:VN Binding Studies

PAI-1 was immobilized on the ELISA plate, and VN, or equimolar mixtures of PAI-1 and VN were added prior to detection via a polyclonal rabbit αVN antibody that was generated by our lab. Binding curves were generated by creating serial dilutions of equimolar mixtures of PAI-1 and VN. Data were normalized to the highest A_{450} value for this experiment to render the data more easily comparable. Solid lines represent data collected when a VN binding PAI-1 variant was mixed with VN just prior to plate addition. Dashed lines represent data collected when a VN binding deficient PAI-1 variant was mixed with VN just prior to plate addition. Data shown in red are from a Wt PAI-1 coat with Wt, or RMQW PAI-1 mixed with VN added. Data shown in blue are from an RMQW PAI-1 coat with Wt, or RMQW PAI-1 mixed with VN added. Data shown in green are from a W175F PAI-1 coat with a mixture of W175F, or RMQW PAI-1 and VN added. Data shown in purple are from an RMQW PAI-1 coat with W175F, or RMQW PAI-1 mixed with VN added. There is a clearly observable difference between PAI-1:VN interactions when a VN binding PAI-1 is present. While RMQW PAI-1:VN mixtures produced almost no complex, RMQW PAI-1 was incorporated into complexes when Wt or W175F PAI-1 were present, indicating the existence of a PAI-1:PAI-1:VN interaction.

facilitate binding between binding deficient RMQW PAI-1 and VN. These data support the hypothesis that a PAI-1:PAI-1:VN complex exists when PAI-1 interacts with VN.

3.3.e SPR provides insight into the PAI-1:VN interaction

In order to study the PAI-1:VN interaction at lower concentrations we also turned to SPR. VN was immobilized on a CM5 chip, and PAI-1 was passed over the chip as the analyte. Preliminary experiments were conducted to measure the K_d of VN binding to the various PAI-1 constructs (table 3.2). An overlay of several PAI-1 construct's binding curves at 100nM is shown in figure 3.15. As the data demonstrate, the RMQ set of PAI-1 variants has a significantly reduced affinity for VN. This not only confirmed the efficacy of these mutations in eliminating PAI-1:VN interactions, it also demonstrated that the RMQ PAI-1 variant was a good candidate for study in the AUC.

We utilized the S338C mutation and labeled the P9 position of several PAI-1 variants with biotin to allow detection of labeled PAI-1 independently of a change in response units (figure 3.16). However, streptavidin appeared to pull some of the P9*biotin PAI-1 off of the chip, particularly at higher concentrations of PAI-1. We determined a lower concentration of streptavidin should be used for future experiments and this alleviated most of the PAI-1 removal.

Further SPR experiments were conducted with RMQ PAI-1 variants with and without the biotin label. Our results indicated that W175F PAI-1 may be able to facilitate incorporation of RMQP*biotin PAI-1 into complex with VN. This phenomenon is more noticeable at lower (5nM and 20nM) concentrations of the RMQP*b PAI-1 variant (figure 3.17). During the course of our SPR experiments we observed that the biotin label affects the ability of W175F PAI-1 to

Table 3.2 K_d for Selected PAI-1 Variants

SPR was used to determine the dissociation constant for VN and several PAI-1 constructs. In several cases multiple experiments allowed for an average of the measured K_d values, however not all binding experiments were replicated.

Measured K_d values for PAI-1 Variants			
PAI-1 Variant	*K_d*	*Std. Dev.*	*# data sets*
Wt	3 nM	n/a	(1)
W175F	2 nM	1.8 nM	(4)
P9	3 nM	1.8 nM	(4)
RMQ	1,430 nM	304 nM	(3)
RMQW	719 nM	n/a	(1)
RMQP*biotin	1,410 nM	n/a	(1)

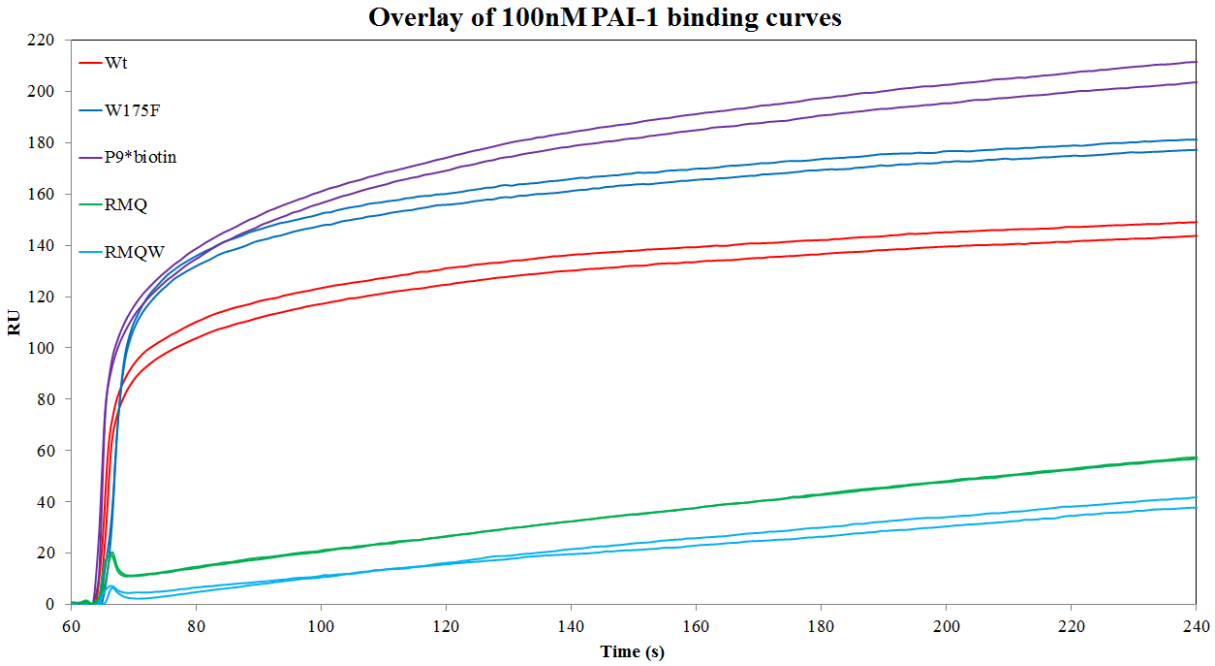

Figure 3.15 SPR Binding Curves for Several PAI-1 Variants to VN at 100nM

Several PAI-1 variants were flowed over immobilized VN at a concentration of 100nM. As can be seen in the data, RMQ PAI-1 (green) and RMQW PAI-1 (cyan) have diminished affinity for VN in comparison to Wt PAI-1 (red), W175F PAI-1 (blue), and P9*biotin PAI-1 (purple). Duplicates of all conditions are shown.

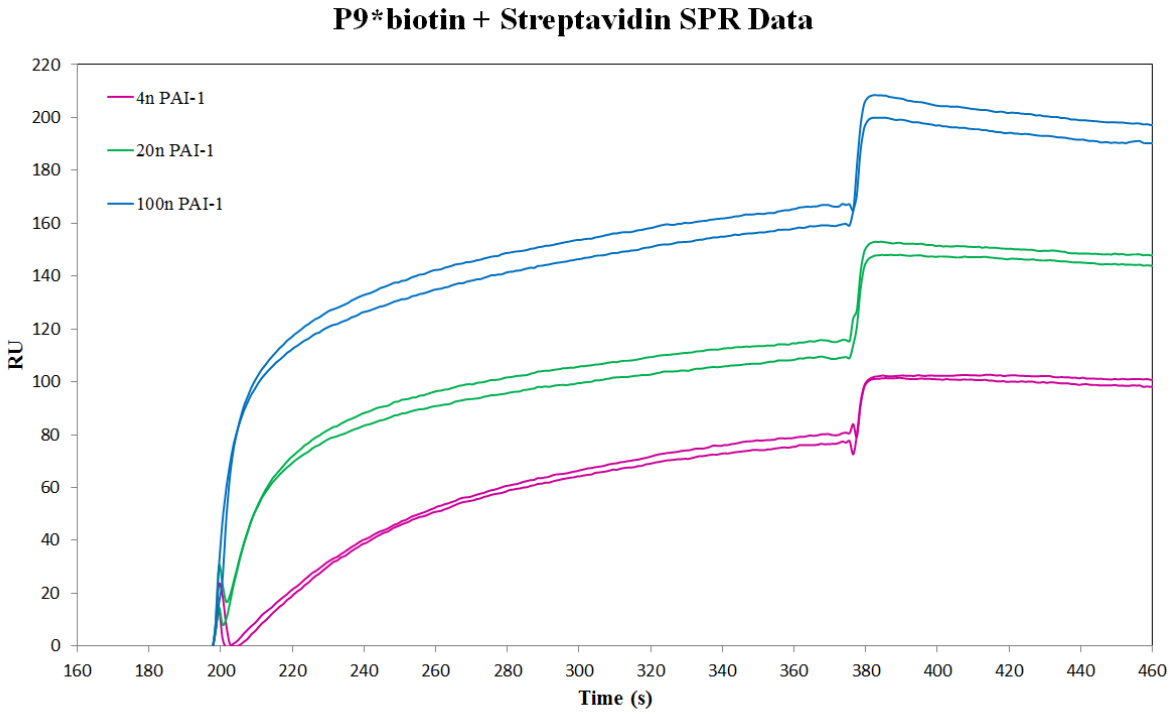

Figure 3.16 Streptavidin Confirms the Presence of Biotin Labeled PAI-1 in PAI-1:VN Complex on SPR Chip

Three concentrations of P9*biotin PAI-1 were flowed over the VN immobilized CM5 chip and binding was measured in response units (RU). Duplicates of each concentration are shown. Immediately following the P9*biotin PAI-1 injection, at ~375s, streptavidin was added at a concentration of .2mg/mL. The data demonstrate that streptavidin interacts with biotin labeled PAI-1 on the SPR chip. Controls were performed, not shown, which demonstrate that streptavidin does not interact with unlabeled PAI-1 or immobilized VN. Duplicates of all conditions are shown.

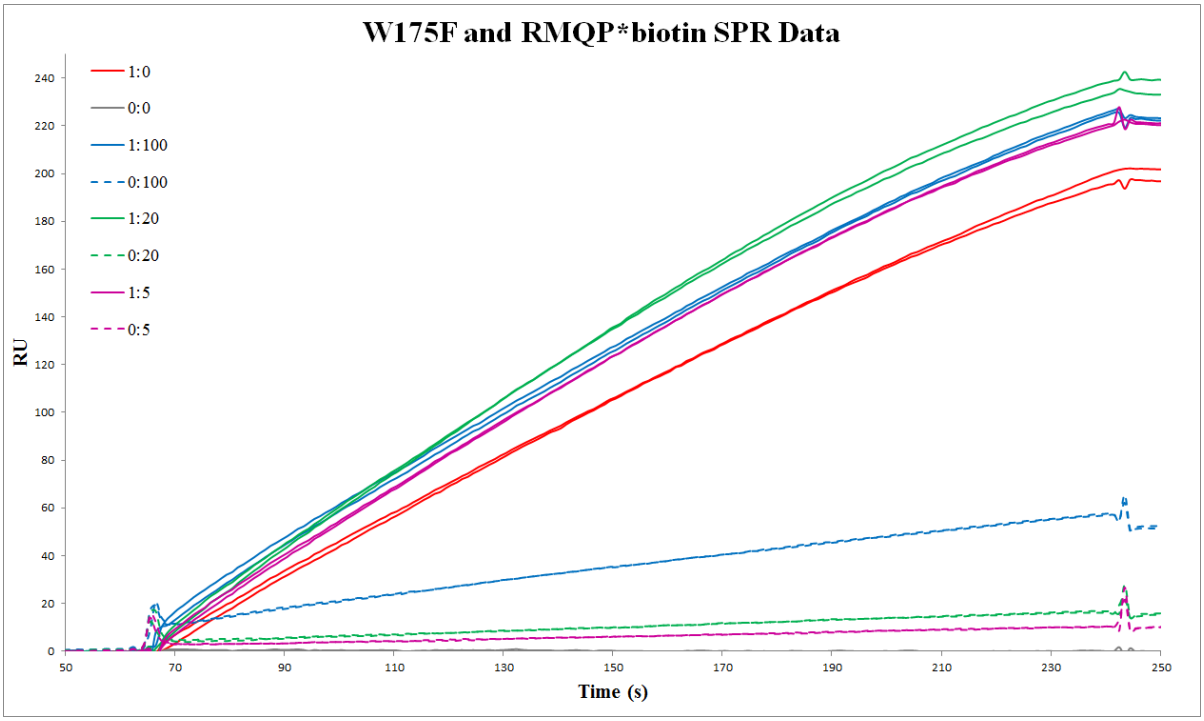

Figure 3.17 SPR Binding Data of W175F PAI-1 and RMQP*biotin PAI-1

1nM of W175F PAI-1 was mixed with varying concentrations of RMQ PAI-1 so that it could facilitate the interaction of RMQ PAI-1 with the VN chip. RMQ PAI-1 was also added to the chip without W715F PAI-1 present as a control. The labeling system in the legend is (concentration of W175F PAI-1):(concentration of RMQ PAI-1), thus the 1:0 data shown in red are from 1nM W175F PAI-1 with no RMQ PAI-1. Our results indicate that W175F PAI-1 may be able to facilitate incorporation of RMQP*biotin PAI-1 into complex with VN. This phenomenon is more noticeable in the difference between RMQP*biotin PAI-1 alone and in the presence of W175F PAI0-1 at lower (5nM and 20nM) concentrations of the RMQP*b PAI-1 variant. Duplicates of all conditions are shown.

mediate an interaction between the labeled RMQ PAI-1 variant and VN (3.17, 3.18 and 3.19). When mixtures of unlabeled RMQ PAI-1 and W175F were injected over the VN chip, an increase in PAI-1 concentration resulted in an increase in RUs. However, when biotin labeled RMQWP PAI-1, or RMQP PAI-1, was mixed with W175F, an increase in biotin labeled PAI-1 resulted in a decrease in RU at concentrations above 50nM of the labeled proteins. This phenomenon was observed for multiple biotin labeled PAI-1 constructs. These data suggest that the biotin label interferes with complex formation, and possible PAI-1 dimerization.

It is interesting to note that the biotin label only affects the PAI-1:PAI-1 interaction as labeled and un-labeled bind to the VN chip equally (data not shown). These data supports a mechanism of interaction wherein the RCL of the second PAI-1 molecule is involved in binding to the first PAI-1. Further studies would need to be performed in order to fully confirm this finding. Due to the disrupting effect that the biotin label has in the presence of W175F PAI-1, SPR was not utilized for further study of the complex. However, it has provided useful data regarding the affinity of PAI-1 variants for VN, and also suggests a possible mechanism by which the two PAI-1 molecules interact.

3.3.f Probing the PAI-1:VN complex with AUC – Revisiting the Method

Following the generation of the RMQ PAI-1 variants, we decided to study the complex using AUC again, reasoning that since the RMQ PAI-1 variants have such a low affinity for VN (table 3.2) they would result in more meaningful AUC data than we were previously able to collect. Following standard AUC protocol, RMQP PAI-1, freshly labeled with NBD, was dialyzed overnight in PBS pH 7.4. The next day several samples were generated, RMQP*NBD PAI-1

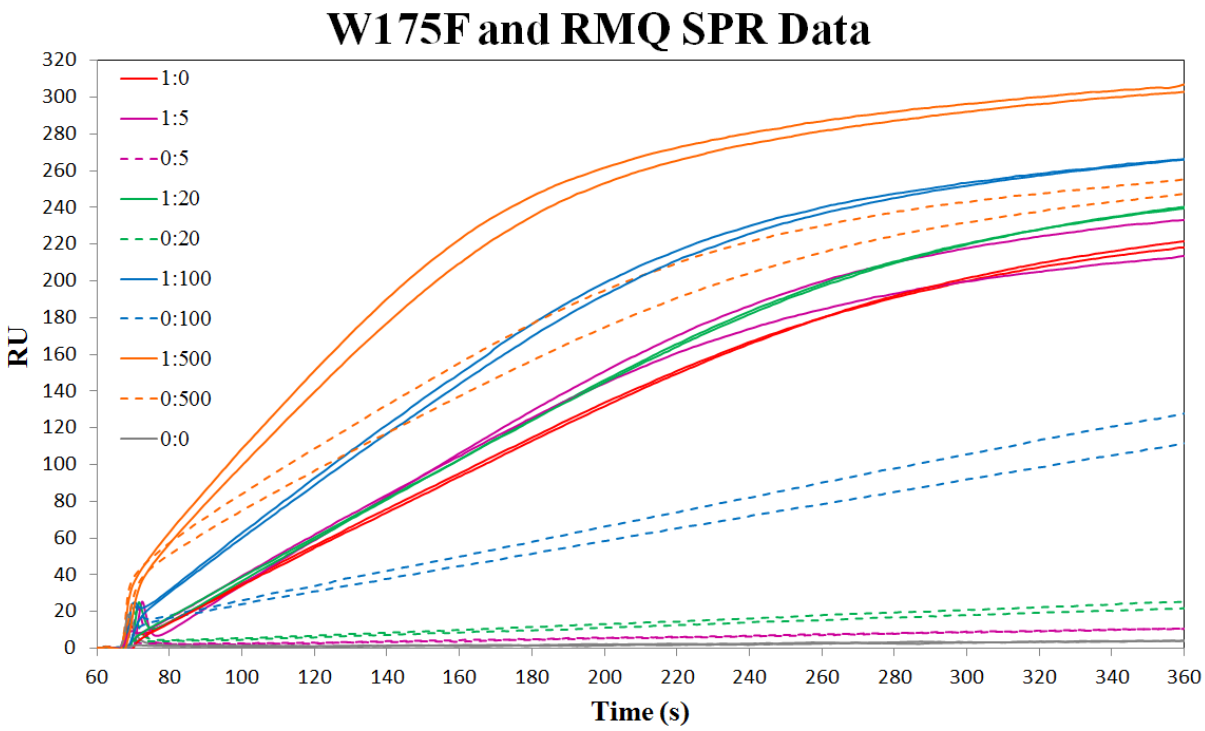

Figure 3.18 SPR Binding Data of W175F PAI-1 and RMQ PAI-1on a VN Chip

1nM of W175F PAI-1 was mixed with varying concentrations of RMQ PAI-1 so that it could facilitate the interaction of RMQ PAI-1 with the VN chip. RMQ PAI-1 was also added to the chip without W715F PAI-1 present as a control. The labeling system in the legend is (concentration of W175F PAI-1):(concentration of RMQ PAI-1), thus the 1:0 data shown in red are from 1nM W175F PAI-1 with no RMQ PAI-1. Data from samples with W175F PAI-1 present are shown as solid lines. Data without W175F PAI-1 are displayed with dashed lines. These data shows that as RMQ PAI-1 concentration increases, RU increases, both with and without W175F PAI-1 to facilitate the interaction. Duplicates of all conditions are shown.

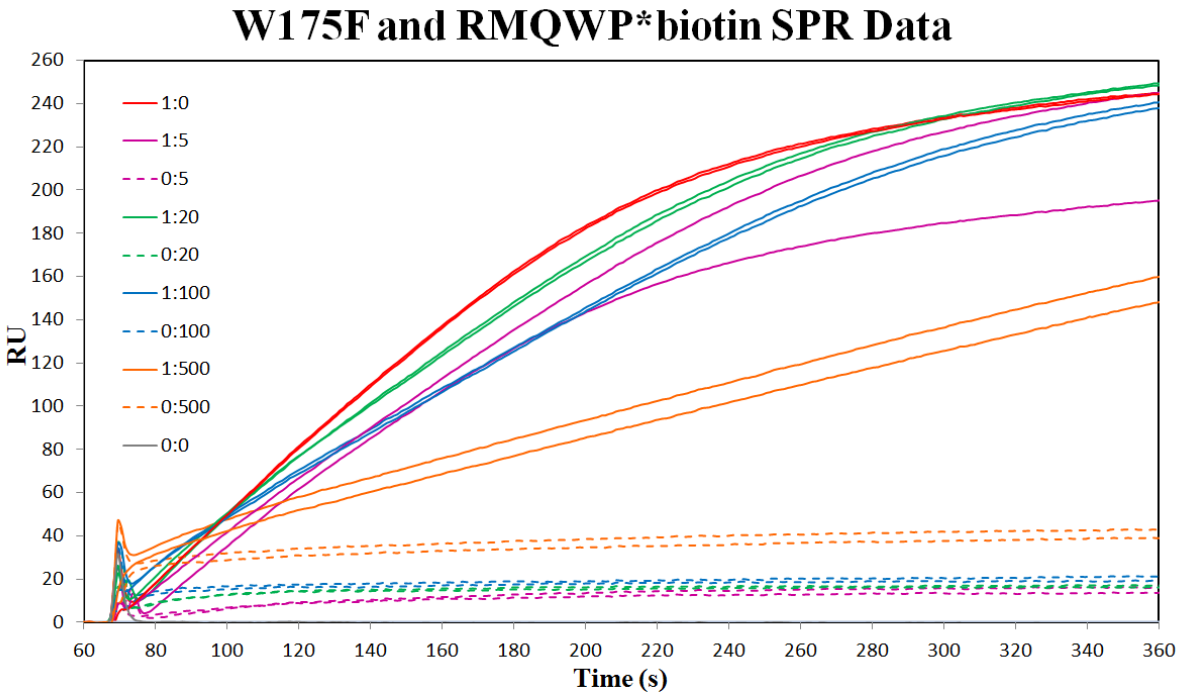

Figure 3.19 SPR Binding Data of W175F PAI-1 and RMQ*biotin PAI-1on a VN Chip

1nM W175F PAI-1 was mixed with varying concentrations of RMQWP*biotin PAI-1 so that it could facilitate the interaction of RMQQP*biotin PAI-1 with the VN chip. RMQWP*biotin PAI-1 was also added to the chip without W715F PAI-1 present as a control. The labeling system in the legend is (concentration of W175F PAI-1):(concentration of RMQWP*biotin PAI-1), thus the 1:0 data shown in red is 1nM W175F PAI-1 with no RMQWP*biotin PAI-1. Data from samples with W175F PAI-1 present are shown as solid lines. Data without W175F PAI-1 are displayed with dashed lines. The data show that as RMQWP*biotin PAI-1 concentration increases, RU decreases when in the presence of W175F PAI-1. It appears that the biotin label has a negative effect on the ability of RMQWP*biotin PAI-1 to interact with W175F PAI-1and/or VN. This dampening effect is seen throughout our data. Duplicates of all conditions are shown.

alone, RMQP*NBD PAI-1 & VN, RMQP*NBD PAI-1, Wt PAI-1, & VN, as well as controls without NBD labeled RMQP PAI-1. These samples were and promptly loaded into pre-assembled AUC cells. Data were collected at A_{500} in order to detect the NBD label only. Interference data were also collected to act as a control. Once the AUC had equilibrated for ~45min the centrifuge was brought up to speed and data were collected for ~20 hours overnight.

Data were analyzed in Sedfit and the distribution tables were used to generate data overlays so that the samples would be more readily comparable. As can be seen in the AUC data in figures 3.20 and 3.21, NBD labeled RMQP PAI-1 was only detectable in complexes when Wt PAI-1 was present to mediate the interaction. Additionally RMQP*NBD PAI-1 was only observed in complexes of 2:1 and higher (S = 6.5 and above). In order to confirm these findings we repeated the experiment with freshly purified and NBD labeled RMQP PAI-1 at a higher concentration of protein and observed that RMQP*NBD PAI-1 incorporation into higher order complexes was increased when Wt PAI-1 was present (figures 3.22 and 3.23). A small amount of RMQP*NBD PAI-1:VN appears to have formed, but no significant presence in higher order complexes was observed without Wt PAI-1 present. These data positively confirm our hypothesis that PAI-1 forms a dimer when in 2:1 complexes with VN.

3.4 Discussion

Using a multitude of experimental techniques, we sought to test the hypothesis that PAI-1 and VN interact in a PAI-1:PAI-1:VN manner when in higher order complexes. Our initial AUC experiments were unable to fully probe this hypothesis due to the residual affinity that the QRE PAI-1 variants retained for VN and the high concentration of protein required for AUC

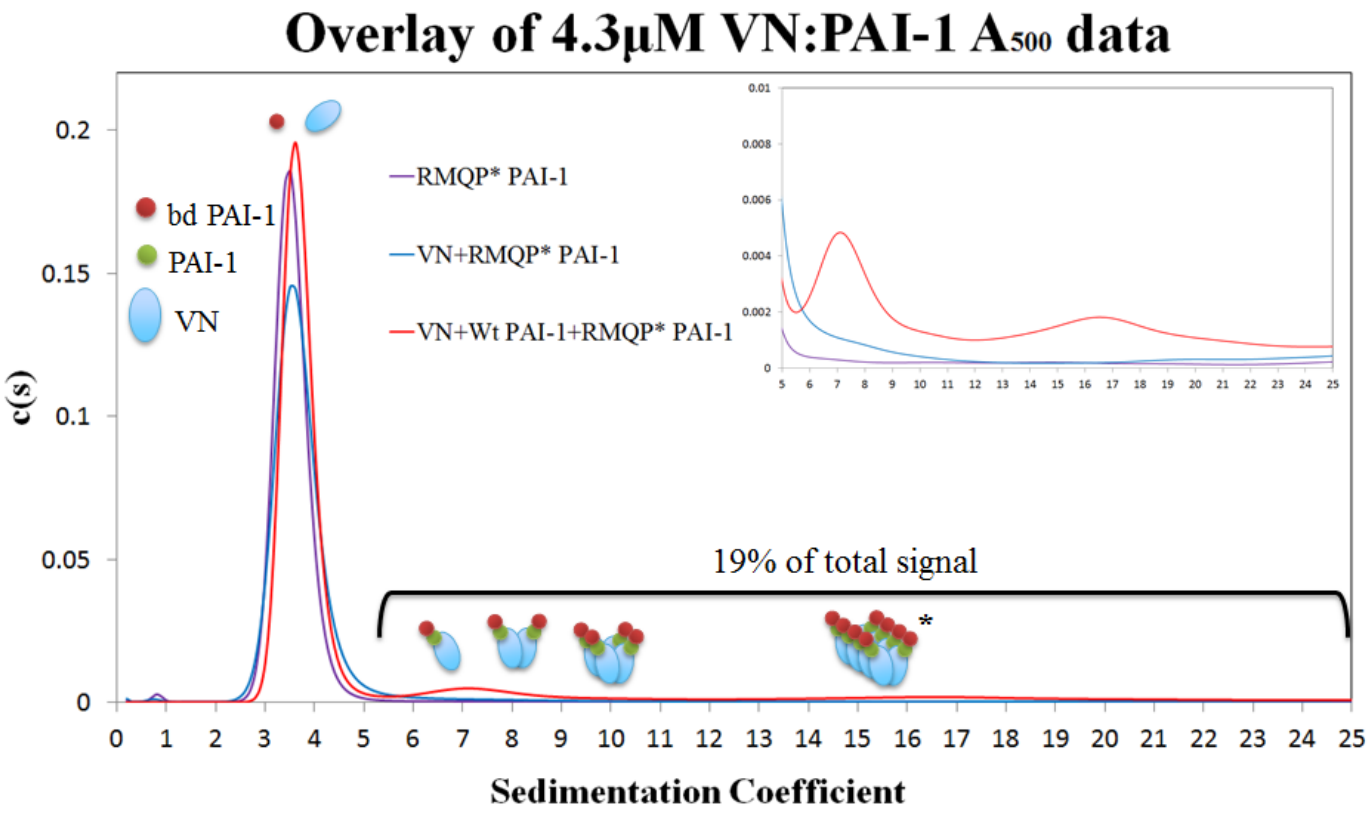

Figure 3.20 4.3µM A_{500} AUC Data for RMQP*NBD PAI-1:VN complex formation

PAI-1 and VN were dialyzed overnight in PBS pH 7.4. Following dialysis, proteins were spun to remove precipitants. Immediately before loading into preassembled AUC cells, PAI-1 and VN were mixed in equimolar ratios. These samples were then incubated at 25°C for ~45min prior to data collection overnight. Absorbance was measured at 500nm in order to detect signal from the NBD label. The inset in the top right corner is a close up view of the data from 5S to 25S. The data demonstrate that when Wt PAI-1 is present, RMQP*NBD PAI-1 is incorporated into higher order PAI-1:VN complexes.

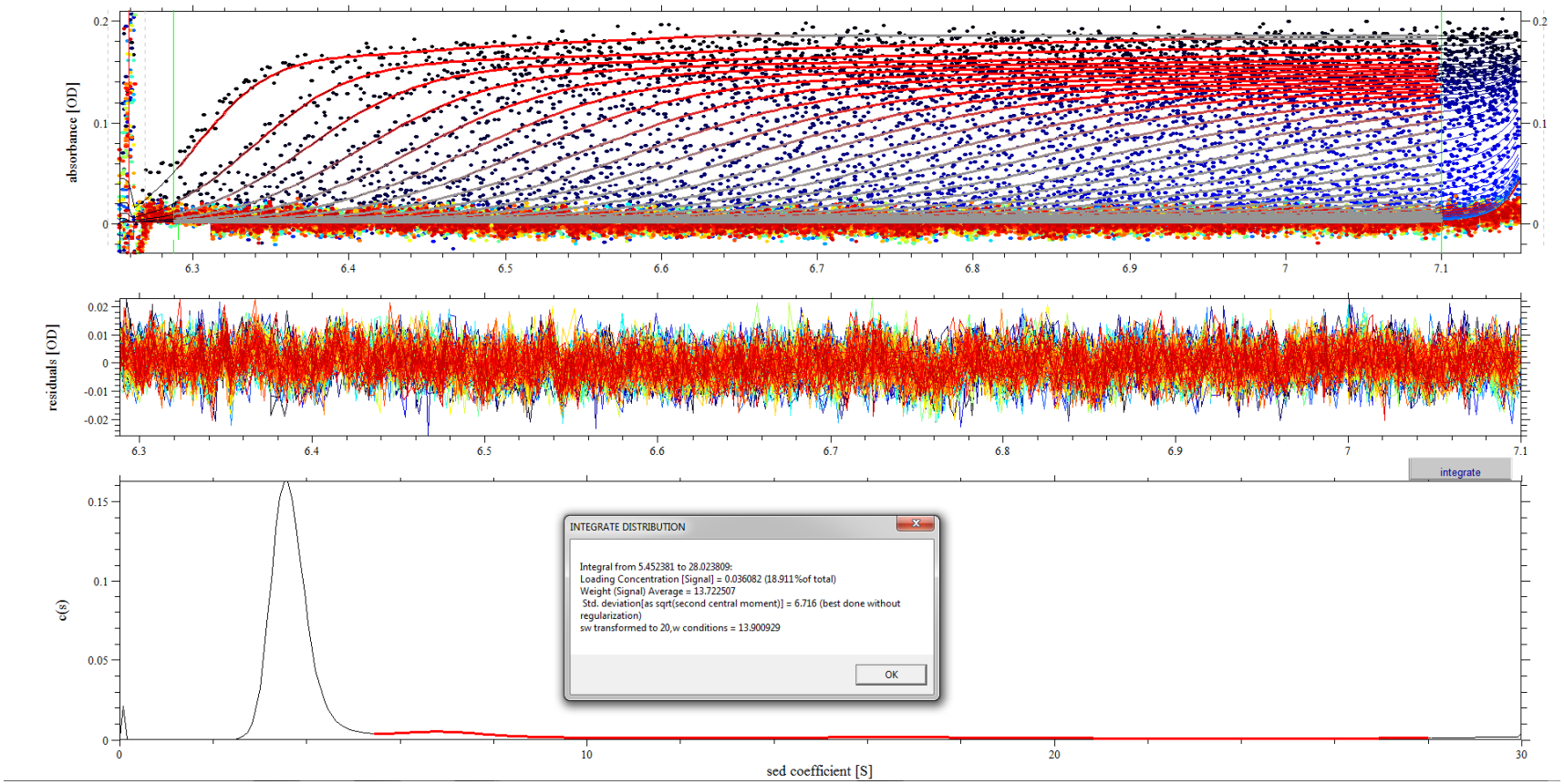

Figure 3.21 AUC Data: Amount of Higher Order Complex in 4µM Data Set

We used the built in integration tool in Sedfit to determine the percentage of higher order complex found in the total AUC signal. Data were integrated starting at 5.45 [S], just below the sedimentation coefficient for 1:1 complexes to 28 [S]. It was determined that 19% of the total signal was found in higher order complexes, clearly demonstrating the incorporation of RMQP*NBD into the PAI-1 VN complex.

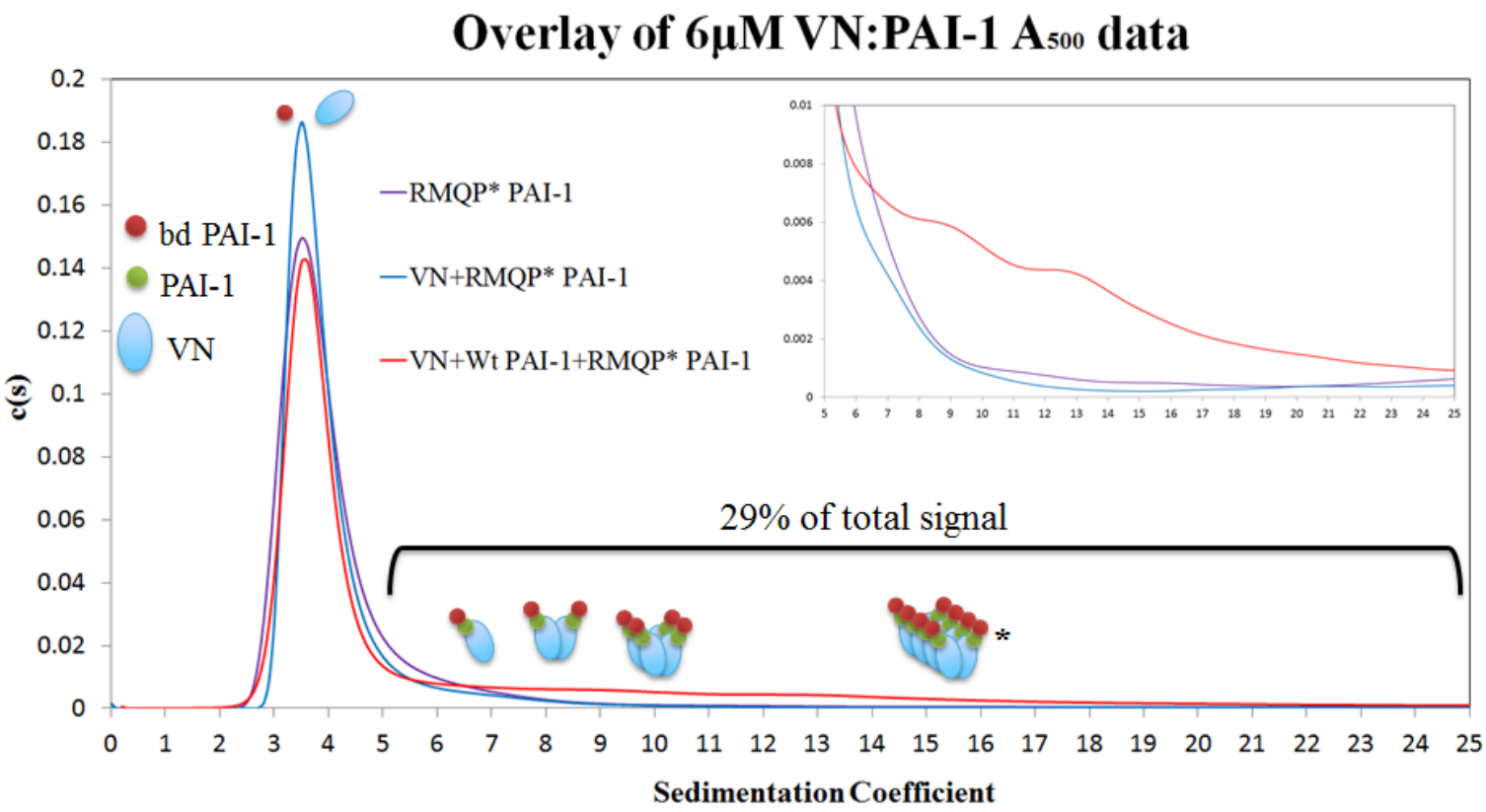

Figure 3.22 6µM A_{500} AUC Data for RMQP*NBD PAI-1:VN complex formation

PAI-1 and VN were dialyzed overnight in PBS pH 7.4. Following dialysis, proteins were spun to remove precipitants. Immediately before loading into preassembled AUC cells, PAI-1 and VN were mixed in equimolar ratios. These samples were then incubated at 25°C for ~45min prior to data collection overnight. Absorbance was measured at 500nm in order to detect signal from the NBD label. The inset in the top right corner is a close up view of the data from 5S to 25S. The data demonstrate that when Wt PAI-1 is present, RMQP*NBD PAI-1 is incorporated into higher order PAI-1:VN complexes.

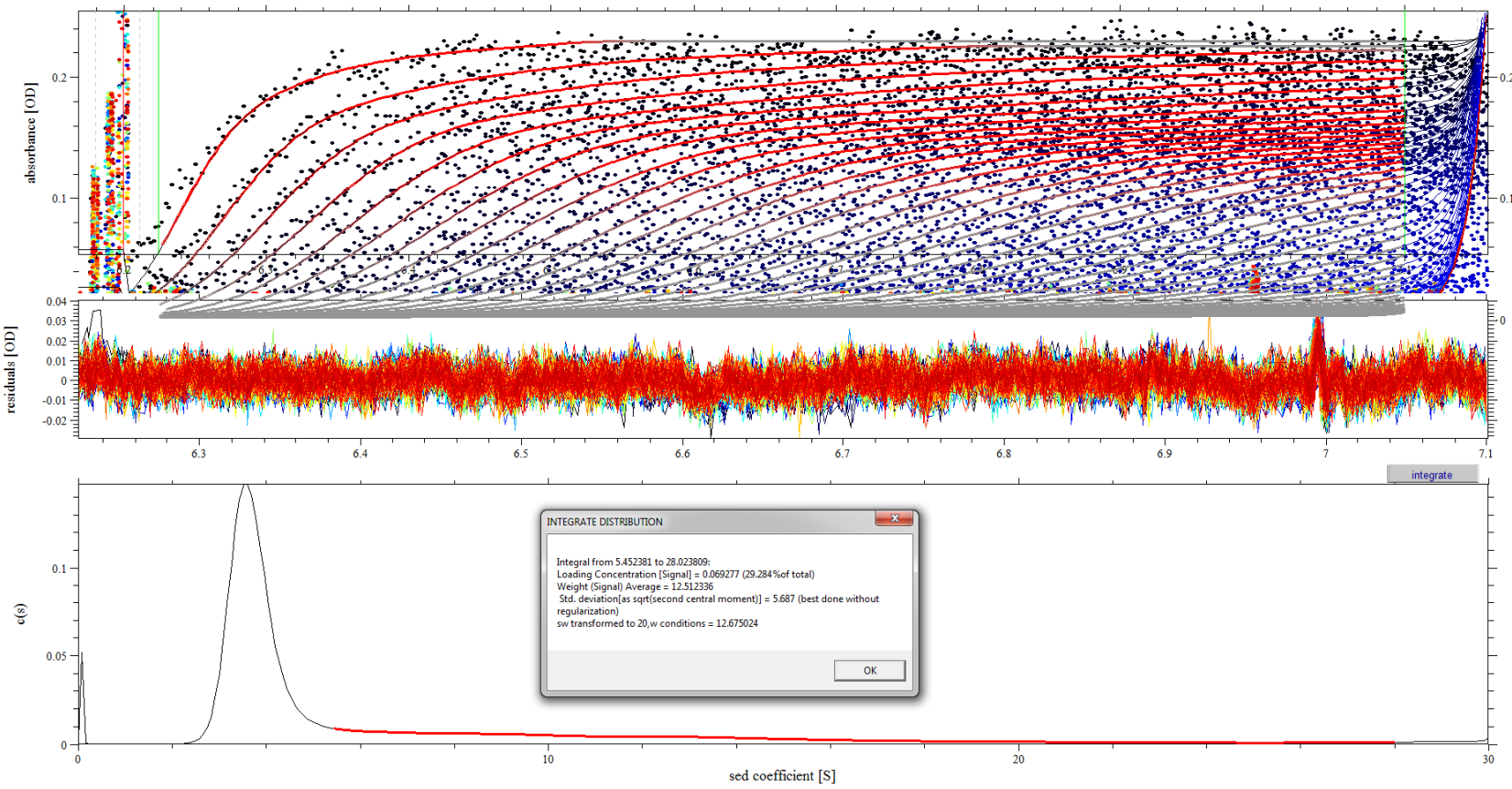

Figure 3.23 AUC Data: Amount of Higher Order Complex in 6µM Data Set

We used the built in integration tool in Sedfit to determine the percentage of higher order complex found in the total AUC signal. Data were integrated starting at 5.45 [S], just below the sedimentation coefficient for 1:1 complexes to 28 [S]. It was determined that 29% of the total signal was found in higher order complexes, clearly demonstrating the incorporation of RMQP*NBD into the PAI-1 VN complex.

experiments. We sought to utilize HPLC, but again discovered that the method was not sensitive enough for our needs. We also studied the complex using ELISAs however; the QRE PAI-1 variants retained too great an affinity for VN. We concluded that the QRE PAI-1 variant was not useful for these studies and turned to a new binding deficient PAI-1 for further investigation of the PAI-1:VN interaction.

We began using a new PAI-1 variant, RMQ PAI-1. This new PAI-1 construct was a much more effective tool for studying the PAI-1:VN complex. Our ELISA data demonstrate that RMQW PAI-1 was able to participate in PAI-1:VN complexes when Wt or W175F PAI-1were present, but not with VN alone, or when RMQW PAI-1 was added in conjunction with VN.

The data from our AUC experiments, performed with the RMQ PAI-1 variant also confirm that Wt PAI-1 is able to mediate incorporation of VN binding deficient PAI-1 into a PAI-1:VN complex. These results also provided insight into the distribution of RMQ*NBD PAI-1, confirming that it is able to assemble into higher order complexes, when in the presence of Wt PAI-1: and VN.

Together, our ELISA and AUC data support our hypothesis via two independent methods. These data, combined with the SANS model, support a new model for PAI-1:VN interactions. This model greatly advances the field and facilitates efforts into developing therapeutic agents that target the PAI-1:VN complex. New therapies can be developed that focus on disrupting PAI-1:PAI-1 dimers. Additionally, the confirmation that a single PAI-1 interacts at both the primary and secondary site will facilitate binding studies and development of inhibitors that seek to target the PAI-1:VN interface.

Our SPR data reveal that the biotin label interferes with the ability of W175F to mediate an interaction between biotin labeled RMQ PAI-1 variants and VN. These findings provide

insight into the mechanism by which the PAI-1 molecules interact. An alternative labeling site could be used to better monitor PAI-1 interactions. While no specific information about the exact interaction has been revealed, the SPR results indicate that the RCL of the second PAI-1 is responsible for interaction with the first PAI-1 molecule. Future research will focus on the finer details of this interaction, such as how the two PAI-1 molecules interact with each other. Zhou *et al* proposed several different methods by which PAI-1 could polymerize and these models would be an excellent starting point for future study (figure 3.24) [33]. It is important to note PAI-1 has been seen to adopt the s7A linkage under crystallization conditions [191], but whether this polymerization method is valid for PAI-1 under physiological conditions remains to be seen. The crystalized PAI-1 polymer formed a long chain, which is not seen under physiological conditions. Thus, even if PAI-1 interacts via an s7a linkage there are definitive differences between physiological PAI-1:VN interactions and the long chain polymer seen in the literature.

It would also be valuable to determine if both PAI-1 molecules in the 2:1 complex are fully active, and also if both can act simultaneously. In their study, Zhou *et al* noted that PAI-1 polymers are unique in that they can dissociate into functional monomers. This indicates that both PAI-1s are active in complex, but does not address the question of whether both PAI-1 molecules are able to function as inhibitors simultaneously. It is improbable that both can simultaneously inhibit proteases, as the RCL mediated dimerization is the most likely mode of interaction. More likely, one of the two PAI-1 molecules is available for PA inactivation, and upon cleavage and loop insertion of one PAI-1 molecule, the other becomes free to inhibit PAs.

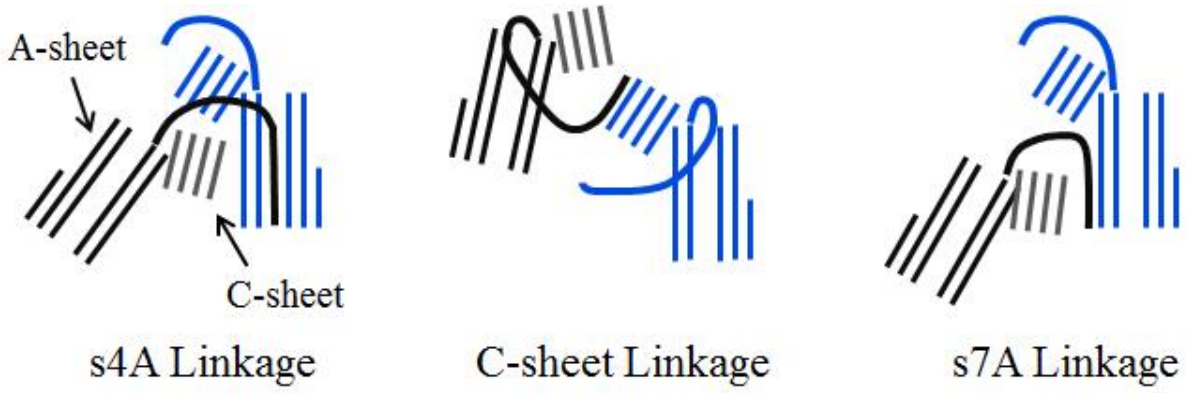

Figure 3.24 Illustrated Scheme of Serpin Polymerization

Three possible mechanisms by which PAI-1 could form dimers are shown in this figure adapted from Zhou *et al* (for more details, and three dimensional structural representation of see the original work) [81]. Due to the fact that PAI-1 is still able to act against PAs when in higher order complexes, it is unlikely that PAI-1 dimerizes via the s4A linkage model, leaving two possible models for interaction. PAI-1 has been shown to form a long chain s7A linkage polymer under crystallization conditions [191] making this mode of interaction an ideal model to test in initial experiments to probe the method by which PAI-1 can dimerize.

Chapter 4 - Effect of PAI-1 binding on the IDD of VN

4.1 Introduction

4.1.a Vitronectin Overview

Vitronectin (VN) was first identified as a serum spreading factor that enabled mammalian cells to adhere to culture vessels [192, 193]. Through the application of antibodies, it was found that VN is present at the cell surface and is a component of the ECM [194]. Additionally, it was found that application of antibodies against VN was sufficient to inhibit the rate of cell migration, thus confirming the role of VN as a serum spreading factor [195]. Over the years, many binding partners have been identified for VN including plasminogen [196], fibrinogen [197], a variety of intergrins [198-200], uPAR [201], heparin [202], and PAI-1[167]. These binding partners affect VN structure and function and have been the subject of many studies.

The structure of full-length VN has not been experimentally determined. However, a combination of computational analysis, experimental studies, and the high resolution crystal and solution structures of the n-terminal SMB domain have been combined to generate three-dimensional models [89, 92, 94, 203, 204], one of which is shown in figure 1.5. The SMB domain is composed of the first 44-50 amino acids. The only classic secondary structural elements in the SMB domain are a single turn alpha helix, and a partial 3-10 helix. The remainder of this domain is composed of unstructured loops and coils, held in place by four disulfide linkages.

The next domain of VN is composed of residues from approximately 48 through 130. This domain contains no secondary structure, and conforms to the requirements for classification as an intrinsically disordered domain (IDD) [122]. The IDD is an understudied domain of this

glycoprotein, likely due in part to the difficulty of studying a disordered protein region. Lastlly, the central domain consists of residues 131 - 342, and the C-terminal domain includes residues 347 - 359. These domains are rich in β secondary structure and have been computationally predicted to fold into a β-propeller type structure and β-blade (half a propeller) type structure respectively [83, 89].

4.1.b Intrinsically Disordered Proteins and VN

For decades, the concept of protein function was intimately tied to protein structure [102, 103, 205]. Lack of protein structure was often associated with a lack of function [206]. However, in recent years, the role of disorder has attracted new interest. Studies of intrinsically disordered proteins and protein domains have shown that these disordered regions have a functional aspect [207, 208]. In many cases, intrinsically disordered proteins, or domains, have been seen to adopt various structures and conformations based on their binding partners [209]. Even when classical secondary structure is not adopted by the IDD/IDP, the disordered region may associate with the binding partner through "disordered" loops. This unique ability allows proteins containing a disordered region to have an increased versatility in binding partners compared to traditional proteins due to the adaptable nature of disordered domains [107, 110]. The second domain of VN has not been a focus of much study over the years. However, with the recent interest in intrinsic disorder, there are new insights into the possible role of the IDD of VN in its many biological functions. The IDD of VN could play a key role in the adaptability of VN, diverse binding interactions, incorporation into the ECM, and more.

4.1.c A Brief Review of PAI-1:VN interactions

PAI-1 binding to VN causes a conformational change in VN that is associated with a permanent conformational change in VN leading to the formation of VN oligomers. Notably, this conformational change occurs on a much faster time scale than that of VN oligomerization, which indicates that the conformational change is specifically due to PAI-1 binding [21]. The specific nature, of this conformational change is currently unknown, and further insight into this change would be beneficial to the field of VN biochemistry and the study of disordered proteins.

PAI-1 and VN interact at two separate sites. The primary site of interaction is well characterized [77, 136]. However, only small details are known about the secondary sites of interaction between these two proteins. A secondary binding site for VN has been identified on PAI-1 through mutagenesis and binding studies. This site overlaps with the PAI-1 heparin binding region and contains a number of key, basic, residues (figure 3.2) [137].

The secondary binding site for PAI-1 on VN is still under debate [142]. There are two regions that have been proposed to contain a secondary PAI-1 binding site. The first, is found in the heparin binding region of VN, comprising residues 348-370, found in the C-terminal domain [140, 144]. Another proposed binding site is found in 115 - 131, of the disordered domain of VN [143, 210]. Further studies are needed to conclusively localize the secondary PAI-1 binding domain in VN. However, the number of positively charged residues that are crucial to the binding interface support the localization of the secondary binding to the acidic disordered domain, rather than the basic HBD in VN.

4.1.d Research Goals

With this branch of the project we sought to better understand the effect of PAI-1 binding on VN. More specifically, we studied the impact of PAI-1:VN interactions on the IDD of VN. Our discoveries will further the field by lending insight in to an understudied domain of VN and potentially provide answers about how PAI-1 affects conformational changes in VN.

Intrinsically disordered proteins have been shown to have an important role in many key biological processes, and we wish to better understand how the IDD affects this aspect of the role of VN. We have used two primary techniques to study the IDD in this work, CD and SANS. The hypothesis that guided this branch of the project is the disordered domain of VN is an IDD and will undergo a disorder to order transition upon interaction with PAI-1.

In addition to our study of the structural effect of PAI-1 binding on the IDD, we also sought to gain further understanding regarding the secondary binding site for PAI-1 on VN. There are two regions in VN that have been proposed to contain the secondary binding site for PAI-1. The first region is located in the C-terminal domain, near the heparin binding domain (HBD), and the second is located in the IDD. We hypothesize that the secondary binding site for PAI-1 on VN is found in the IDD of VN. Our rationale for this hypothesis stems from the inherent conflict of two basic HBDs interacting [203] whereas the IDD site is acidic and is thus more likely to participate in an electrostatic interaction [138]. Additionally, the heparin binding domain of VN is cryptic until exposed due to conformational changes induced by binding to PAI-1 and a handful of other partners [179]. The cryptic nature of the HBD prior to PAI-1 binding indicates that it cannot serve as the secondary binding site, since it would remain cryptic until after the interaction of PAI-1 at both the primary and secondary binding locations [21].

Finally, due to its flexible nature, the IDD site is more likely to be readily positioned in close proximity to the primary binding site.

4.2 Methods

4.2.a Expression and purification of a VN fragment in *E. coli*

The SMB-IDD fragment of VN was expressed in *E. coli*, under control of a T7 promoter, with a thioredoxin and His tag. The purpose of the His tag was for ease of purification, and the Thioredoxin was added to ensure that the small protein fragment was not degraded by the cell. Following expression of the SMB-IDD, the Thioredoxin tagged protein was isolated from the cell lysate by an IMAC affinity column. After elution of the recombinant protein from the column, the SMB-IDD was isolated from the Thioredoxin and His tags via thrombin cleavage. Following cleavage, the SMB-IDD was isolated, and then flowed over a PAI-1 affinity column to isolate SMB-IDD constructs that can bind PAI-1. This step was performed to ensure that the *E. coli* expressed SMB-IDD, was also functional and properly folded. More detail on this process can be found in 2.2.n. The size of the SMB-IDD was confirmed via HPLC, Mass Spectrometry, and gel electrophoresis.

4.2.b Expression and purification of deuterated W175F PAI-1

We utilized two different methods for the deuteration of PAI-1. Initially we relied on deuterated rich media. *E. coli* expressing the W175F PAI-1 construct was then grown in this media as described in 2.2.h. Briefly, we used a small volume of the deuterated media to generate starter culture from glycerol stocks. This culture was then used to inoculate the remaining 1L of

deuterated media. Cultures were grown at 37°C until they reached an OD_{600} of ~2, then cooled to 15°C prior to induction with 1mM IPTG. Following an 18 hour induction, cells were spun down and frozen at -80°C.

Our second method of deuterating W175F PAI-1 utilized minimal media and fermentation. In order to grow the cells in deuterated minimal media, we spent several weeks adapting the cultures to a new media. Once we had cell stocks that grew and expressed PAI-1 well in minimal media, we created a glycerol stock for use with creating a starter culture when working at ORNL. This stock was then used to inoculate deuterated minimal media for use as a starter culture. After an overnight growth at 37°C, this culture was used to inoculate 1L of deuterated minimal media. The culture was then grown in a fermenter to OD_{600} 35. The culture was then cooled and induced with 1mM IPTG. Cells were spun down and frozen at -80°C.

Deuterated W175F PAI-1 was purified using our standard purification protocol, described in 2.2.j, using a series of three columns. All buffers were prepared with H2O, and the final purified protein was immediately dialyzed into PBS in D2O, and kept at 4°C until use for SANS. PAI-1 yield was much higher for the fermentation method, and extra protein was frozen at -80°C for future experiments. This caused some aggregation of PAI-1, so all frozen PAI-1 was run over an s-100 column a second time prior to use.

4.2.c Circular Dichroism

Circular Dichroism experiments were performed on an Aviv Circular Dichroism Spectrometer, model 202. Samples were placed in 1mm path length quartz cuvettes and then

placed in the instrument to be scanned. Data were analyzed using the online tool, Dichroweb [211, 212].

4.2.d Small Angle Neutron Scattering

SANS experiments were performed on the BioSANS or EQ SANS beam lines at ORNL. More information on data collection and analysis can be found in 2.2.t.

Data analysis was conducted using the ATSAS and SASSIE suite of tools. These processes are described in detail in 2.2.v and 2.2.w. Both EOM and SASSIE rely on generating a large pool of structures and then comparing those structures to the experimental data. This combination of computational and experimental techniques allows for a robust analysis that yields high resolution data.

4.3 Results

4.3.a Studying the effect of osmolytes on the IDD structure with Circular Dichroism

In our quest to explore the role of the IDD in PAI-1:VN interactions, we first studied the effect of osmolytes on the structure of the IDD. In order to study this disordered domain, we expressed it as a part of a two domain construct that also included the SMB domain of VN. The inclusion of the SMB domain provided a stable anchor for the IDD and allowed for affinity purification of the VN fragment. The SMB domain is largely free of classical secondary structural elements, and thus would not contribute greatly to the CD spectra.

To begin our studies we utilized CD and examined the effect of osmotic pressure on the IDD. Osmotic pressure is frequently used to simulate binding or cellular conditions on a protein in order to isolate structural changes that would be masked in the presence of binding partners. In our experiments, we used Ethelyne Glycol (EG) and Polyethylene glycol (PEG) 400 to study the structure of the IDD under osmotic pressure. Our findings showed the SMB-IDD domain alone has an elipticity that is devoid of classical structural features (figure 4.1). However, upon addition of EG and PEG 400 we observed the SMB-IDD elipticity shift towards 220nm indicating a reduction in disorder and a possible adoption of secondary structure. We analyzed our CD data using the free online tool, Dichroweb. The results supported our hypothesis and observation that the IDD underwent a disorder to order transition upon addition of osmolytes (figure 4.2).

4.3.b Computationally examining the IDD for potential to adopt structure

In order to determine if the IDD of VN was, like so many other IDDs, able to adopt secondary structure upon interaction with a binding partner, we collaborated with Dr. Uversky to utilize his Molecular Recognition Feature (MoRF) prediction software [213]. MoRFs are small segments in intrinsically disordered proteins (IDPs) that transition from disorder, to order, upon ligand binding. This ordered state can be anything from adoption of classic secondary structure, to an ordered loop region [214]. Dr. Uversky's software is designed to identify these MoRFs within an IDP and predict the adoption of structure upon binding to a ligand. The results of the MoRF prediction are shown in figure 4.3. The model predicts the presence of two regions in the IDD that may to adopt alpha helical structure upon interaction with a ligand (VN residues

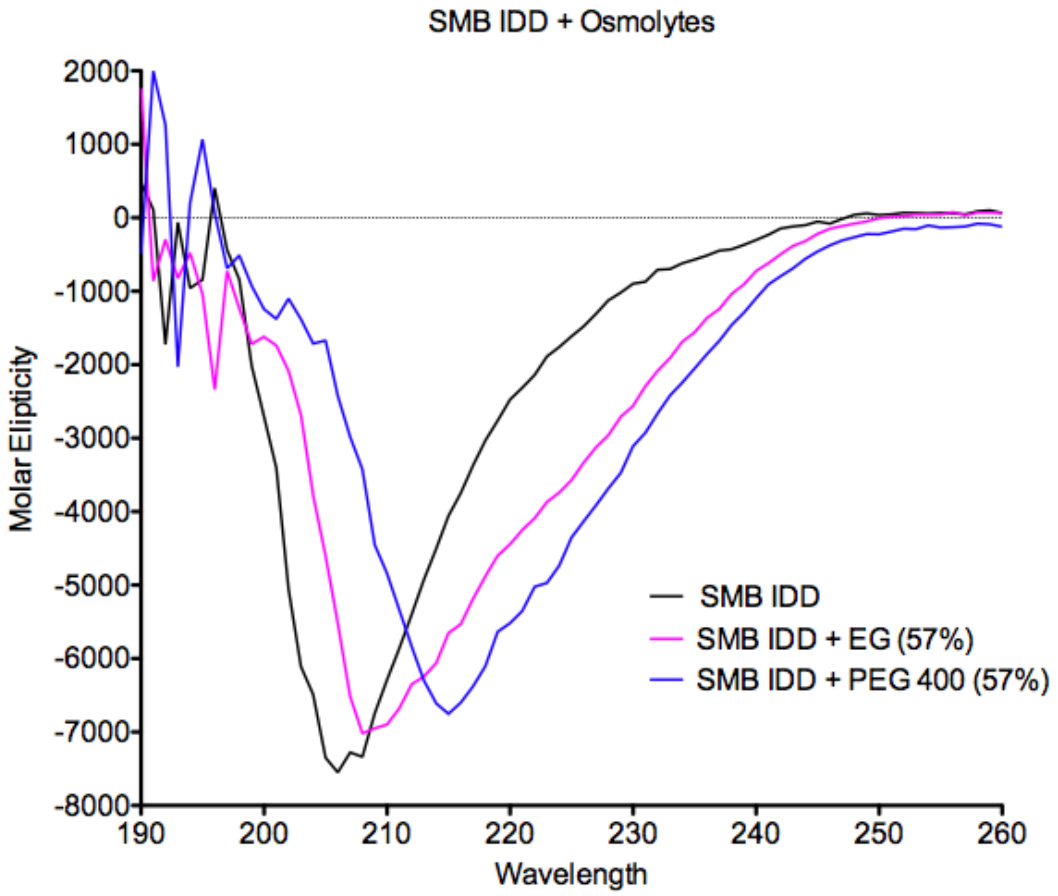

Figure 4.1 CD Data

CD spectra of the SMB-IDD fragment of VN. Black line: SMB-IDD alone in solution. Pink line: SMB-IDD in the presence of 57% ethylene glycol. Blue line: SMB-IDD in the presence of 57% polyethylene glycol 400. Increase in osmotic pressure causes a shift in elipticity toward 220nm, indicative of a more ordered state.

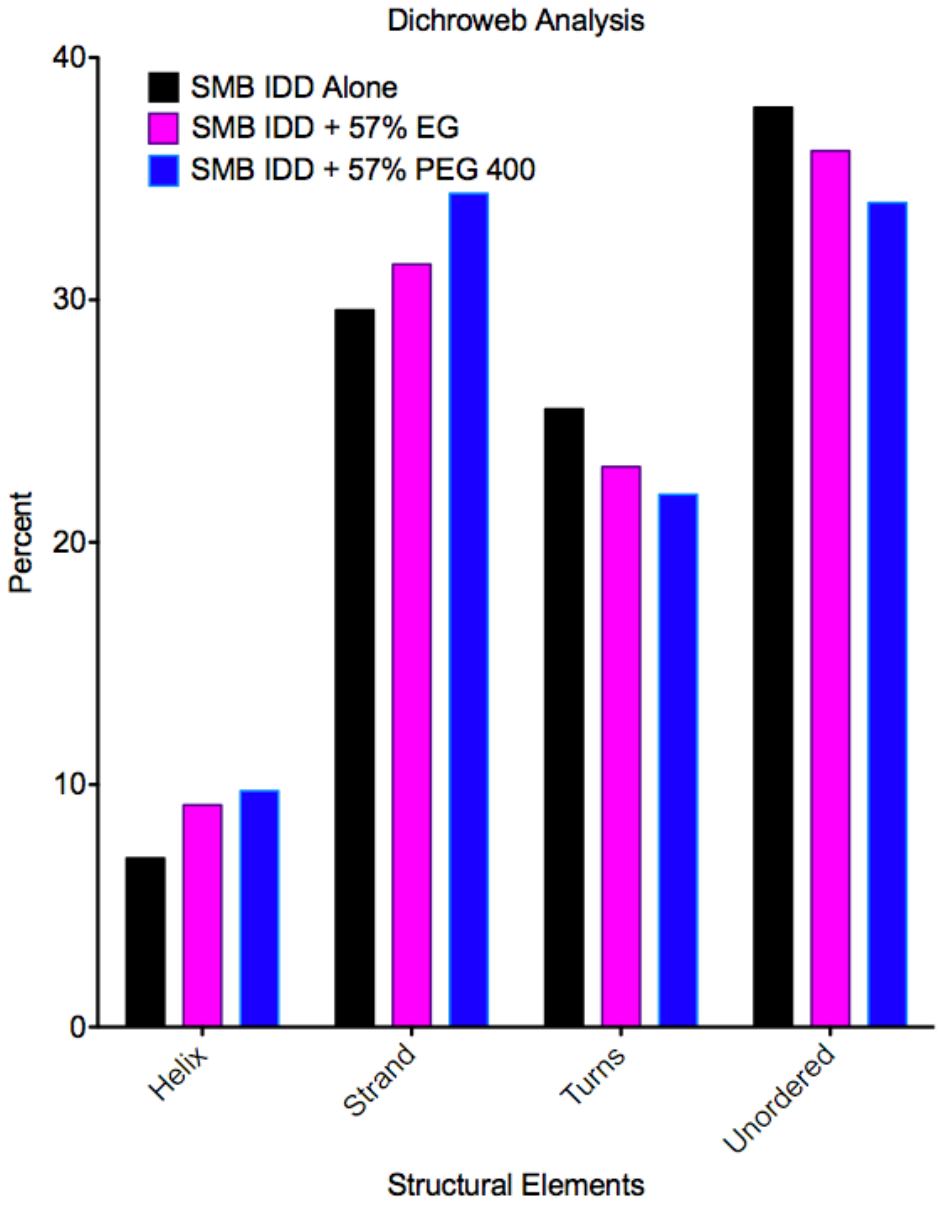

Figure 4.2 Dichroweb Analysis of CD data

Dichroweb analysis of the CD spectra confirms an increase in order and a decrease in disorder in the IDD of VN under increasing osmotic pressure. Black: SMB-IDD alone in solution. Pink: SMB-IDD in the presence of 57% ethylene glycol. Blue: SMB-IDD in the presence of 57% polyethylene glycol 400.

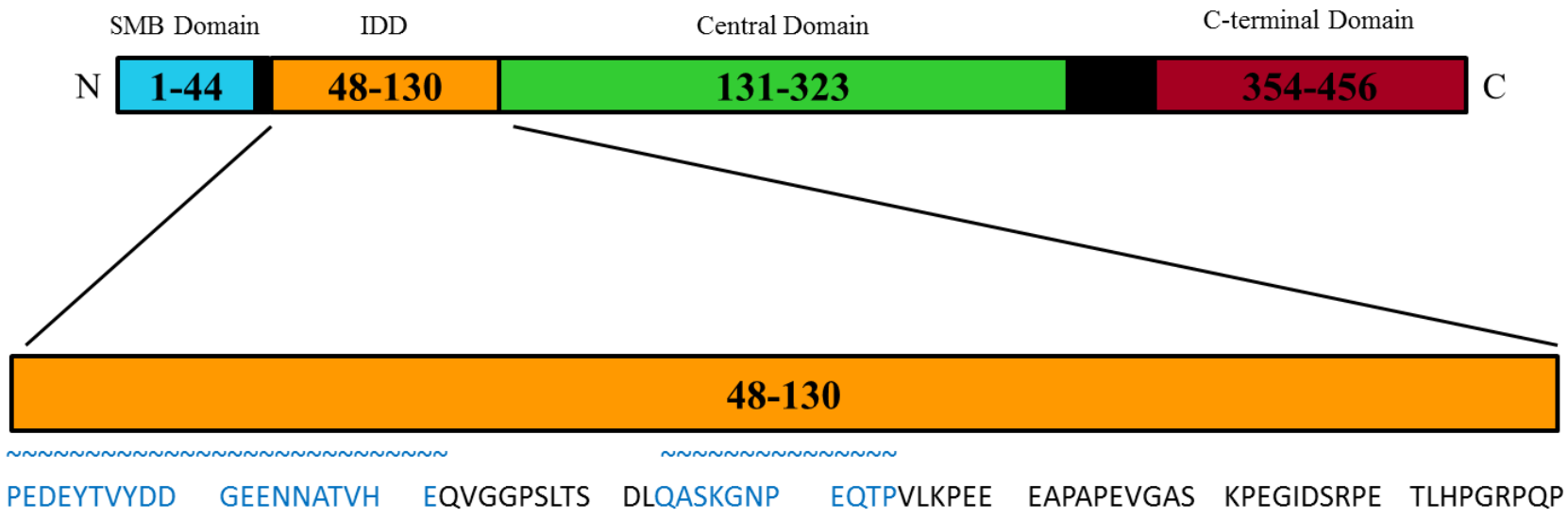

Figure 4.3 Analysis Of The IDD Sequence Indicates Potential To Adopt Helical Structure

Two regions of the IDD were predicted to adopt alpha helical secondary structure upon interaction with PAI-1 using MoRF prediction software [213]. The sequence of the IDD is shown below the main cartoon of the VN domain structure. The two regions predicted to adopt structure are shown in blue.

52-72 and 84-95). These data are in support the hypothesis that PAI-1:VN interactions cause a conformational change in the IDD of VN.

4.3.c Studying the effect of osmolytes on the IDD structure with SANS

In order to further test our hypothesis we studied the SMB-IDD using SANS. By working with fully deuterated osmolytes we eliminated the need to perform contrast variation experiments. Instead, we measured scattering of the SMB IDD in a buffer that matched out signal from the osmolytes so that we only gathered data from our protein of interest (figure 4.4).

Upon data analysis we observed that addition of osmolytes caused a reduction in the radius of gyration (R_g) of the SMB IDD (figure 4.5). This reduction in R_g indicated that the IDD was less flexible and elongated in solution when under osmotic stress. We further analyzed the data by performing an ensemble optimization method (EOM). We generated 10,000 structures for the SMB-IDD, and selected the top 10% based on best fit to the experimental data. Using these structures, we generated a heat map comparing the Rg of these 100 structures with osmolyte concentration. Our results demonstrate that the IDD is very flexible alone in solution, but samples a much smaller area when under osmotic stress (Figure 4.6). This structural change could be due to secondary structure adoption, or an overall compaction of the IDD. However, the low resolution of SANS is unable to differentiate between these two possibilities.

4.3.d Studying the effect of PAI-1 binding on the IDD structure using cvSANS.

Together the CD and SANS data support our hypothesis that the IDD experiences a structural change under osmotic pressure. These findings generated the preliminary rationale for

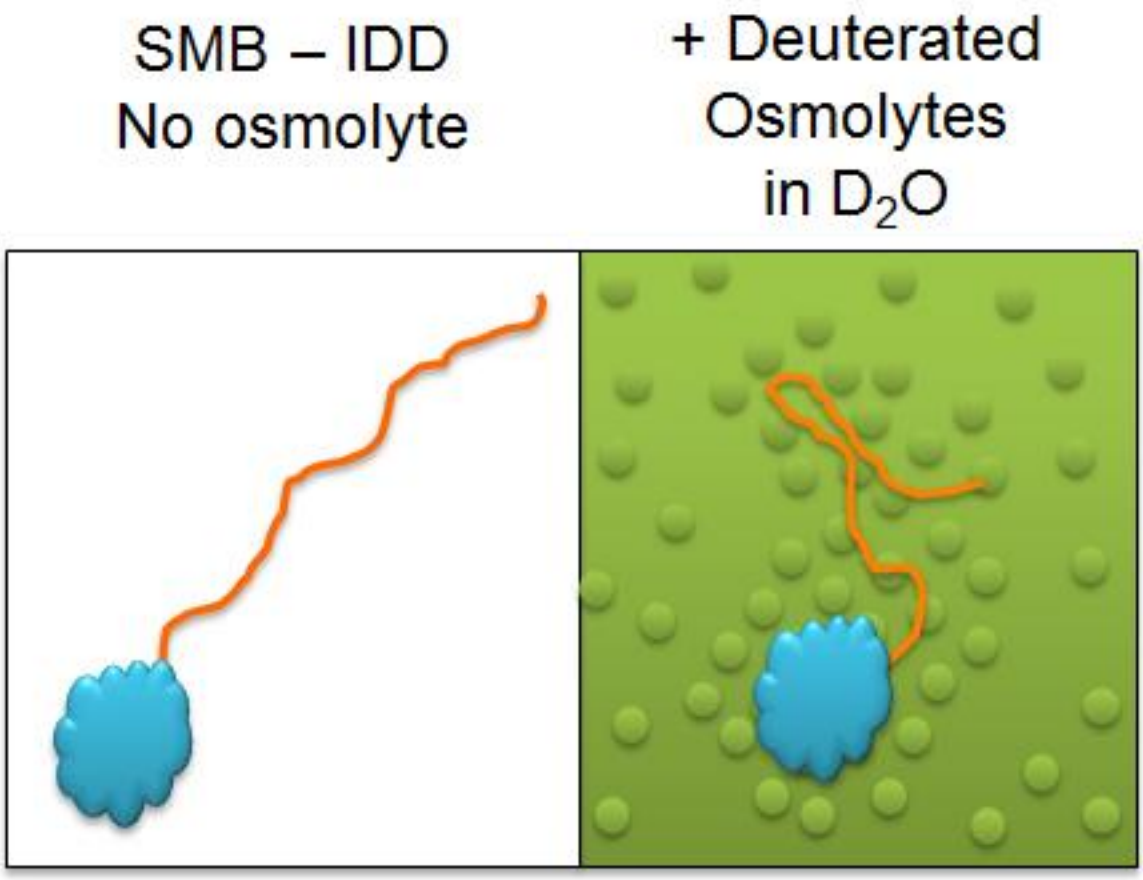

Figure 4.4 Contrast Matching SANS Experimental Scheme

Using deuterated osmolytes we are able to "match out" the scattering signal using buffer D_2O percentage. This allows us to conduct measurements with a single buffer condition, speeding data collection and simplifying data analysis.

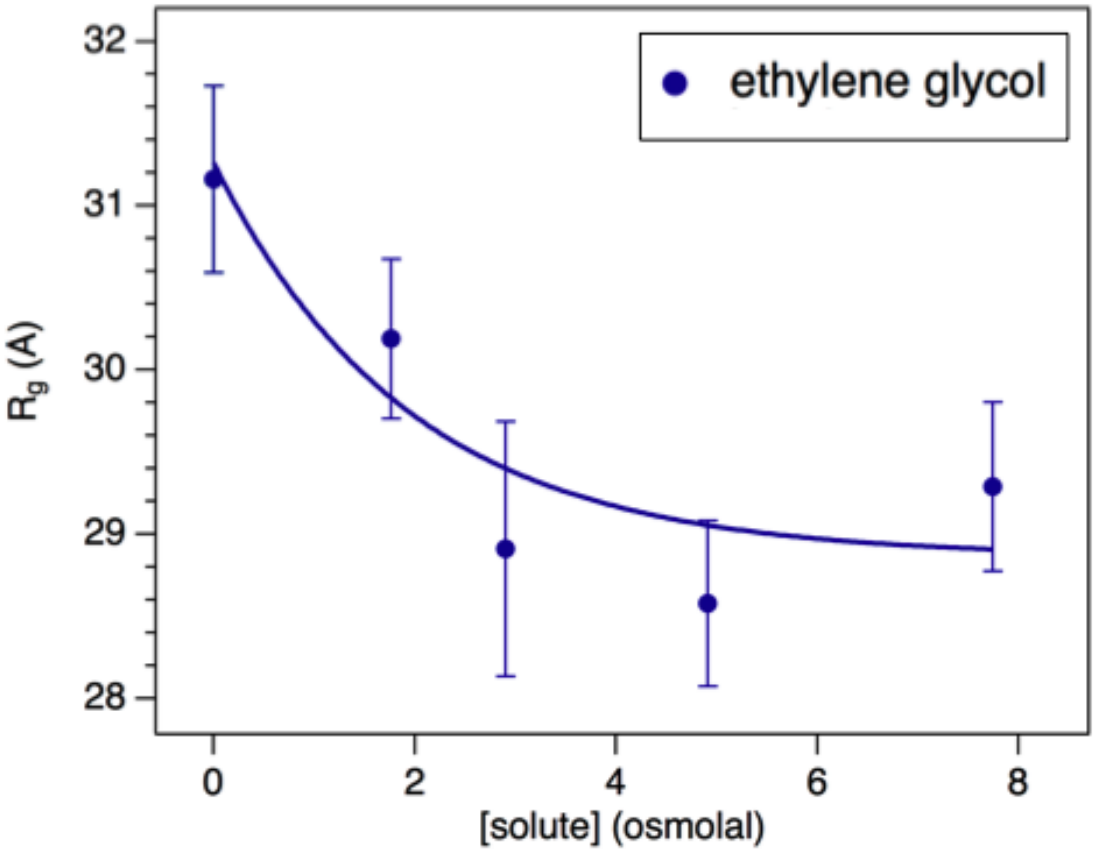

Figure 4.5 SANS Osmolyte Data

SANS experiments were conducted under five different osmolyte concentrations. The average Rg for each data set was calculated from the gunier region in the software package Igor. These data were plotted as a measure of Rg vs osmolytes concentration. The data demonstrate that increasing osmotic pressure results in a decreased Rg.

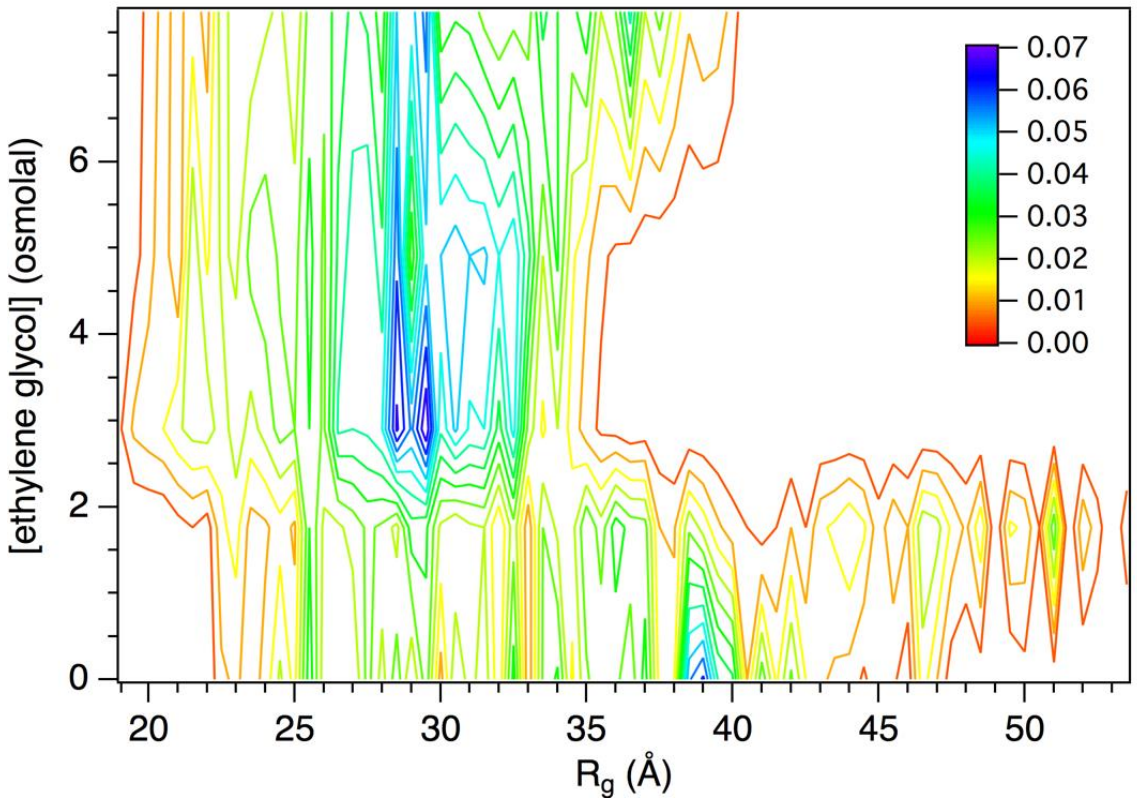

Figure 4.6 EOM Heat Map

For each osmolyte condition, 1000 structures were selected that best fit the scattering data. The Rg for these structures was then used to construct a heat map that displays the relationship between osmotic stress and RG for the SMB-IDD. The Rg values for each of the 1,000 structures are plotted on the x-axis. Five osmolal conditions (0, 2, 4, 6, and 8 osmolals of EG) were analyzed and are shown on the y-axis. The data demonstrate that in the absence of osmolytes, the Rg peaks in the high 30's. however, in the presence of osmolytes, this peak shifts by nearly 10 angstroms, confirming that osmotic pressure effects the conformation of the IDD.

testing PAI-1 and the SMB-IDD in complex to see how a native ligand affects the structure of the IDD. We used deuterated W175F PAI-1 so that we could isolate scattering data from the complex components via contrast variation experiments (Figure 4.7).

Following data collection, a variety of methods were utilized to analyze the data. First, we used the MONSA and SUPCOMB software packages from the ATSAS suite to generate a low resolution representation of the data, and then super imposed the co-crystal structure of PAI and SMB in order to gauge the appropriateness of the model. This method, while able to generate a model that fit the data relatively well, was unable to fully model the IDD portion of the data due to the inherent flexibility of the protein domain (figure 4.8). Consequently, this analysis method was set aside in favor of other, more refined, approaches.

In order to accurately model the flexible IDD we again turned to two separate approaches. First, we used EOM to generate a pool of 10,000 unique structures. From this pool we selected 2000 structures that best fit each contrast condition. These structures were used to generate a new pool of 10,000 structures from which we ran EOM again, to select 1000 structures that best fit the 100% D_2O condition. From this new collection of structures we isolated the signal from the SMB-IDD. We then compared the Rgs for bound, vs unbound SMB IDD. The data show that PAI-1 binding results in a much narrower R_g range for the SMB-IDD, indicating that the IDD cannot move as freely in solution when bound to PAI-1 (Figure 4.9).

We also collaborated with Susan Kreuger and Joseph Curtis at NIST, using the SASSIE software suite to generate a model for the PAI-1:SMB-IDD complex. Several starting structures were generated so that we could explore the possible structures adopted by the IDD of VN (Figures 4.10 and 4.11). Starting structure 1 was generated with no constraints on the IDD.

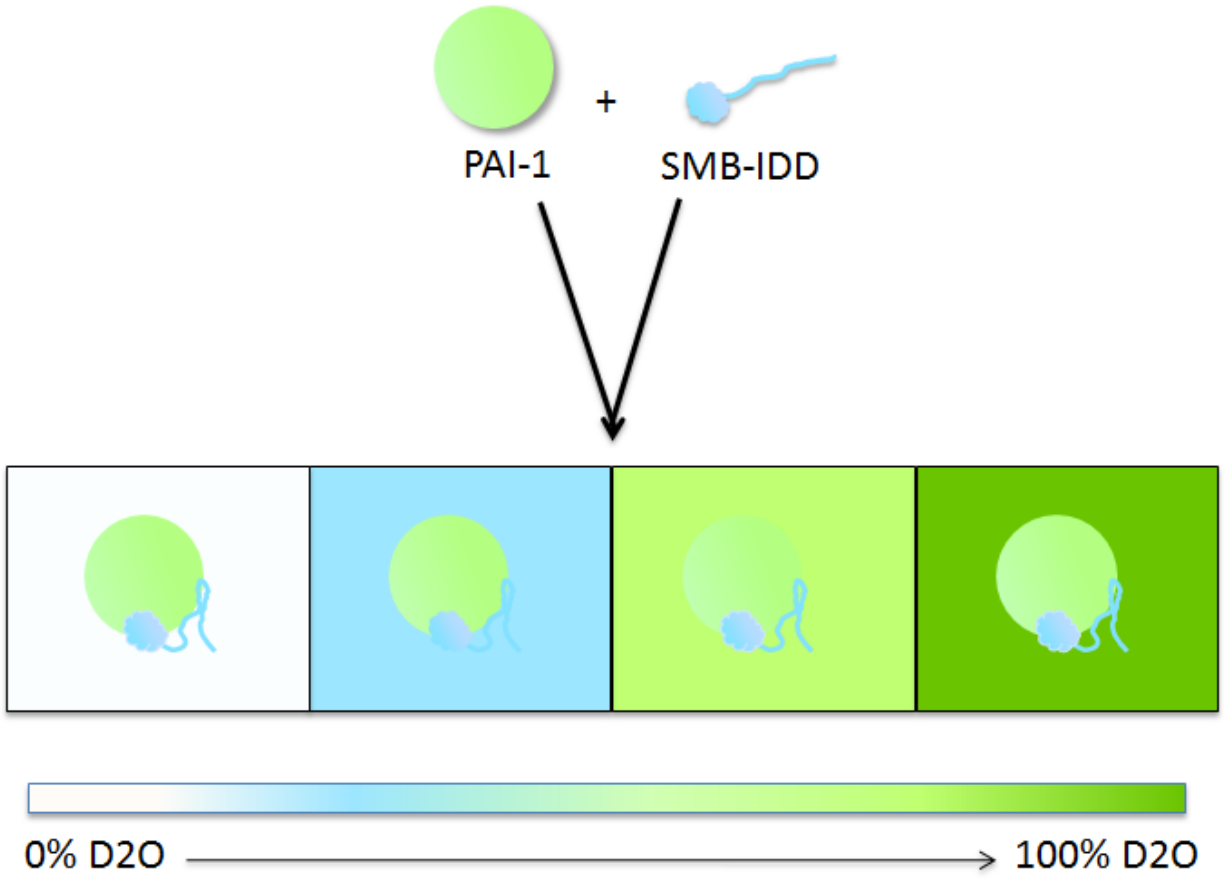

Figure 4.7 Illustration of the PAI-1:SMB-IDD cvSANS

We used contrast variation SANS to gather data on deuterated PAI-1 and protonated SMB-IDD. We studied the complex in buffer with varied D_2O compositions in order to change the signal contribution from each of the complex components. Neither of the complex components were completely matched out in any buffer condition with this method, but the buffer variation allowed one component of the complex to dominate the signal under different conditions.

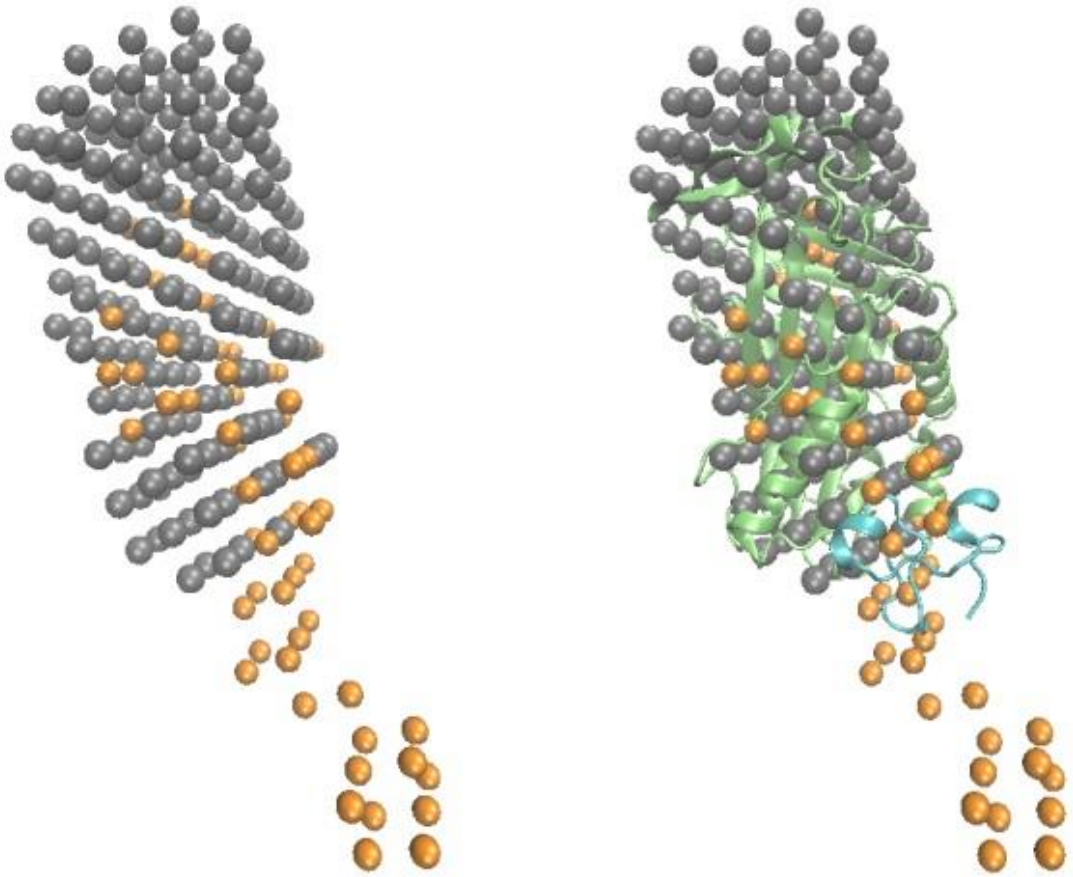

Figure 4.8 MONSA model of PAI-1:SMB-IDD SANS data

A low resolution model was generated using the MONSA software package. PAI-1 is represented by gray, and the SMB-IDD is represented by orange. The left structure is a representative model generated using MONSA. The right structure is an overlay of the low resolution MONSA structure with the PAI-1:SMB co-crystal structure (green and cyan respectively) to demonstrate goodness of fit.

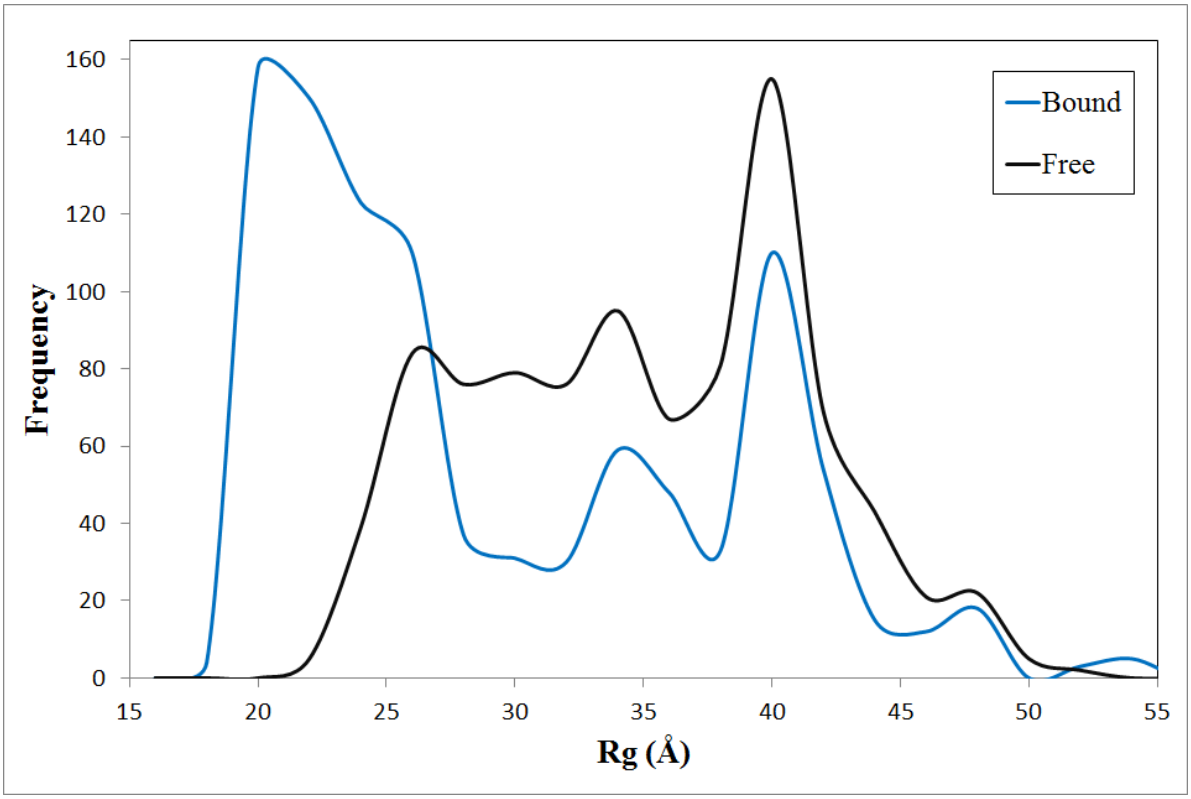

Figure 4.9 EOM Analysis of PAI-1:SMB-IDD and free SMB-IDD SANS data

EOM analysis of SANS data on the SMB-IDD VN fragment demonstrates that the IDD of VN samples a broad range of space in solution. The above graph illustrates the change in the SMB-IDD when unbound (black) or bound (blue). These data demonstrate that that the IDD exists predominantly in conformations with a smaller Rgs upon interaction with PAI-1.

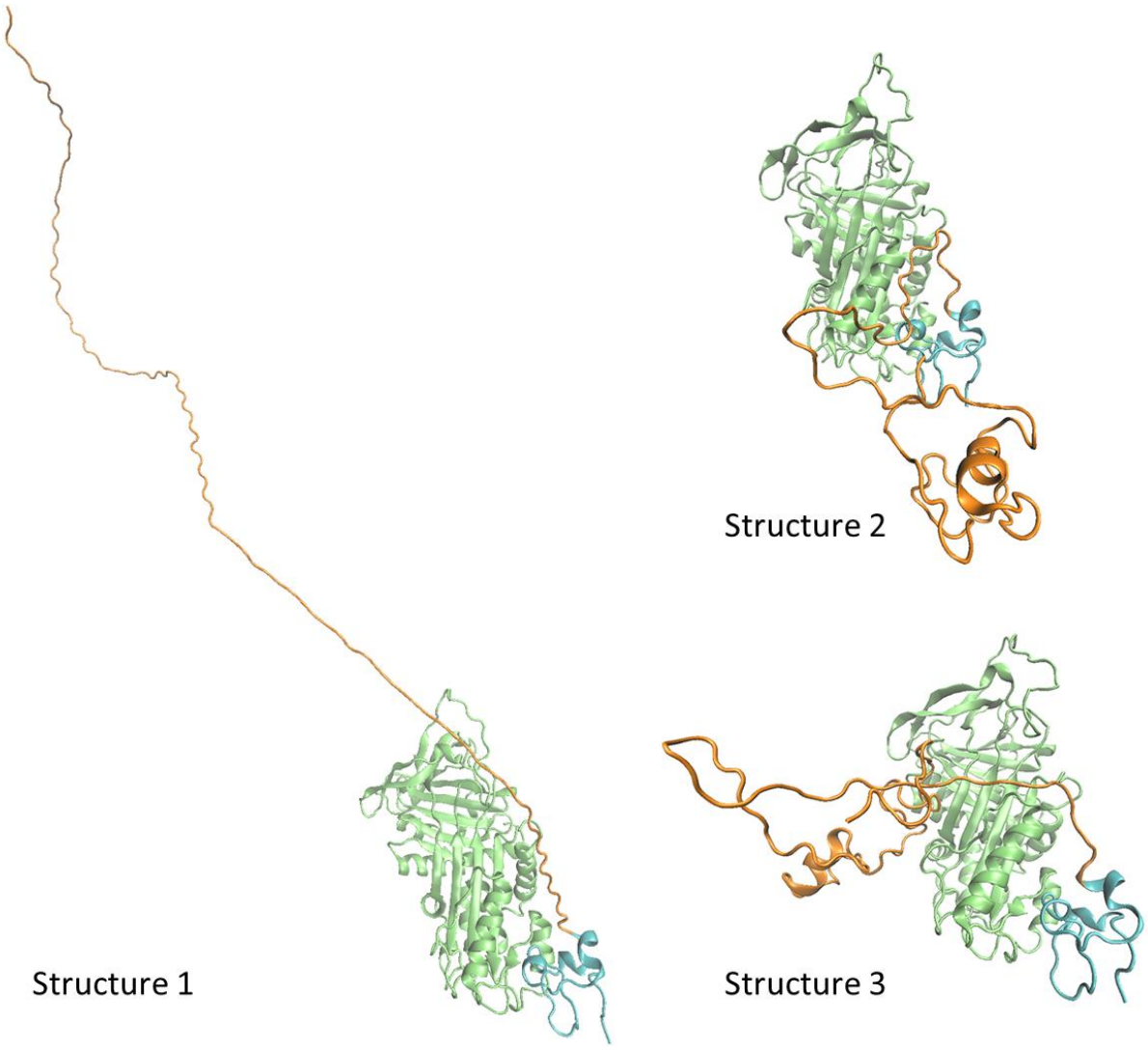

Figure 4.10 Starting Structures for PAI-1:SMB-IDD SANS analysis

Three starting structures were generated using the all atom calculator that is part of the SASSIE tool suite in order to analyze the PAI-1:SMB-IDD SANS data. Structure 1 had no constraints built into the IDD. Structure 2 was created with the IDD in a more compact starting position. Structure 3 was created with the IDD in a compact state and wrapping around PAI-1. These structures were used as starting points to generate large, conformationally diverse, structure pools for further data analysis.

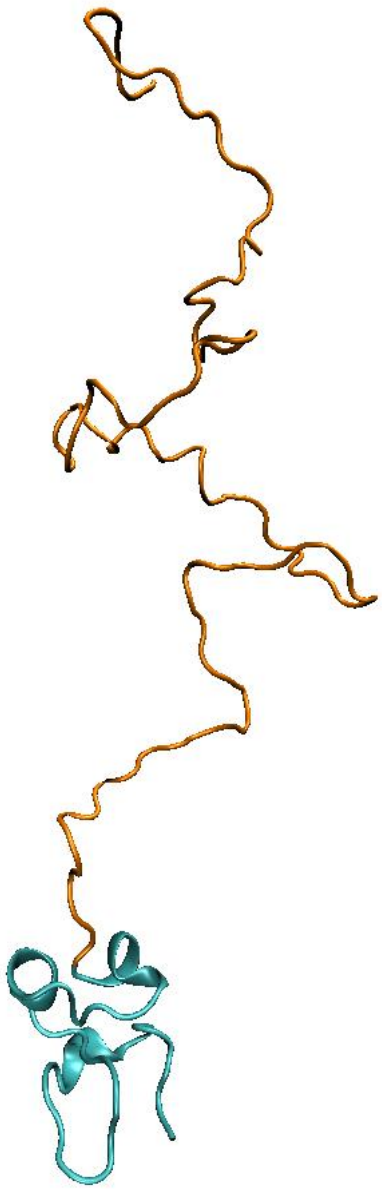

Figure 4.11 Starting Structure for unbound SMB-IDD SANS analysis

A single starting structure was used to analyze the unbound SMB-IDD SANS data. This structure was used as starting point to generate a large, conformationally diverse, structure pool for further data analysis.

Starting structure 2 was generated with the IDD in a more condensed starting position that agreed better with the experimental data. Starting structure 3 was generated with Rg constraints as well as starting partially wrapped around the PAI-1 molecule in order to better simulate the center of mass that was calculated from the experimental data. Additionally, a structure for the SMB-IDD alone in solution was generated with no constraints on the IDD.

From each of these starting structures, pools of 50,000 conformations were generated under varied simulated conditions (Figure 4.12). These pools were then analyzed in comparison with the experimental data and X^2 values were used to determine goodness of fit. A comparison of the X^2 versus Rg values for each structure compared to the 85% contrast condition is shown in figure 4.12. This contrast condition was favored for data analysis because the deuterated PAI-1 is nearly matched out, allowing the SMB-IDD the greatest signal contribution at this contrast. As can be seen in figure 4.12, the best fit to the data came from the two pools generated using starting structure 1 (shown in red and black). A similar comparison of the two pools was made with the global data set, taking all contrast conditions into account (Figure 4.13). In this case the structure with a constrained Rg better fit the global data. Additionally, a X^2 versus Rg comparison was performed for the SMB-IDD data set alone and is shown in figure 4.14. As with the complex, the unbound SMB-IDD pool has a number of structures that do not fit as well to the experimental data, and a good selection of structures that have a reasonable X^2 value.

Using X^2 values, a best fit structure was selected for the global data set, as well as a best fit structure for the 85% data set (Figure 4.15). Curves were calculated for each of these two structures at 0%, 20%, 85%, and 100% D_2O conditions and compared with the interpolated experimental data (Figure 4.16). The global best fit structure correlates well with experimental data at 0% and 20% D_2O, but not well at the 85% or 100% conditions. Conversely, the best fit

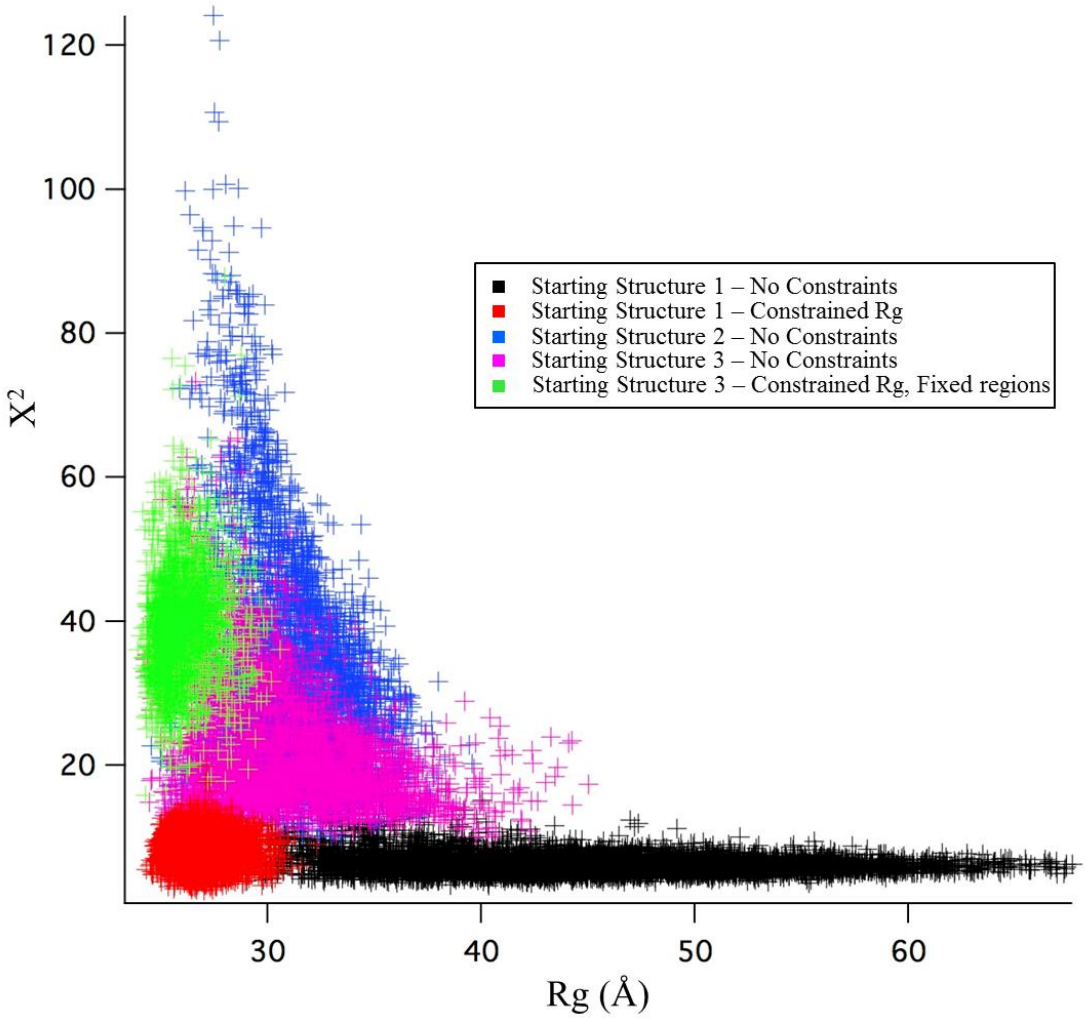

Figure 4.12 X^2 vs Rg Plot for 85% D_2O PAI-1:SMB-IDD Contrast Condition

The three starting structures were used to generate large, conformationally diverse structure pools. In the creation of these pools, constraints could be used to affect the resulting structural pool. Starting structure 1 was used to generate two pools. The first pool (black) was not subjected to any constraints. The second pool (red) was constrained to Rgs below 35 Å. The single pool generated from starting structure 2 (blue) was not subjected to any constraints. Starting structure 3 was also used to generate two separate pools. The first pool (pink) was not subjected to any constraints. The second pool (green) was constrained to Rgs below 35Å and also had fixed regions introduced into the IDD forced the IDD to remain wrapped around PAI-1. The structures from these pools were compared with the 85% experimental condition for goodness of fit and are displayed here in a X^2 vs Rg plot. As can be seen from this data, both pools from structure 1 had the best fit to the 85% contrast data.

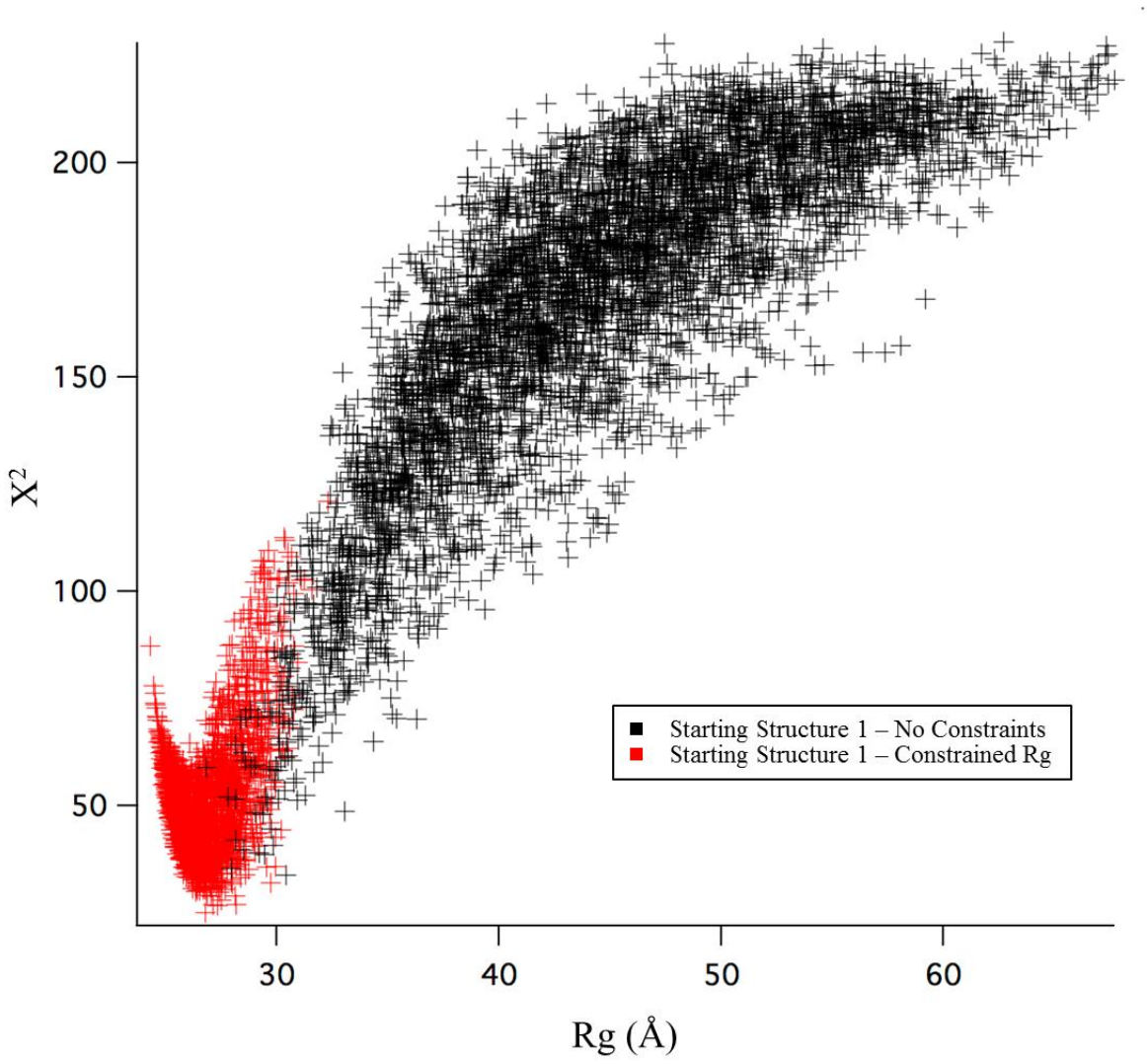

Figure 4.13 X^2 vs Rg Plot for Global PAI-1:SMB-IDD Complex Data

The pools from starting structure 1 were compared with the global SANS data set. Under these conditions, the red pool, in which Rg was constrained, contained structures that best fit the experimental data.

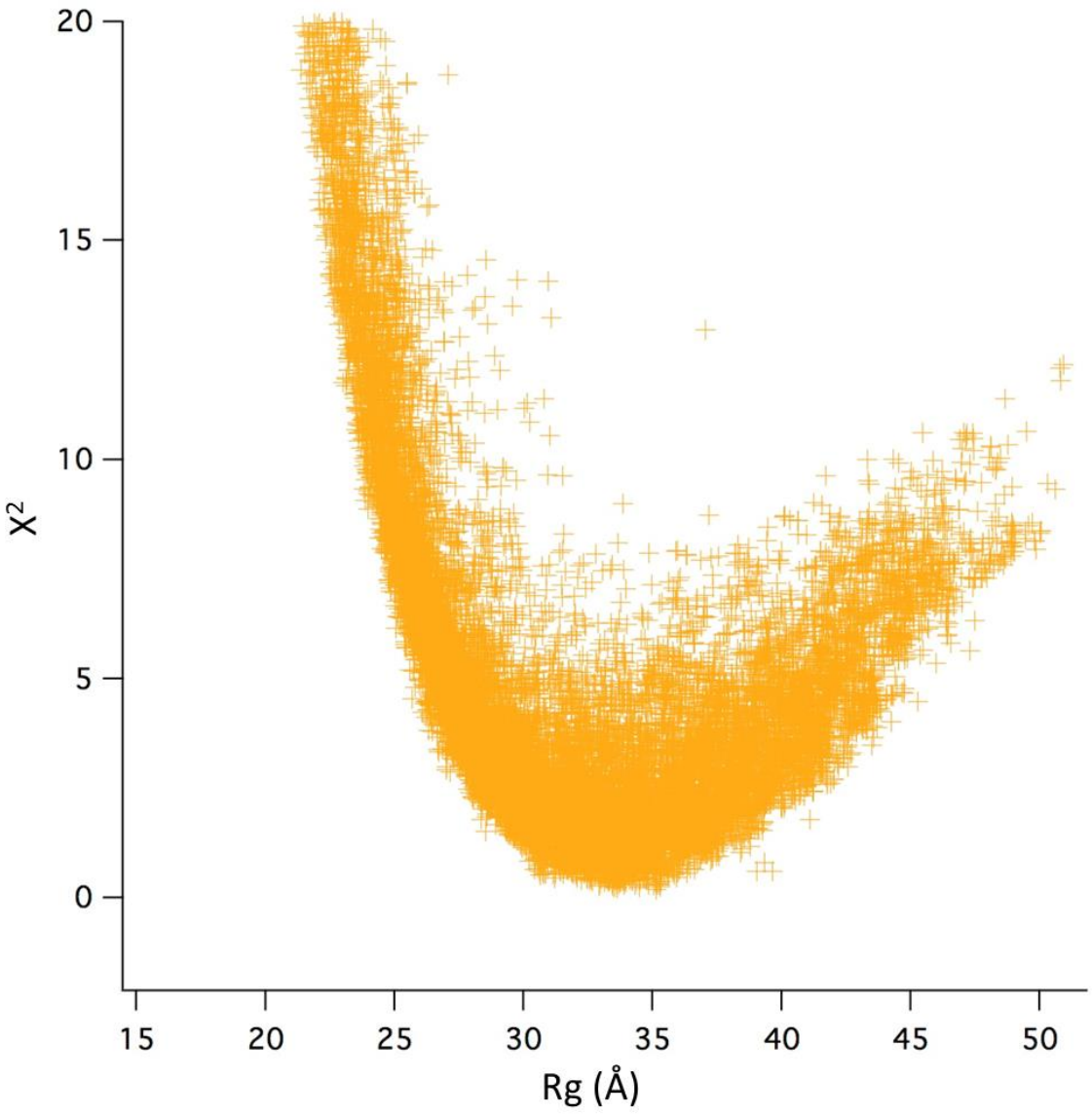

Figure 4.14 X^2 vs Rg Plot for Unbound SMB-IDD Experimental Conditions

All structures in the pool were compared with the global SANS data set. Overall, the structures fit reasonably well to the data.

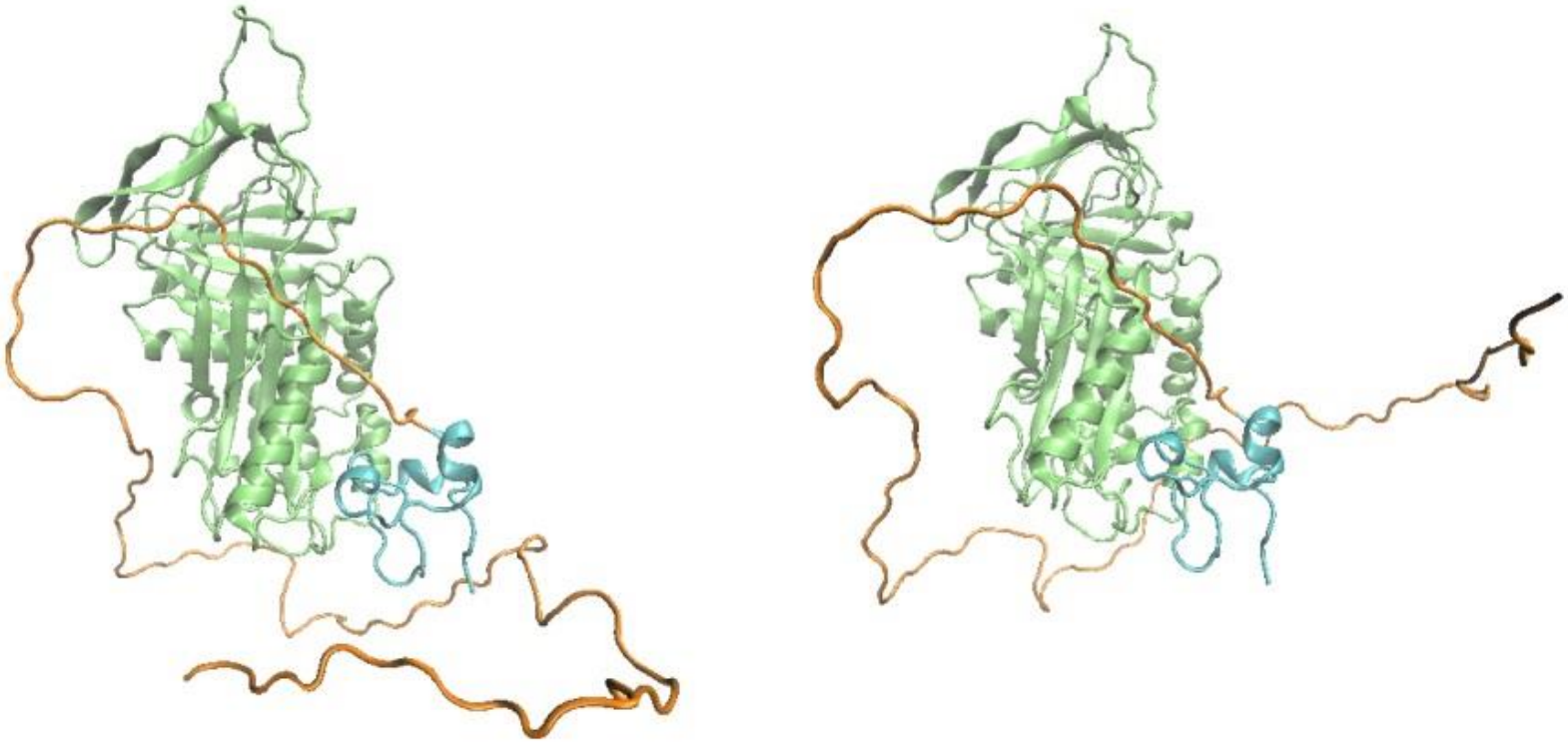

Figure 4.15 Best fit PAI-1:SMB-IDD structures

While no single structure can fully capture the flexible, disordered domain of VN, we selected the two best fitting structures from the ensemble to show as representative conformational states. The structure on the left is the best fit to the global PAI-1:SMB-IDD data set. The structure on the right is the best fit to the 85% contrast condition.

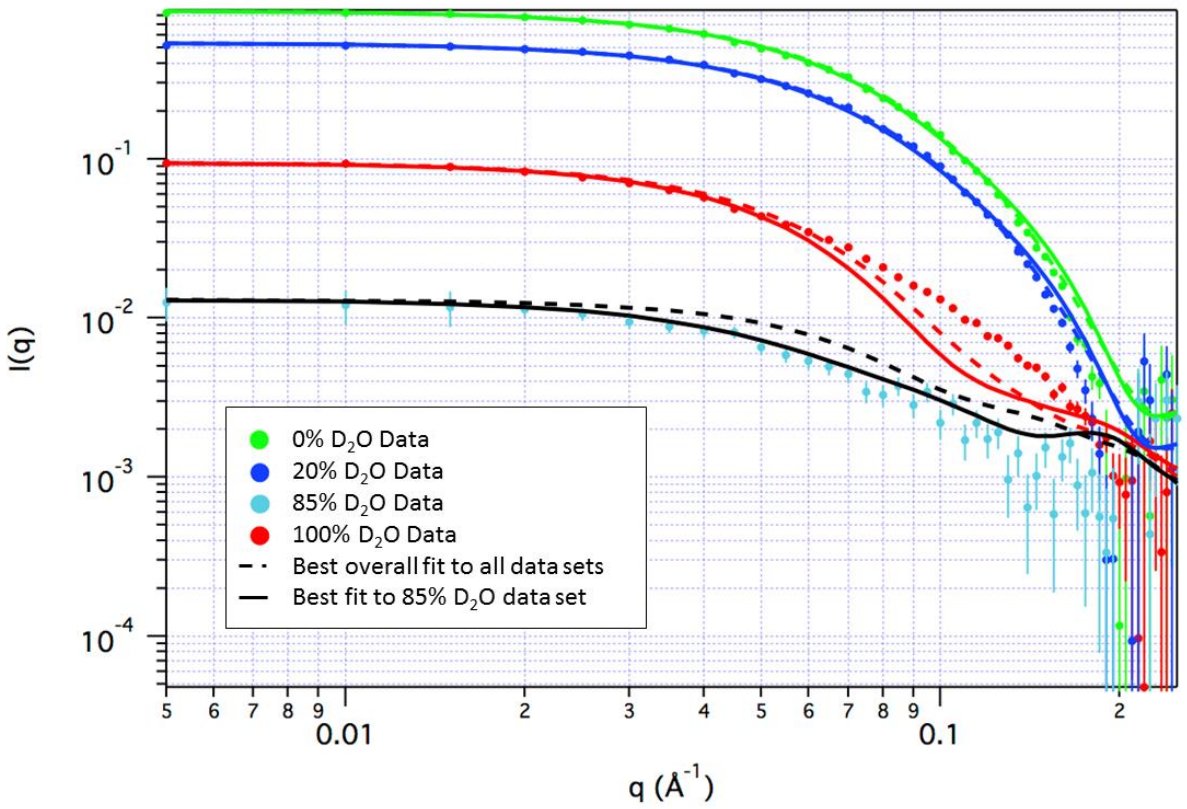

Figure 4.16 SANS data curves

Interpolated experimental SANS data are shown as dots for four contrast conditions. Curves for the global best fit structure under different contrast conditions are displayed as a dashed line in corresponding colors. Curves for the best fit structure to the 85% contrast condition are shown as solid lines in corresponding colors. The global best fit structure only fit the 0% and 20% data, whereas the 85% conditions fits well to all conditions other than 100% D_2O.

structure for 85% conditions fits well to all conditions other than 100% D_2O. No structure fit well to all experimental conditions. This is likely due to some aggregation that occurred in the 100% D_2O sample.

In addition to selecting a single, best fit, structure from the selected pools, we also generated density plots to more accurately display the conformational space sampled by the flexible IDD of VN. Figure 4.17 is a density plot of all structures with a X^2 <5 to the unbound SMB-IDD data. The cyan shape, fixed in the center of the plot, represents the SMB. The gray cloud is a representation of all the conformational space sampled by the IDD.

The density plot in figure 4.18 is an overlay of the unbound SMB-IDD data shown in figure 4.17, and the data from bound SMB-IDD. The green and cyan shapes in the center represent PAI-1 and the SMB domain respectively. The orange cloud is a representation of all the conformational space sampled by the IDD when the VN fragment is bound to PAI-1. As can be seen from the overlay, the selected IDD conformations inhabit the region surrounding PAI-1. This result agrees with the EOM analysis and expands upon it by visualizing the space in which the IDD localizes.

4.4 Discussion

We sought to better understand the effect of PAI-1 binding on VN, specifically studying the IDD. We hypothesized that PAI-1 binding would have a structural effect on the IDD, causing a disorder to order transition in the domain. Our CD and SANS experiments support this hypothesis and confirm that the IDD becomes less disordered and more compact when bound to PAI-1. Due to the low resolution of SANS data no firm conclusions could be reached regarding

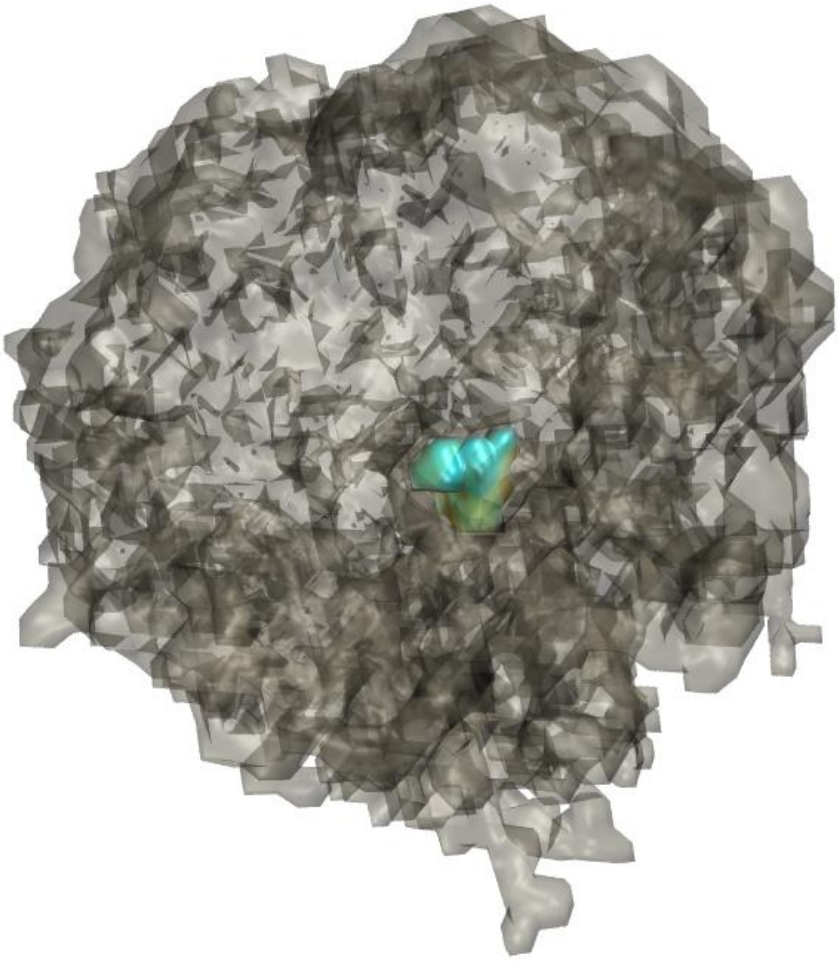

Figure 4.17 Density Plot for Unbound SMB-IDD

The SMB domain is shown at the core in cyan. The outer gray cloud represents the conformational space inhabited by the IDD in all structures with a X^2 value of <5. The data show that unbound, the IDD samples a range of conformational space around the SMB core. When viewed in three dimensional space (not shown) the IDD samples space around the SMB core relatively equally.

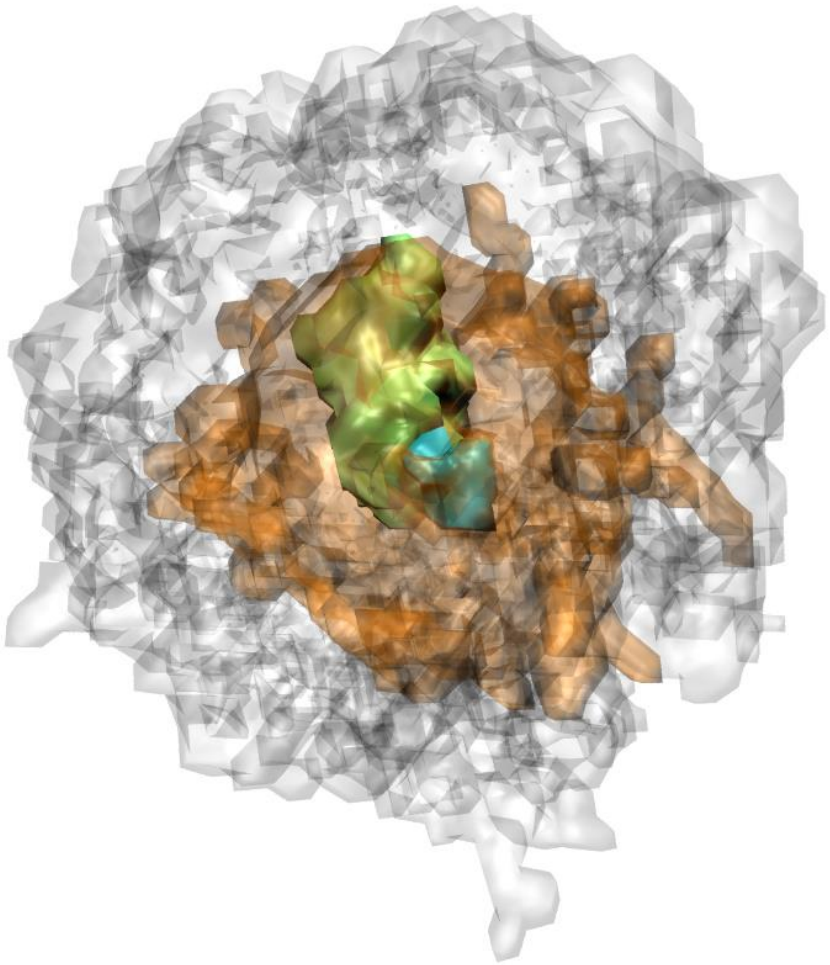

Figure 4.18 Overlay of Bound and Unbound Density Plots

The PAI-1:SMB complex is shown at the core in green and cyan respectively. The outer gray cloud displays **unbound** IDD structures with a X^2 value of <5. The smaller orange cloud displays all **bound** IDD structures with a X^2 value of <5. The data demonstrate that when bound, the IDD samples a smaller range of conformational space around the PAI-1:SMB core in comparison to the space sampled by unbound SMB-IDD. When viewed in three dimensional space (not shown) the bound IDD localizes around the front (shown) and sides of the PAI-1:SMB core, with little density behind the PAI-1 molecule.

the adoption of secondary structure in the IDD from the SANS data alone. However, in both of the "best-fit" structures, the IDD wraps around the PAI-1 molecule in what appears to be an ordered coil. Also, in both structures, the IDD is located near the secondary binding site on PAI-1. This finding does not serve to independently confirm our hypothesis that the IDD houses the secondary PAI-1 binding site, but it does provide a possible mechanism by which the two sites could interact. Further experimental efforts will be needed to determine the location of the secondary binding site for PAI-1 on VN.

Future experiments could address the question of structure in the IDD through the use of N^{15} labeled SMB-IDD in NMR studies. However, it is entirely possible that the MoRFs that Uversky predicted do not adopt structure upon PAI-1 binding. VN has many interaction partners, and even if PAI-1 does not induce a disorder to order transition in the IDD, that finding would not eliminate the possibility of such a transition occurring upon interaction with another binding partner of VN.

Localization of the secondary interaction site between PAI-1 and VN is another important direction of study for the future. The IDD serves as a likely location for this site due to the complementary binding regions and the inherent flexibility, which would allow the two binding sites to simultaneously interact with PAI-1. Possible avenues of experimentation include the use of fluorescent probes on PAI-1 or the IDD, however this could serve to disrupt binding. Another avenue of study would be limited proteolysis of the PAI-1:SMB-IDD complex. However, the flexible nature of the IDD and the weaker affinity for PAI-1 at the secondary site may cause difficulty in performing proteolysis. Whatever method of study is chosen, identification of the secondary binding site for PAI-1 on VN is an important next step in the study of this interaction.

Chapter 5 – Discussion

5.1 Probing the Existence of a PAI-1 Dimer

With this study we sought to further explore the interaction between PAI-1 and VN. Our goal was to gain greater insight into the global interaction between these proteins, as well as take a closer look at a specific, understudied, domain in VN. Through our experimental efforts we discovered that binding deficient PAI-1 can be incorporated into the PAI-1:VN complex when a Wt PAI-1 molecule is present. This finding supports the revised model revealed through analysis of SANS data (figure 1.10) [147]. Future studies could expand on our experimental design in figure 3.3 to confirm our findings using FRET. Previous work by our lab has demonstrated that the two PAI-1 molecules in the PAI-1:VN complex are 57Å apart [138]. Performing FRET experiments using our investigational set up would serve to tie both studies together and would be another method to examine the hypothesis that PAI-1 forms a dimer when in complex with VN.

Our discovery of a potentially functional serpin dimer is an exciting new prospect in the field of serpin biology. Many serpins can form polymers under pathophysiological conditions, but free PAI-1 has not been seen to undergo polymerization under pathophysiological or physiological conditions. However, in one study, free PAI-1 was shown to form dimers under certain non-physiological conditions [81]. Not only did this study demonstrate that PAI-1 can form dimers in certain circumstances, it also revealed that the PAI-1 dimers dissociate into functional PAI-1 monomers. This unique trait suggests a physiological, rather than pathophysiological, role for the PAI-1 dimer that we observe in PAI-1:VN complexes. Future studies will target the mechanism by which the PAI-1 molecules interact. It is likely that PAI-1

interacts via and RCL mediated linkage (figure 3.22). Peptide studies, site directed mutagenesis studies, and antibody blocking studies could be used to elucidate the site of interaction between the two PAI-1 molecules.

5.2 Exploring PAI-1:VN binding sites

Two sites have been proposed to bind to PAI-1 outside the SMB domain. One of these sites is housed in the disordered domain of VN, and the other site is found in the HBD, housed in the C-terminal domain of VN [142-144]. Due to the flexible and versatile nature of the disordered domain of VN, as well as its special proximity to the SMB, it is a promising site for housing the second PAI-1 binding domain. Additionally, the HBD in VN is cryptic until exposed by conformational changes induced by interaction with binding partners such as PAI-1. Together, these facts led to our hypothesis that the second binding site for PAI-1 on VN resides in the disordered domain of VN. The models provided by our SASSIE analysis lend support to this hypothesis. However, further studies will be required to fully probe the location of the second PAI-1 binding site on VN. Such studies could include limited proteolysis of bound SMB-IDD to determine if regions of the IDD are protected from cleavage by interaction with PAI-1.

In addition to the localization of the secondary PAI-1 binding site on VN, this work, and previous studies from our lab, support a change in the way we refer to the PAI-1:VN binding sites. Data from this study, and previous studies [21, 137], support the reclassification of the two binding sites to a single extended interface on PAI-1. Our data support a model in which a single PAI-1 interacts at both VN binding sites simultaneously. Indeed, the key residues in both the

primary and secondary binding sites on PAI-1 have some overlap, further supporting the idea that there is a single, extended interface on the PAI-1 molecule. While the two PAI-1 binding sites on VN are housed in separate domains, they come together in three dimensional space to form an extended interface for a single PAI-1 molecule.

When taken alone, this data could support a model in which the HBD is a valid, "third" binding site for PAI-1. Following the conformational change that occurs in VN upon binding of the first PAI-1 molecule at an extended interface, the HBD could become accessible for binding of the second PAI-1 molecule. However, the proximity of the two PAI-1 molecules (57 Å) does not support the HBD as a binding site for the second PAI-1 molecule. Additionally, future studies following the experimental model from figure 3.3, with NBD labeled bdPAI-1 and the SMB-IDD, will be performed to determine if the SMB IDD fragment is sufficient to promote 2:1 PAI-1:VN complex formation. These experiments will not only address the PAI-1 dimerization hypothesis, but will also probe the location outside the SMB domain that binds to the extended PAI-1 interface.

5.3 Classifying the Disordered Domain of VN as an IDD

The study of intrinsically disordered proteins is a field of emerging importance. Intrinsically disordered proteins play key roles in neural development, synaptic transmission, cell cycle regulation [105, 106], and are found in many signaling sequences and scaffolding proteins [107-111]. Intrinsic disorder is considered an important aspect to the versatility of living systems, providing simultaneous promiscuity and specificity in binding interactions [112]. Not all disorder is functional however. In order for a protein to be classified as "intrinsically

disordered" there are several requirements. IDPs have a high content of acidic residues (Asp and Glu), as well as Gln, and are depleted in Cys and Gly residues. They also have an overall negative charge and exhibit negative charge repulsion interactions [122]. The disordered domain of VN shares these key features which lead to our hypothesis that the domain can be classified as intrinsically disordered.

In order to fully test the classification we examined the disordered domain of VN for another feature of IDPs, disorder to order transition. The inherent versatility of IDPs is in part due to their ability to adopt a variety of structures upon interaction with binding partners. The regions of the protein that adopt these structures are referred to as molecular recognition features (MoRFs) [213]. We utilized MoRF prediction software to identify the presence of MoRFs in the disordered domain of VN. In addition to this prediction, we experimentally confirmed that the disordered domain of VN undergoes a disorder to order transition upon interaction with PAI-1. Together these data support the classification of the disordered domain of VN as an IDD. This classification provides insight into the function of this understudied domain of VN, and opens new research avenues for studying VN interactions with partners other than PAI-1.

The presence of an IDD in VN also provides insight into the versatility of VN in binding partners and physiological functions. Future research on the IDD of VN may include efforts to obtain higher resolution structural data that SANS provides. We have already generated cell stocks to allow N^{15} labeling of the SMB-IDD for study in the NMR when bound to PAI-1. Additionally, while the IDD is still flexible when in complex with VN, there may be enough induced order to allow for crystallization. Even if some portions of the IDD are flexible, and unresolvable in a crystal structure, if the IDD houses part of the PAI-1 binding domain, we would be able to resolve that region with crystallization.

5.4 Glycosylation and the IDD of VN

For the purposes of our break through study, we did not attempt to generate glycosylated SMB-IDD. However, it is important to acknowledge the fact that VN is a glycoprotein, and one of the key glycosylation sites exists in the IDD [95]. The glycosylation of VN is versatile, and changes in the glycosylation state affect cell survival and formation of the ECM [215]. Additionally, the conformational change induced by PAI-1 binding causes a rearrangement of VN that repositions carbohydrates, allowing for multimerization [216]. These data demonstrate that there is still more to the PAI-1 VN interaction to discover, but important strides have been made with this study to further our understanding of VN.

The presence of a carbohydrate likely affects the flexibility of the IDD. Additionally, the two remaining domains of VN would also affect the conformational space sampled by the IDD in our studies. Likely, several of the conformational states sampled by the IDD in our SASSIE analysis would not be feasible with the additional bulk provided by glycosylation and additional domains. This illuminates the need for future studies that incorporate glycosylation and additional domains. Our lab has previously used S2 cells to recombinantly express glycosylated VN, and these could be used to generate glycosylated SMB-IDD for additional SANS studies. These studies would lend insight into the importance of glycosylation in PAI-1:VN interactions, and the flexibility of the IDD when bound.

When comparing our SANS data to the full-length VN SAXS envelope generated by Lynn *et al*. we observed that the unbound IDD has an average Rg of ~39Å. The narrowest point of the SAXS model, where the IDD is thought to reside, is ~35Å. The difference of 4Å between our data could be a result of the truncation of VN allowing the IDD to sample a greater

conformational space. It could also be due to the fact that the IDD is not fully contained in the narrowest portion of the SAXS model. Due to the flexible nature of the IDD a difference of 4Å is not outside the margin of error when comparing data such as these. However, it will still be beneficial for future studies to focus on a way to better study full length VN, and the structure of each of the four domains.

References

1. Binder, B.R., et al., *Plasminogen activator inhibitor 1: physiological and pathophysiological roles.* News Physiol Sci, 2002. **17**: p. 56-61.
2. Al-Horani, R.A., *Serpin regulation of fibrinolytic system: implications for therapeutic applications in cardiovascular diseases.* Cardiovasc Hematol Agents Med Chem, 2014. **12**(2): p. 91-125.
3. Mulligan-Kehoe, M.J., G.N. Schwartz, and L.R. Zacharski, *The functions of plasminogen activator inhibitor-1: do we have all the pieces of PAI?* Thromb Res, 2006. **117**(5): p. 483-6.
4. Myohanen, H. and A. Vaheri, *Regulation and interactions in the activation of cell-associated plasminogen.* Cell Mol Life Sci, 2004. **61**(22): p. 2840-58.
5. Declerck, P.J. and A. Gils, *Three decades of research on plasminogen activator inhibitor-1: a multifaceted serpin.* Semin Thromb Hemost, 2013. **39**(4): p. 356-64.
6. Didiasova, M., et al., *From plasminogen to plasmin: role of plasminogen receptors in human cancer.* Int J Mol Sci, 2014. **15**(11): p. 21229-52.
7. Law, R.H., D. Abu-Ssaydeh, and J.C. Whisstock, *New insights into the structure and function of the plasminogen/plasmin system.* Curr Opin Struct Biol, 2013. **23**(6): p. 836-41.
8. Draxler, D.F. and R.L. Medcalf, *The fibrinolytic system-more than fibrinolysis?* Transfus Med Rev, 2015. **29**(2): p. 102-9.
9. Dano, K., et al., *Plasminogen activation and cancer.* Thromb Haemost, 2005. **93**(4): p. 676-81.
10. Lin, Z., et al., *Structural basis for recognition of urokinase-type plasminogen activator by plasminogen activator inhibitor-1.* J Biol Chem, 2011. **286**(9): p. 7027-32.
11. Gong, L., et al., *Crystal Structure of the Michaelis Complex between Tissue-type Plasminogen Activator and Plasminogen Activators Inhibitor-1.* J Biol Chem, 2015. **290**(43): p. 25795-804.
12. Kraut, J., *Serine proteases: structure and mechanism of catalysis.* Annu Rev Biochem, 1977. **46**: p. 331-58.
13. Grinnell, F., D.G. Hays, and D. Minter, *Cell adhesion and spreading factor. Partial purification and properties.* Exp Cell Res, 1977. **110**(1): p. 175-90.
14. Huntington, J.A., R.J. Read, and R.W. Carrell, *Structure of a serpin-protease complex shows inhibition by deformation.* Nature, 2000. **407**(6806): p. 923-6.
15. Gettins, P.G., *Serpin structure, mechanism, and function.* Chem Rev, 2002. **102**(12): p. 4751-804.
16. Czekay, R.P., et al., *PAI-1: An Integrator of Cell Signaling and Migration.* Int J Cell Biol, 2011. **2011**: p. 562481.
17. Kamikubo, Y., J.G. Neels, and B. Degryse, *Vitronectin inhibits plasminogen activator inhibitor-1-induced signalling and chemotaxis by blocking plasminogen activator inhibitor-1 binding to the low-density lipoprotein receptor-related protein.* Int J Biochem Cell Biol, 2009. **41**(3): p. 578-85.
18. Lademann, U.A. and M.U. Romer, *Regulation of programmed cell death by plasminogen activator inhibitor type 1 (PAI-1).* Thromb Haemost, 2008. **100**(6): p. 1041-6.
19. Gettins, P.G. and K. Dolmer, *The High Affinity Binding Site on Plasminogen Activator Inhibitor-1 (PAI-1) for the Low Density Lipoprotein Receptor-related Protein (LRP1) Is Composed of Four Basic Residues.* J Biol Chem, 2016. **291**(2): p. 800-12.
20. Zmijewski, J.W., et al., *Inhibition of neutrophil apoptosis by PAI-1.* Am J Physiol Lung Cell Mol Physiol, 2011. **301**(2): p. L247-54.
21. Blouse, G.E., et al., *Interactions of plasminogen activator inhibitor-1 with vitronectin involve an extensive binding surface and induce mutual conformational rearrangements.* Biochemistry, 2009. **48**(8): p. 1723-35.
22. Mehta, R. and A.D. Shapiro, *Plasminogen activator inhibitor type 1 deficiency.* Haemophilia, 2008. **14**(6): p. 1255-60.
23. Jankun, J. and E. Skrzypczak-Jankun, *Plasminogen activator inhibitor with very long half-life (VLHL PAI-1) can reduce bleeding in PAI-1-deficient patients.* Cardiovasc Hematol Disord Drug Targets, 2013. **13**(2): p. 144-50.

24. Qian, J., et al., *[Effects of urokinase type plasminogen activator and plasminogen activator inhibitor-1 expressions on the formation of aneurysm of perimembranous ventricular septal defect].* Zhonghua Er Ke Za Zhi, 2015. **53**(6): p. 453-8.
25. Repine, T. and M. Osswald, *Menorrhagia due to a qualitative deficiency of plasminogen activator inhibitor-1: case report and literature review.* Clin Appl Thromb Hemost, 2004. **10**(3): p. 293-6.
26. Schleef, R.R., et al., *Bleeding diathesis due to decreased functional activity of type 1 plasminogen activator inhibitor.* J Clin Invest, 1989. **83**(5): p. 1747-52.
27. Kahl, B.S., B.S. Schwartz, and D.F. Mosher, *Profound imbalance of pro-fibrinolytic and anti-fibrinolytic factors (tissue plasminogen activator and plasminogen activator inhibitor type 1) and severe bleeding diathesis in a patient with cirrhosis: correction by liver transplantation.* Blood Coagul Fibrinolysis, 2003. **14**(8): p. 741-4.
28. Zhang, J., et al., *A plasminogen activator inhibitor type 1 mutant retards diabetic nephropathy in db/db mice by protecting podocytes.* Exp Physiol, 2014. **99**(5): p. 802-15.
29. Cale, J.M. and D.A. Lawrence, *Structure-function relationships of plasminogen activator inhibitor-1 and its potential as a therapeutic agent.* Curr Drug Targets, 2007. **8**(9): p. 971-81.
30. Chen, H., et al., *Silencing of plasminogen activator inhibitor-1 suppresses colorectal cancer progression and liver metastasis.* Surgery, 2015.
31. Cartier-Michaud, A., et al., *Matrix-bound PAI-1 supports cell blebbing via RhoA/ROCK1 signaling.* PLoS One, 2012. **7**(2): p. e32204.
32. Gveric, D., et al., *Impaired fibrinolysis in multiple sclerosis: a role for tissue plasminogen activator inhibitors.* Brain, 2003. **126**(Pt 7): p. 1590-8.
33. Liu, R.M., et al., *Knockout of plasminogen activator inhibitor 1 gene reduces amyloid beta peptide burden in a mouse model of Alzheimer's disease.* Neurobiol Aging, 2011. **32**(6): p. 1079-89.
34. Yamamoto, K., K. Takeshita, and H. Saito, *Plasminogen activator inhibitor-1 in aging.* Semin Thromb Hemost, 2014. **40**(6): p. 652-9.
35. Juhan-Vague, I., et al., *Plasminogen activator inhibitor-1, inflammation, obesity, insulin resistance and vascular risk.* J Thromb Haemost, 2003. **1**(7): p. 1575-9.
36. Lemaire, R., et al., *Neutralization of the anti-fibrinolytic function of plasminogen activator inhibitor-1 resolves skin fibrosis.* Arthritis Rheumatol, 2015.
37. Oishi, K., et al., *Ketogenic diet disrupts the circadian clock and increases hypofibrinolytic risk by inducing expression of plasminogen activator inhibitor-1.* Arterioscler Thromb Vasc Biol, 2009. **29**(10): p. 1571-7.
38. Shetty, S., et al., *Regulation of plasminogen activator inhibitor-1 expression by tumor suppressor protein p53.* J Biol Chem, 2008. **283**(28): p. 19570-80.
39. White, M.J., et al., *Genetics of Plasminogen Activator Inhibitor-1 (PAI-1) in a Ghanaian Population.* PLoS One, 2015. **10**(8): p. e0136379.
40. Arteel, G.E., *New role of plasminogen activator inhibitor-1 in alcohol-induced liver injury.* J Gastroenterol Hepatol, 2008. **23 Suppl 1**: p. S54-9.
41. Miles, L.A. and R.J. Parmer, *PAI-1: cardiac friend or foe?* Blood, 2010. **115**(10): p. 1862-3.
42. Vaughan, D.E., *PAI-1 antagonists: the promise and the peril.* Trans Am Clin Climatol Assoc, 2011. **122**: p. 312-25.
43. Mashiko, S., et al., *Inhibition of plasminogen activator inhibitor-1 is a potential therapeutic strategy in ovarian cancer.* Cancer Biol Ther, 2015. **16**(2): p. 253-60.
44. Simon, D.I. and N.M. Simon, *Plasminogen activator inhibitor-1: a novel therapeutic target for hypertension?* Circulation, 2013. **128**(21): p. 2286-8.
45. Simone, T.M. and P.J. Higgins, *Low Molecular Weight Antagonists of Plasminogen Activator Inhibitor-1: Therapeutic Potential in Cardiovascular Disease.* Mol Med Ther, 2012. **1**(1): p. 101.

46. Simone, T.M. and P.J. Higgins, *Small Molecule PAI-1 Functional Inhibitor Attenuates Vascular Smooth Muscle Cell Migration and Survival: Implications for the Therapy of Vascular Disease.* New Horiz Transl Med, 2014. **2**(1): p. 16-19.
47. Simone, T.M., et al., *Targeted Inhibition of PAI-1 Activity Impairs Epithelial Migration and Wound Closure Following Cutaneous Injury.* Adv Wound Care (New Rochelle), 2015. **4**(6): p. 321-328.
48. Brown, N.J., *Therapeutic potential of plasminogen activator inhibitor-1 inhibitors.* Ther Adv Cardiovasc Dis, 2010. **4**(5): p. 315-24.
49. Jankun, J., et al., *Very long half-life plasminogen activator inhibitor type 1 reduces bleeding in a mouse model.* BJU Int, 2010. **105**(10): p. 1469-76.
50. Lee, S.H., et al., *A plasminogen activator inhibitor-1 inhibitor reduces airway remodeling in a murine model of chronic asthma.* Am J Respir Cell Mol Biol, 2012. **46**(6): p. 842-6.
51. Simone, T.M., et al., *A small molecule PAI-1 functional inhibitor attenuates neointimal hyperplasia and vascular smooth muscle cell survival by promoting PAI-1 cleavage.* Cell Signal, 2015. **27**(5): p. 923-33.
52. Fjellstrom, O., et al., *Characterization of a small molecule inhibitor of plasminogen activator inhibitor type 1 that accelerates the transition into the latent conformation.* J Biol Chem, 2013. **288**(2): p. 873-85.
53. Simone, T.M., et al., *Chemical Antagonists of Plasminogen Activator Inhibitor-1: Mechanisms of Action and Therapeutic Potential in Vascular Disease.* J Mol Genet Med, 2014. **8**(3).
54. Tani, S., et al., *Effect of dipeptidyl peptidase-4 inhibitor, vildagliptin on plasminogen activator inhibitor-1 in patients with diabetes mellitus.* Am J Cardiol, 2015. **115**(4): p. 454-60.
55. Liu, J., et al., *Green tea polyphenols inhibit plasminogen activator inhibitor-1 expression and secretion in endothelial cells.* Blood Coagul Fibrinolysis, 2009. **20**(7): p. 552-7.
56. Zagotta, I., et al., *Resveratrol suppresses PAI-1 gene expression in a human in vitro model of inflamed adipose tissue.* Oxid Med Cell Longev, 2013. **2013**: p. 793525.
57. Placencio, V.R., et al., *Small Molecule Inhibitors of Plasminogen Activator Inhibitor-1 Elicit Anti-Tumorigenic and Anti-Angiogenic Activity.* PLoS One, 2015. **10**(7): p. e0133786.
58. Silverman, G.A., et al., *Serpins flex their muscle: I. Putting the clamps on proteolysis in diverse biological systems.* J Biol Chem, 2010. **285**(32): p. 24299-305.
59. Law, R.H., et al., *An overview of the serpin superfamily.* Genome Biol, 2006. **7**(5): p. 216.
60. Steenbakkers, P.J., et al., *A serpin in the cellulosome of the anaerobic fungus Piromyces sp. strain E2.* Mycol Res, 2008. **112**(Pt 8): p. 999-1006.
61. Lomas, D.A. and R.W. Carrell, *Serpinopathies and the conformational dementias.* Nat Rev Genet, 2002. **3**(10): p. 759-68.
62. Whisstock, J.C., et al., *Serpins flex their muscle: II. Structural insights into target peptidase recognition, polymerization, and transport functions.* J Biol Chem, 2010. **285**(32): p. 24307-12.
63. Irving, J.A., et al., *Serpins in prokaryotes.* Mol Biol Evol, 2002. **19**(11): p. 1881-90.
64. Zhou, A., R.W. Carrell, and J.A. Huntington, *The serpin inhibitory mechanism is critically dependent on the length of the reactive center loop.* J Biol Chem, 2001. **276**(29): p. 27541-7.
65. Declerck, P., *[Plasminogen activator-inhibitor 1: biochemical, structural and functional studies].* Verh K Acad Geneeskd Belg, 1993. **55**(5): p. 457-73.
66. Yasar Yildiz, S., et al., *Functional stability of plasminogen activator inhibitor-1.* ScientificWorldJournal, 2014. **2014**: p. 858293.
67. Trelle, M.B., et al., *Local transient unfolding of native state PAI-1 associated with serpin metastability.* Angew Chem Int Ed Engl, 2014. **53**(37): p. 9751-4.
68. Chorostowska-Wynimko, J., E. Skrzypczak-Jankun, and J. Jankun, *Plasminogen activator inhibitor type-1 controls the process of the in vitro sprout formation.* J Physiol Pharmacol, 2004. **55 Suppl 3**: p. 49-56.

69. Hansen, M., M.N. Busse, and P.A. Andreasen, *Importance of the amino-acid composition of the shutter region of plasminogen activator inhibitor-1 for its transitions to latent and substrate forms.* Eur J Biochem, 2001. **268**(23): p. 6274-83.
70. Wright, H.T. and J.N. Scarsdale, *Structural basis for serpin inhibitor activity.* Proteins, 1995. **22**(3): p. 210-25.
71. Mangs, H., G.C. Sui, and B. Wiman, *PAI-1 stability: the role of histidine residues.* FEBS Lett, 2000. **475**(3): p. 192-6.
72. Kvassman, J.O., D.A. Lawrence, and J.D. Shore, *The acid stabilization of plasminogen activator inhibitor-1 depends on protonation of a single group that affects loop insertion into beta-sheet A.* J Biol Chem, 1995. **270**(46): p. 27942-7.
73. Thompson, L.C., et al., *Metals affect the structure and activity of human plasminogen activator inhibitor-1. I. Modulation of stability and protease inhibition.* Protein Sci, 2011. **20**(2): p. 353-65.
74. Berkenpas, M.B., D.A. Lawrence, and D. Ginsburg, *Molecular evolution of plasminogen activator inhibitor-1 functional stability.* EMBO J, 1995. **14**(13): p. 2969-77.
75. Jensen, J.K. and P.G. Gettins, *High-resolution structure of the stable plasminogen activator inhibitor type-1 variant 14-1B in its proteinase-cleaved form: a new tool for detailed interaction studies and modeling.* Protein Sci, 2008. **17**(10): p. 1844-9.
76. Jensen, J.K., et al., *Crystal structure of plasminogen activator inhibitor-1 in an active conformation with normal thermodynamic stability.* J Biol Chem, 2011. **286**(34): p. 29709-17.
77. Zhou, A., et al., *How vitronectin binds PAI-1 to modulate fibrinolysis and cell migration.* Nat Struct Biol, 2003. **10**(7): p. 541-4.
78. Stout, T.J., et al., *Structures of active and latent PAI-1: a possible stabilizing role for chloride ions.* Biochemistry, 2000. **39**(29): p. 8460-9.
79. Blouse, G.E., et al., *Mutation of the highly conserved tryptophan in the serpin breach region alters the inhibitory mechanism of plasminogen activator inhibitor-1.* Biochemistry, 2003. **42**(42): p. 12260-72.
80. Li, S.H., et al., *Structural differences between active forms of plasminogen activator inhibitor type 1 revealed by conformationally sensitive ligands.* J Biol Chem, 2008. **283**(26): p. 18147-57.
81. Zhou, A., et al., *Polymerization of plasminogen activator inhibitor-1.* J Biol Chem, 2001. **276**(12): p. 9115-22.
82. Preissner, K.T. and D. Seiffert, *Role of vitronectin and its receptors in haemostasis and vascular remodeling.* Thromb Res, 1998. **89**(1): p. 1-21.
83. Preissner, K.T., *Structure and biological role of vitronectin.* Annu Rev Cell Biol, 1991. **7**: p. 275-310.
84. Koschnick, S., et al., *Thrombotic phenotype of mice with a combined deficiency in plasminogen activator inhibitor 1 and vitronectin.* J Thromb Haemost, 2005. **3**(10): p. 2290-5.
85. Singh, B., Y.C. Su, and K. Riesbeck, *Vitronectin in bacterial pathogenesis: a host protein used in complement escape and cellular invasion.* Mol Microbiol, 2010. **78**(3): p. 545-60.
86. Gechtman, Z., et al., *The cluster of basic amino acids in vitronectin contributes to its binding of plasminogen activator inhibitor-1: evidence from thrombin-, elastase- and plasmin-cleaved vitronectins and anti-peptide antibodies.* Biochem J, 1997. **325 (Pt 2)**: p. 339-49.
87. Leavesley, D.I., et al., *Vitronectin--master controller or micromanager?* IUBMB Life, 2013. **65**(10): p. 807-18.
88. Conlan, M.G., et al., *Plasma vitronectin polymorphism in normal subjects and patients with disseminated intravascular coagulation.* Blood, 1988. **72**(1): p. 185-90.
89. Xu, D., et al., *Model for the three-dimensional structure of vitronectin: predictions for the multi-domain protein from threading and docking.* Proteins, 2001. **44**(3): p. 312-20.
90. Horn, N.A., et al., *Assignment of the four disulfides in the N-terminal somatomedin B domain of native vitronectin isolated from human plasma.* J Biol Chem, 2004. **279**(34): p. 35867-78.

91. Kamikubo, Y., Y. Okumura, and D.J. Loskutoff, *Identification of the disulfide bonds in the recombinant somatomedin B domain of human vitronectin.* J Biol Chem, 2002. **277**(30): p. 27109-19.
92. Kamikubo, Y., et al., *Disulfide bonding arrangements in active forms of the somatomedin B domain of human vitronectin.* Biochemistry, 2004. **43**(21): p. 6519-34.
93. Kjaergaard, M., et al., *Solution structure of recombinant somatomedin B domain from vitronectin produced in Pichia pastoris.* Protein Sci, 2007. **16**(9): p. 1934-45.
94. Mayasundari, A., et al., *The solution structure of the N-terminal domain of human vitronectin: proximal sites that regulate fibrinolysis and cell migration.* J Biol Chem, 2004. **279**(28): p. 29359-66.
95. Lynn, G.W., et al., *A model for the three-dimensional structure of human plasma vitronectin from small-angle scattering measurements.* Biochemistry, 2005. **44**(2): p. 565-74.
96. Chow, S. and N. Di Girolamo, *Vitronectin: a migration and wound healing factor for human corneal epithelial cells.* Invest Ophthalmol Vis Sci, 2014. **55**(10): p. 6590-600.
97. Stefansson, S., C.C. Haudenschild, and D.A. Lawrence, *Beyond fibrinolysis: the role of plasminogen activator inhibitor-1 and vitronectin in vascular wound healing.* Trends Cardiovasc Med, 1998. **8**(4): p. 175-80.
98. Madsen, C.D., et al., *uPAR-induced cell adhesion and migration: vitronectin provides the key.* J Cell Biol, 2007. **177**(5): p. 927-39.
99. Aaboe, M., et al., *Vitronectin in human breast carcinomas.* Biochim Biophys Acta, 2003. **1638**(1): p. 72-82.
100. Rea, V.E., et al., *Discovery of new small molecules targeting the vitronectin-binding site of the urokinase receptor that block cancer cell invasion.* Mol Cancer Ther, 2013. **12**(8): p. 1402-16.
101. Upton, Z., et al., *Vitronectin: growth factor complexes hold potential as a wound therapy approach.* J Invest Dermatol, 2008. **128**(6): p. 1535-44.
102. Kendrew, J.C., *Architecture of a protein molecule.* Nature, 1958. **182**(4638): p. 764-7.
103. Pauling, L., R.B. Corey, and H.R. Branson, *The structure of proteins; two hydrogen-bonded helical configurations of the polypeptide chain.* Proc Natl Acad Sci U S A, 1951. **37**(4): p. 205-11.
104. Bennett, W.S. and R. Huber, *Structural and functional aspects of domain motions in proteins.* CRC Crit Rev Biochem, 1984. **15**(4): p. 291-384.
105. Tantos, A., L. Kalmar, and P. Tompa, *The role of structural disorder in cell cycle regulation, related clinical proteomics, disease development and drug targeting.* Expert Rev Proteomics, 2015. **12**(3): p. 221-33.
106. Tovo-Rodrigues, L., et al., *The role of protein intrinsic disorder in major psychiatric disorders.* Am J Med Genet B Neuropsychiatr Genet, 2016.
107. Uversky, V.N., *The multifaceted roles of intrinsic disorder in protein complexes.* FEBS Lett, 2015. **589**(19 Pt A): p. 2498-506.
108. Cortese, M.S., V.N. Uversky, and A.K. Dunker, *Intrinsic disorder in scaffold proteins: getting more from less.* Prog Biophys Mol Biol, 2008. **98**(1): p. 85-106.
109. Uversky, V.N., C.J. Oldfield, and A.K. Dunker, *Showing your ID: intrinsic disorder as an ID for recognition, regulation and cell signaling.* J Mol Recognit, 2005. **18**(5): p. 343-84.
110. Dunker, A.K., et al., *The unfoldomics decade: an update on intrinsically disordered proteins.* BMC Genomics, 2008. **9 Suppl 2**: p. S1.
111. Dyson, H.J. and P.E. Wright, *Coupling of folding and binding for unstructured proteins.* Curr Opin Struct Biol, 2002. **12**(1): p. 54-60.
112. Dyson, H.J. and P.E. Wright, *Role of Intrinsic Protein Disorder in the Function and Interactions of the Transcriptional Coactivators CREB-binding Protein (CBP) and p300.* J Biol Chem, 2016. **291**(13): p. 6714-22.
113. Meng, F., et al., *Compartmentalization and Functionality of Nuclear Disorder: Intrinsic Disorder and Protein-Protein Interactions in Intra-Nuclear Compartments.* Int J Mol Sci, 2016. **17**(1).

114. Varadi, M., et al., *Functional Advantages of Conserved Intrinsic Disorder in RNA-Binding Proteins.* PLoS One, 2015. **10**(10): p. e0139731.
115. Uversky, V.N., C.J. Oldfield, and A.K. Dunker, *Intrinsically disordered proteins in human diseases: introducing the D2 concept.* Annu Rev Biophys, 2008. **37**: p. 215-46.
116. Dyson, H.J. and P.E. Wright, *Intrinsically unstructured proteins and their functions.* Nat Rev Mol Cell Biol, 2005. **6**(3): p. 197-208.
117. Vacic, V., et al., *Disease-associated mutations disrupt functionally important regions of intrinsic protein disorder.* PLoS Comput Biol, 2012. **8**(10): p. e1002709.
118. Schuch, J.B., et al., *The contribution of protein intrinsic disorder to understand the role of genetic variants uncovered by autism spectrum disorders exome studies.* Am J Med Genet B Neuropsychiatr Genet, 2016. **171**(3): p. 479-91.
119. DeForte, S. and V.N. Uversky, *Resolving the ambiguity: Making sense of intrinsic disorder when PDB structures disagree.* Protein Sci, 2016. **25**(3): p. 676-88.
120. Vincent, M. and S. Schnell, *A collection of intrinsic disorder characterizations from eukaryotic proteomes.* Sci Data, 2016. **3**: p. 160045.
121. Luna-Martinez, O.D., et al., *Simple approach for ranking structure determining residues.* PeerJ, 2016. **4**: p. e2136.
122. Rani, P., A. Baruah, and P. Biswas, *Does lack of secondary structure imply intrinsic disorder in proteins? A sequence analysis.* Biochim Biophys Acta, 2014. **1844**(10): p. 1827-34.
123. Podor, T.J., et al., *Type 1 plasminogen activator inhibitor binds to fibrin via vitronectin.* J Biol Chem, 2000. **275**(26): p. 19788-94.
124. Preissner, K.T. and U. Reuning, *Vitronectin in vascular context: facets of a multitalented matricellular protein.* Semin Thromb Hemost, 2011. **37**(4): p. 408-24.
125. Andreasen, P.A., et al., *Solvent effects on activity and conformation of plasminogen activator inhibitor-1.* Thromb Haemost, 1999. **81**(3): p. 407-14.
126. Jensen, S., et al., *The role of beta-strand 5A of plasminogen activator inhibitor-1 in regulation of its latency transition and inhibitory activity by vitronectin.* Biochim Biophys Acta, 2002. **1597**(2): p. 301-10.
127. Stefansson, S., et al., *Inhibition of angiogenesis in vivo by plasminogen activator inhibitor-1.* J Biol Chem, 2001. **276**(11): p. 8135-41.
128. Minor, K.H., et al., *A mechanism for assembly of complexes of vitronectin and plasminogen activator inhibitor-1 from sedimentation velocity analysis.* J Biol Chem, 2005. **280**(31): p. 28711-20.
129. Stefansson, S., D.A. Lawrence, and W.S. Argraves, *Plasminogen activator inhibitor-1 and vitronectin promote the cellular clearance of thrombin by low density lipoprotein receptor-related proteins 1 and 2.* J Biol Chem, 1996. **271**(14): p. 8215-20.
130. Zhong, J., et al., *Vitronectin-binding PAI-1 protects against the development of cardiac fibrosis through interaction with fibroblasts.* Lab Invest, 2014. **94**(6): p. 633-44.
131. Gibson, A., et al., *The use of fluorescent probes to characterize conformational changes in the interaction between vitronectin and plasminogen activator inhibitor-1.* J Biol Chem, 1997. **272**(8): p. 5112-21.
132. Minor, K.H. and C.B. Peterson, *Plasminogen activator inhibitor type 1 promotes the self-association of vitronectin into complexes exhibiting altered incorporation into the extracellular matrix.* J Biol Chem, 2002. **277**(12): p. 10337-45.
133. Podor, T.J., et al., *Vimentin exposed on activated platelets and platelet microparticles localizes vitronectin and plasminogen activator inhibitor complexes on their surface.* J Biol Chem, 2002. **277**(9): p. 7529-39.
134. Alessi, M.C., et al., *Association of vitronectin and plasminogen activator inhibitor-1 levels with the risk of metabolic syndrome and type 2 diabetes mellitus. Results from the D.E.S.I.R. prospective cohort.* Thromb Haemost, 2011. **106**(3): p. 416-22.

135. Garg, N., et al., *Plasminogen activator inhibitor-1 and vitronectin expression level and stoichiometry regulate vascular smooth muscle cell migration through physiological collagen matrices.* J Thromb Haemost, 2010. **8**(8): p. 1847-54.
136. Seiffert, D., et al., *The somatomedin B domain of vitronectin. Structural requirements for the binding and stabilization of active type 1 plasminogen activator inhibitor.* J Biol Chem, 1994. **269**(4): p. 2659-66.
137. Schar, C.R., et al., *Characterization of a site on PAI-1 that binds to vitronectin outside of the somatomedin B domain.* J Biol Chem, 2008. **283**(42): p. 28487-96.
138. Schar, C.R., et al., *A deletion mutant of vitronectin lacking the somatomedin B domain exhibits residual plasminogen activator inhibitor-1-binding activity.* J Biol Chem, 2008. **283**(16): p. 10297-309.
139. Booth, N.A., et al., *Plasminogen activator inhibitor (PAI-1) in plasma and platelets.* Br J Haematol, 1988. **70**(3): p. 327-33.
140. Podor, T.J., et al., *New insights into the size and stoichiometry of the plasminogen activator inhibitor type-1.vitronectin complex.* J Biol Chem, 2000. **275**(33): p. 25402-10.
141. Deng, G., et al., *Structural and functional analysis of the plasminogen activator inhibitor-1 binding motif in the somatomedin B domain of vitronectin.* J Biol Chem, 1996. **271**(22): p. 12716-23.
142. Schroeck, F., et al., *Interaction of plasminogen activator inhibitor type-1 (PAI-1) with vitronectin (Vn): mapping the binding sites on PAI-1 and Vn.* Biol Chem, 2002. **383**(7-8): p. 1143-9.
143. Mimuro, J., et al., *Identification of the plasminogen activator inhibitor-1 binding heptapeptide in vitronectin.* Biochemistry, 1993. **32**(9): p. 2314-20.
144. Kost, C., et al., *Mapping of binding sites for heparin, plasminogen activator inhibitor-1, and plasminogen to vitronectin's heparin-binding region reveals a novel vitronectin-dependent feedback mechanism for the control of plasmin formation.* J Biol Chem, 1992. **267**(17): p. 12098-105.
145. Deng, G., et al., *Is plasminogen activator inhibitor-1 the molecular switch that governs urokinase receptor-mediated cell adhesion and release?* J Cell Biol, 1996. **134**(6): p. 1563-71.
146. Germer, M., et al., *Kinetic analysis of integrin-dependent cell adhesion on vitronectin--the inhibitory potential of plasminogen activator inhibitor-1 and RGD peptides.* Eur J Biochem, 1998. **253**(3): p. 669-74.
147. Goswami, S., *Studies on the Role of Vitronectin and Plasminogen-Activator Inhibitor-1 Complexes Beyond Inhibiting Proteases: Binding to the Extracellular Matrix, Cell Interactions and Pathogenesis.* . PhD dissertation, University of Tennessee, 2010.
148. Chillakuri, C.R., C. Jones, and H.J. Mardon, *Heparin binding domain in vitronectin is required for oligomerization and thus enhances integrin mediated cell adhesion and spreading.* FEBS Lett, 2010. **584**(15): p. 3287-91.
149. Dahlback, B. and E.R. Podack, *Characterization of human S protein, an inhibitor of the membrane attack complex of complement. Demonstration of a free reactive thiol group.* Biochemistry, 1985. **24**(9): p. 2368-74.
150. Schuck, P., *Size-distribution analysis of macromolecules by sedimentation velocity ultracentrifugation and lamm equation modeling.* Biophys J, 2000. **78**(3): p. 1606-19.
151. Petoukhov, M.V., et al., *New developments in the program package for small-angle scattering data analysis.* J Appl Crystallogr, 2012. **45**(Pt 2): p. 342-350.
152. Svergun, D.I., *Restoring low resolution structure of biological macromolecules from solution scattering using simulated annealing.* Biophys J, 1999. **76**(6): p. 2879-86.
153. Kozin, M.B. and D.I. Svergun, *Automated matching of high- and low-resolution structural models.* Journal of Applied Crystallography, 2001. **34**: p. 33-41.
154. Bernado, P., et al., *Structural characterization of flexible proteins using small-angle X-ray scattering.* J Am Chem Soc, 2007. **129**(17): p. 5656-64.

155. Svergun, D.I., et al., *Protein hydration in solution: experimental observation by x-ray and neutron scattering.* Proc Natl Acad Sci U S A, 1998. **95**(5): p. 2267-72.
156. Tria, G., et al., *Advanced ensemble modelling of flexible macromolecules using X-ray solution scattering.* IUCrJ, 2015. **2**(Pt 2): p. 207-17.
157. Curtis, J.E., et al., *SASSIE: A program to study intrinsically disordered biological molecules and macromolecular ensembles using experimental scattering restraints.* Computer Physics Communications, 2012. **183**(2): p. 382-389.
158. Phillips, J.C., et al., *Scalable molecular dynamics with NAMD.* J Comput Chem, 2005. **26**(16): p. 1781-802.
159. Jones, D.T., *Protein secondary structure prediction based on position-specific scoring matrices.* J Mol Biol, 1999. **292**(2): p. 195-202.
160. Kelley, L.A. and M.J. Sternberg, *Protein structure prediction on the Web: a case study using the Phyre server.* Nat Protoc, 2009. **4**(3): p. 363-71.
161. Kelley, L.A., et al., *The Phyre2 web portal for protein modeling, prediction and analysis.* Nat Protoc, 2015. **10**(6): p. 845-58.
162. Fasman, G.D., *Prediction of Protein-Structure from Sequence.* Nature, 1985. **316**(6023): p. 22-22.
163. Prevelige, P.F., G.D., *Chou-Fasman Prediction of the Secondary Structure of Proteins*, in *Prediction of Protein Structure and the Principles of Protein Conformation*, G. Fasman, Editor. 1989, Springer US, Boston, MA. p. 391-416.
164. Garnier, J., D.J. Osguthorpe, and B. Robson, *Analysis of the accuracy and implications of simple methods for predicting the secondary structure of globular proteins.* J Mol Biol, 1978. **120**(1): p. 97-120.
165. Buchan, D.W., et al., *Scalable web services for the PSIPRED Protein Analysis Workbench.* Nucleic Acids Res, 2013. **41**(Web Server issue): p. W349-57.
166. Humphrey, W., A. Dalke, and K. Schulten, *VMD: Visual molecular dynamics.* Journal of Molecular Graphics & Modelling, 1996. **14**(1): p. 33-38.
167. Declerck, P.J., et al., *Purification and characterization of a plasminogen activator inhibitor 1 binding protein from human plasma. Identification as a multimeric form of S protein (vitronectin).* J Biol Chem, 1988. **263**(30): p. 15454-61.
168. Mimuro, J., R.R. Schleef, and D.J. Loskutoff, *Extracellular matrix of cultured bovine aortic endothelial cells contains functionally active type 1 plasminogen activator inhibitor.* Blood, 1987. **70**(3): p. 721-8.
169. Seiffert, D., N.N. Wagner, and D.J. Loskutoff, *Serum-derived vitronectin influences the pericellular distribution of type 1 plasminogen activator inhibitor.* J Cell Biol, 1990. **111**(3): p. 1283-91.
170. van Meijer, M., et al., *Determination of the vitronectin binding site on plasminogen activator inhibitor 1 (PAI-1).* FEBS Lett, 1994. **352**(3): p. 342-6.
171. Lawrence, D.A., et al., *Localization of vitronectin binding domain in plasminogen activator inhibitor-1.* J Biol Chem, 1994. **269**(21): p. 15223-8.
172. Arroyo De Prada, N., et al., *Interaction of plasminogen activator inhibitor type-1 (PAI-1) with vitronectin.* Eur J Biochem, 2002. **269**(1): p. 184-92.
173. Ehrlich, H.J., et al., *Elucidation of structural requirements on plasminogen activator inhibitor 1 for binding to heparin.* J Biol Chem, 1992. **267**(16): p. 11606-11.
174. Seiffert, D. and D.J. Loskutoff, *Evidence that type 1 plasminogen activator inhibitor binds to the somatomedin B domain of vitronectin.* J Biol Chem, 1991. **266**(5): p. 2824-30.
175. Sigurdardottir, O. and B. Wiman, *Identification of a PAI-1 binding site in vitronectin.* Biochim Biophys Acta, 1994. **1208**(1): p. 104-10.
176. Seiffert, D. and D.J. Loskutoff, *Kinetic analysis of the interaction between type 1 plasminogen activator inhibitor and vitronectin and evidence that the bovine inhibitor binds to a thrombin-derived amino-terminal fragment of bovine vitronectin.* Biochim Biophys Acta, 1991. **1078**(1): p. 23-30.

177. Salonen, E.M., et al., *Interaction of plasminogen activator inhibitor (PAI-1) with vitronectin.* J Biol Chem, 1989. **264**(11): p. 6339-43.
178. Seiffert, D., et al., *Interactions between type 1 plasminogen activator inhibitor, extracellular matrix and vitronectin.* Cell Differ Dev, 1990. **32**(3): p. 287-92.
179. Seiffert, D. and J.W. Smith, *The cell adhesion domain in plasma vitronectin is cryptic.* J Biol Chem, 1997. **272**(21): p. 13705-10.
180. Boyd, N.A., A.R. Bradwell, and R.A. Thompson, *Quantitation of vitronectin in serum: evaluation of its usefulness in routine clinical practice.* J Clin Pathol, 1993. **46**(11): p. 1042-5.
181. Plow, E.F., *Vitronectin: back into the spotlight.* J Thromb Haemost, 2005. **3**(5): p. 873-4.
182. Seiffert, D. and R.R. Schleef, *Two functionally distinct pools of vitronectin (Vn) in the blood circulation: identification of a heparin-binding competent population of Vn within platelet alpha-granules.* Blood, 1996. **88**(2): p. 552-60.
183. Lawrence, D.A., et al., *Characterization of the binding of different conformational forms of plasminogen activator inhibitor-1 to vitronectin. Implications for the regulation of pericellular proteolysis.* J Biol Chem, 1997. **272**(12): p. 7676-80.
184. Yamasaki, M., et al., *Crystal structure of a stable dimer reveals the molecular basis of serpin polymerization.* Nature, 2008. **455**(7217): p. 1255-8.
185. Shore, J.D., et al., *A fluorescent probe study of plasminogen activator inhibitor-1. Evidence for reactive center loop insertion and its role in the inhibitory mechanism.* J Biol Chem, 1995. **270**(10): p. 5395-8.
186. Qureshi, T., et al., *Distinct encounter complexes of PAI-1 with plasminogen activators and vitronectin revealed by changes in the conformation and dynamics of the reactive center loop.* Protein Sci, 2016. **25**(2): p. 499-510.
187. Qureshi, T. and C.B. Peterson, *Single fluorescence probes along the reactive center loop reveal site-specific changes during the latency transition of PAI-1.* Protein Sci, 2016. **25**(2): p. 487-98.
188. Schuck, P., et al., *Size-distribution analysis of proteins by analytical ultracentrifugation: strategies and application to model systems.* Biophys J, 2002. **82**(2): p. 1096-111.
189. Brown, P.H. and P. Schuck, *Macromolecular size-and-shape distributions by sedimentation velocity analytical ultracentrifugation.* Biophys J, 2006. **90**(12): p. 4651-61.
190. Jensen, J.K., et al., *Construction of a plasminogen activator inhibitor-1 variant without measurable affinity to vitronectin but otherwise normal.* FEBS Lett, 2004. **556**(1-3): p. 175-9.
191. Sharp, A.M., et al., *The active conformation of plasminogen activator inhibitor 1, a target for drugs to control fibrinolysis and cell adhesion.* Structure, 1999. **7**(2): p. 111-8.
192. Barnes, D., et al., *Effects of a serum spreading factor on growth and morphology of cells in serum-free medium.* J Supramol Struct, 1980. **14**(1): p. 47-63.
193. Holmes, R., *Preparation from human serum of an alpha-one protein which induces the immediate growth of unadapted cells in vitro.* J Cell Biol, 1967. **32**(2): p. 297-308.
194. Hayman, E.G., et al., *Serum spreading factor (vitronectin) is present at the cell surface and in tissues.* Proc Natl Acad Sci U S A, 1983. **80**(13): p. 4003-7.
195. Barnes, D.W., et al., *Characterization of human serum spreading factor with monoclonal antibody.* Proc Natl Acad Sci U S A, 1983. **80**(5): p. 1362-6.
196. Kost, C., et al., *Limited plasmin proteolysis of vitronectin. Characterization of the adhesion protein as morpho-regulatory and angiostatin-binding factor.* Eur J Biochem, 1996. **236**(2): p. 682-8.
197. Podor, T.J., et al., *Incorporation of vitronectin into fibrin clots. Evidence for a binding interaction between vitronectin and gamma A/gamma' fibrinogen.* J Biol Chem, 2002. **277**(9): p. 7520-8.
198. Defilippi, P., et al., *Tumor necrosis factor alpha and interferon gamma modulate the expression of the vitronectin receptor (integrin beta 3) in human endothelial cells.* J Biol Chem, 1991. **266**(12): p. 7638-45.
199. Schnapp, L.M., et al., *The human integrin alpha 8 beta 1 functions as a receptor for tenascin, fibronectin, and vitronectin.* J Biol Chem, 1995. **270**(39): p. 23196-202.

200. Smith, J.W., et al., *Purification and functional characterization of integrin alpha v beta 5. An adhesion receptor for vitronectin.* J Biol Chem, 1990. **265**(19): p. 11008-13.
201. Wei, Y., et al., *Identification of the urokinase receptor as an adhesion receptor for vitronectin.* J Biol Chem, 1994. **269**(51): p. 32380-8.
202. Preissner, K.T., R. Wassmuth, and G. Muller-Berghaus, *Physicochemical characterization of human S-protein and its function in the blood coagulation system.* Biochem J, 1985. **231**(2): p. 349-55.
203. Suzuki, S., et al., *Domain structure of vitronectin. Alignment of active sites.* J Biol Chem, 1984. **259**(24): p. 15307-14.
204. Zhou, A., *Functional structure of the somatomedin B domain of vitronectin.* Protein Sci, 2007. **16**(7): p. 1502-8.
205. Anson, M.L. and A.E. Mirsky, *On Some General Properties of Proteins.* J Gen Physiol, 1925. **9**(2): p. 169-79.
206. Mirsky, A.E. and L. Pauling, *On the Structure of Native, Denatured, and Coagulated Proteins.* Proc Natl Acad Sci U S A, 1936. **22**(7): p. 439-47.
207. Dunker, A.K., et al., *Intrinsically disordered protein.* J Mol Graph Model, 2001. **19**(1): p. 26-59.
208. Wright, P.E. and H.J. Dyson, *Intrinsically unstructured proteins: re-assessing the protein structure-function paradigm.* J Mol Biol, 1999. **293**(2): p. 321-31.
209. Uversky, V.N., et al., *Pathological unfoldomics of uncontrolled chaos: intrinsically disordered proteins and human diseases.* Chem Rev, 2014. **114**(13): p. 6844-79.
210. Padmanabhan, J. and D.C. Sane, *Localization of a vitronectin binding region of plasminogen activator inhibitor-1.* Thromb Haemost, 1995. **73**(5): p. 829-34.
211. Whitmore, L. and B.A. Wallace, *DICHROWEB, an online server for protein secondary structure analyses from circular dichroism spectroscopic data.* Nucleic Acids Res, 2004. **32**(Web Server issue): p. W668-73.
212. Whitmore, L. and B.A. Wallace, *Protein secondary structure analyses from circular dichroism spectroscopy: methods and reference databases.* Biopolymers, 2008. **89**(5): p. 392-400.
213. Disfani, F.M., et al., *MoRFpred, a computational tool for sequence-based prediction and characterization of short disorder-to-order transitioning binding regions in proteins.* Bioinformatics, 2012. **28**(12): p. i75-83.
214. van der Lee, R., et al., *Classification of intrinsically disordered regions and proteins.* Chem Rev, 2014. **114**(13): p. 6589-631.
215. Sano, K., et al., *Survival signals of hepatic stellate cells in liver regeneration are regulated by glycosylation changes in rat vitronectin, especially decreased sialylation.* J Biol Chem, 2010. **285**(23): p. 17301-9.
216. Sano, K., et al., *Changes in glycosylation of vitronectin modulate multimerization and collagen binding during liver regeneration.* Glycobiology, 2007. **17**(7): p. 784-94.

Vita

Letitia Puster, formerly Letitia Olson, was born in Las Vegas, NV in September 1987. Letitia attended public schools until the 5th grade, at which point she was homeschooled so that she could study at an accelerated pace. Letitia started college in August of 2004, finishing her senior year of high school as a dual enrolled student. After attending Pellissippi State Community College for two years, Letitia formally transferred to the University of Tennessee, Knoxville and completed a bachelor's of science degree in biochemistry, cellular, and molecular biology in May 2008. Letitia spent the next year conducting post-baccalaureate work in the laboratory of her undergraduate mentor, Dr. Barry Bruce. August 2009 found Letitia back in her old department, this time as a graduate student. Letitia joined the laboratory of Dr. Cynthia B. Peterson in 2010 and finished her PhD in August 2016.